

**SEX DIFFERENCES IN CENTRAL NEURAL ACTIVATION DURING
ACUTE HYPERNATREMIA**

by

Nathan Tucker Romberger

A dissertation submitted to the Faculty of the University of Delaware in partial fulfillment of the requirements for the degree of Doctor of Philosophy in Applied Physiology

Spring 2025

© 2025 Nathan Tucker Romberger
All Rights Reserved

**SEX DIFFERENCES IN CENTRAL NEURAL ACTIVATION DURING
ACUTE HYPERNATREMIA**

by

Nathan Tucker Romberger

Approved: _____

David G. Edwards, Ph.D.
Chair of the Department of Kinesiology and Applied Physiology

Approved: _____

William B. Farquhar, Ph.D.
Dean of the College of Health Sciences

Approved: _____

Louis F. Rossi, Ph.D.
Vice Provost for Graduate and Professional Education and
Dean of the Graduate College

I certify that I have read this dissertation and that in my opinion it meets the academic and professional standard required by the University as a dissertation for the degree of Doctor of Philosophy.

Signed:

William B. Farquhar, Ph.D.
Professor in charge of dissertation

I certify that I have read this dissertation and that in my opinion it meets the academic and professional standard required by the University as a dissertation for the degree of Doctor of Philosophy.

Signed:

Roxana G. Burciu, Ph.D.
Member of dissertation committee

I certify that I have read this dissertation and that in my opinion it meets the academic and professional standard required by the University as a dissertation for the degree of Doctor of Philosophy.

Signed:

Megan M. Wenner, Ph.D.
Member of dissertation committee

I certify that I have read this dissertation and that in my opinion it meets the academic and professional standard required by the University as a dissertation for the degree of Doctor of Philosophy.

Signed:

Joseph M. Stock, Ph.D.
Member of dissertation committee

ACKNOWLEDGMENTS

First and most importantly, I thank God for His continued faithfulness. I would not have reached this point without God's grace and mercy. Ephesians 2:8-9 says, "For by grace you have been saved through faith. And this is not your own doing; it is the gift of God, not a result of works so that no one may boast." I have been saved by grace through faith in Jesus' death and resurrection, and God's grace continues to sustain me. I commit this work entirely to God, for His glory and honor.

I am grateful to my advisor, Dr. William Farquhar, for bringing me into his lab and for the many opportunities he has provided for me to develop as a scientist over the past four years. He has been a great mentor, providing me with research guidance and encouragement to pursue additional projects and opportunities to further my career. Dr. Farquhar has also served as an excellent model of how to be a humble, thoughtful leader. I am also grateful to all the scientists who have served on my dissertation committee, helping to greatly enhance this project. I am thankful for the many hours Dr. Burciu has committed to helping me learn how to analyze the fMRI data for my dissertation. I am thankful to Dr. Wenner for her overall mentorship and specifically

her guidance in considering the effects of biological sex and sex hormones in my research. I am thankful to Dr. Stocker for lending his expertise and insight to help us contextualize and interpret our results. I am grateful for Dr. Stock's continuous support throughout my time here and his eagerness to serve on this committee.

I am thankful for my former lab mates, Dr. Joseph Stock and Dr. Ronald McMillan. I thoroughly enjoyed working together, and I appreciate all their assistance, including teaching me lab techniques, helping with data collection, answering any questions I had, and reading drafts of manuscripts, abstracts, and grant applications. Thank you for your mentorship and support in and out of the research lab. I am also thankful for the assistance of Dr. Virginia Nuckols, who helped finish data collection for my project and provided constructive feedback to improve this document. I am thankful to Liza Walker for her assistance with the administrative side of research and the other KAAP faculty, staff, and students who have supported me throughout my time as a PhD student.

I am also thankful for several individuals who provided technical support for my dissertation research. I am grateful to Wendy Nichols for her assistance with IV placements, infusions, and blood draws for this study as well as ensuring the safety of our participants. I am thankful for the staff at the NMPCC for their assistance with screening participants. I am grateful for the assistance of several members of CBBI, including Ibrahim Malik, Sarah Whitman, and Trevor Wigal for their technical

support. I am also thankful to Seran Kahyaoglu for her assistance with blood processing.

I am grateful for my undergraduate mentors, Dr. Scott Kieffer and Dr. Doug Miller, and their encouragement to pursue my interest in research. I am grateful for their professional and spiritual mentorship, the many research opportunities they provided me, and encouraging me to come to the University of Delaware.

Finally, I am grateful for the support of my family and friends. I am thankful to my family for providing the opportunity for me to pursue higher education and for encouraging me and walking/praying with me throughout this experience. I am also thankful for all the friends I have met since starting graduate school through church and Bible study for their encouragement and prayers. I am especially thankful for my wonderful fiancée, Emily, for supporting me and praying with me throughout this process. I could not have finished without all your support and prayers.

TABLE OF CONTENTS

LIST OF TABLES	x
LIST OF FIGURES	xi
ABSTRACT	xvii

Chapter

1	REVIEW OF THE LITERATURE	1
1.1	Hypertension, Cardiovascular Disease, and Dietary Salt Intake in Men and Women	1
1.1.1	Hypertension and Cardiovascular Disease in Men and Women	1
1.1.2	Salt Consumption, Hypertension, and Cardiovascular Disease	2
1.2	Salt Sensitivity of Blood Pressure	2
1.2.1	Prevalence and Clinical Significance of Salt Sensitivity	2
1.2.2	Mechanisms of Salt Sensitivity	8
1.2.2.1	Vascular Responses	8
1.2.2.2	Immune System Responses	10
1.2.2.3	Renal Responses	12
1.2.2.4	Neural Responses	14
1.3	Central Sodium Sensing: Implications for Fluid Balance and Blood Pressure Regulation	18
1.3.1	Central Sodium Sensing	18
1.3.2	Implications for Fluid Balance	22
1.3.3	Implications for Blood Pressure Regulation.....	24
1.3.4	Sex Differences	26
1.3.5	Translational Research in Humans.....	28

1.4	Blood Oxygenation Level Dependent Functional Magnetic Resonance Imaging (BOLD fMRI)	33
1.4.1	Introduction to MRI.....	33
1.4.2	Introduction to BOLD fMRI	34
1.4.3	Resting-State fMRI.....	40
1.5	Summary.....	45
2	SEX DIFFERENCES IN THE ACTIVATION OF SALT SENSING BRAIN REGIONS DURING ACUTE HYPERNATREMIA	48
2.1	Introduction	48
2.2	Methods	52
2.2.1	Subjects.....	52
2.2.2	Experimental Protocol	53
2.2.3	MRI Acquisition.....	55
2.2.4	MRI Analysis.....	56
2.2.5	Statistical Analysis	60
2.3	Results	61
2.3.1	Participant Characteristics	61
2.3.2	Blood Pressure, Thirst, and Biochemical Data Pre- and Post-Infusion.....	61
2.3.3	Head Motion.....	63
2.3.4	Functional Connectivity	63
2.3.5	fALFF.....	65
2.3.6	Correlations	66
2.4	Discussion.....	67
2.5	Conclusion.....	75
3	SEX DIFFERENCES IN THE ACTIVATION OF SYMPATHOREGULATORY BRAIN REGIONS DURING ACUTE HYPERNATREMIA	95
3.1	Introduction	95
3.2	Methods	99
3.2.1	Subjects.....	99
3.2.2	Experimental Protocol	100
3.2.3	MRI Acquisition.....	103

3.2.4	MRI Analysis.....	103
3.2.5	Statistical Analysis	106
3.3	Results	107
3.3.1	Participant Characteristics	107
3.3.2	Blood Pressure, Thirst, and Biochemical Data Pre- and Post- Infusion.....	107
3.3.3	Head Motion.....	109
3.3.4	Functional Connectivity	109
3.3.5	fALFF.....	110
3.3.6	Correlations	111
3.4	Discussion.....	112
3.5	Conclusion.....	119
4	DISSERTATION CONCLUSIONS	134
4.1	Summary.....	134
4.2	Perspectives and Future Directions	136
	REFERENCES.....	137
Appendix		
A	IRB APPROVAL LETTER	158
B	BIORENDER PUBLICATION LICENSE	159

LIST OF TABLES

Table 1	Participant screening characteristics.....	77
Table 2	Blood pressure, thirst, and biochemical data pre- and post-hypertonic saline infusion.....	78
Table 3	Serum sex hormone concentrations on the day of the MRI and infusion visit.	79
Table 4	MNI coordinates for sympathoregulatory brain regions.	120

LIST OF FIGURES

- Figure 1 Experimental design. Participants completed 3 visits, including 1) an informed consent and preliminary MRI screening, 2) a physical screening at the nurse managed primary care center (NMPCC), and 3) the MRI and hypertonic saline (3% NaCl) infusion data collection. All women completed the MRI and infusion visit within the first 12 days of their menstrual cycle. MRI, magnetic resonance imaging. 80
- Figure 2 MRI and hypertonic saline infusion protocol. Participants provided a spot urine sample at baseline to assess urine specific gravity (USG), and a human chorionic gonadotropin (HCG) pregnancy test was performed for all women. Baseline blood pressure (BP), thirst, and blood samples were also obtained. Participants underwent a T1-weighted anatomical scan and BOLD fMRI scan at baseline, followed by a 30-minute BOLD fMRI scan during an IV hypertonic saline infusion. BP, thirst, and blood samples were obtained following the infusion. BOLD fMRI, blood oxygen level dependent functional magnetic resonance imaging; BP, blood pressure; IV, intravenous. 80
- Figure 3 Regions of interest for the resting state fMRI analysis: regions of interest involved in salt sensing and thirst (A) and control regions of interest (B). The name of each brain region is in the upper left with the slice position indicated in the lower left. ACC, anterior cingulate cortex; fMRI, functional magnetic resonance imaging; L, left; M1, primary motor cortex; OVLT, organum vasculosum of the lamina terminalis; PCC, posterior cingulate cortex; R, right; SFO, subfornical organ. 81
- Figure 4 Plasma AVP increases pre- to post-infusion. Data are presented as mean \pm standard deviation. * $p < 0.05$ pre- vs post-infusion. ART, aligned rank transformation; AVP, arginine vasopressin; RM ANOVA, repeated measures analysis of variance. 82

Figure 5	Average TR-to-TR head motion during baseline and the late phase (15-30 minutes) of the hypertonic saline infusion. Head motion was minimal (<0.20 mm) in all participants and there were no significant differences between the phases or sexes. The average response for men is represented by the blue solid squares/line; the average response for women is represented as the red open circles/line. Individual subject responses are shown as blue (men) or red (women) dashed lines. ART, aligned rank transformation; RM ANOVA, repeated measures analysis of variance.	83
Figure 6	Functional connectivity between the subfornical organ (SFO) and organum vasculosum of the lamina terminalis (OVLT). There is a significant phase*sex interaction and post-hoc testing reveals that functional connectivity increased in men (p=0.043) but decreased in women (p=0.004) from baseline to the late phase of the infusion. Data are presented as mean ± standard deviation. RM ANOVA, repeated measures analysis of variance.	84
Figure 7	Functional connectivity between the subfornical organ (SFO) and additional regions of interest including the left (L) and right (R) anterior cingulate cortex (ACC) (A & B), sensory thalamus (C), and L and R insula (D & E). Data are presented as mean ± standard deviation. *p<0.05 for baseline vs late phase. ART, aligned rank transformation; RM ANOVA, repeated measures analysis of variance..	85
Figure 8	Functional connectivity between the organum vasculosum of the lamina terminalis (OVLT) and additional cortical or subcortical regions of interest, including the left (L) and right (R) anterior cingulate cortex (ACC) (A & B), sensory thalamus (C), and L and R insula (D & E). Data are presented as mean ± standard deviation. ART, aligned rank transformation; RM ANOVA, repeated measures analysis of variance.	86
Figure 9	Functional connectivity between the CVOs and our control regions of interest, including the subfornical organ (SFO) with the left (L) and right (R) PCC (A & B) and L and R M1 hand area (C & D), as well as the organum vasculosum of the lamina terminalis (OVLT) with the L and R PCC (E & F) and L and R M1 hand area (G & H). Data are presented as mean ± standard deviation. CVOs, circumventricular organs; M1, primary motor cortex; PCC, posterior cingulate cortex; RM ANOVA, repeated measures analysis of variance.	87

Figure 10	Fractional amplitude of low frequency fluctuations (fALFF) of the subfornical organ (SFO) (A) and organum vasculosum of the lamina terminalis (OVLT) (B). Data are presented as mean \pm standard deviation. * $p < 0.001$ for baseline vs late phase. ART, aligned rank transformation; RM ANOVA, repeated measures analysis of variance..	88
Figure 11	Fractional amplitude of low frequency fluctuations (fALFF) of additional regions of interest. fALFF was calculated for the left (L) and right (R) anterior cingulate cortex (ACC) (A & B), sensory thalamus (C), and L and R insula (D & E). Data are presented as mean \pm standard deviation. * $p < 0.001$ for baseline vs late phase. ART, aligned rank transformation; RM ANOVA, repeated measures analysis of variance.	89
Figure 12	Fractional amplitude of low frequency fluctuations (fALFF) of control regions of interest, including the left (L) and right (R) PCC (A & B) and L and R M1 hand area (C & D). Data are presented as mean \pm standard deviation. * $p < 0.005$ for baseline vs late phase. ART, aligned rank transformation; M1, primary motor cortex; PCC, posterior cingulate cortex; RM ANOVA, repeated measures analysis of variance.....	90
Figure 13	Correlations between serum testosterone and the change in SFO-OVLT functional connectivity with acute relative hypernatremia. Results are presented for the entire cohort (A) and for men separately (B). Blue closed squares represent men; red open circles represent women. OVLT, organum vasculosum of the lamina terminalis; SFO, subfornical organ. Pearson (r) or Spearman's (ρ) correlations were calculated.	91
Figure 14	Correlations between baseline SFO-OVLT functional connectivity and the day of the menstrual cycle on which women were tested (A), serum estradiol (B), and serum progesterone (C) in women. Pearson (r) or Spearman's correlations (ρ) were calculated. E2, estradiol; OVLT, organum vasculosum of the lamina terminalis; SFO, subfornical organ.	92
Figure 15	Correlations between age and the change in functional connectivity between the subfornical organ (SFO) and organum vasculosum of the lamina terminalis (OVLT) in the entire cohort (A), women alone (B), and men alone (C). Blue closed squares represent men; red open circles represent women. Pearson correlations (r) were used.....	93

Figure 16	Correlations between the change in thirst and the change in fALFF in the right and left PCC (A & B) and in the left ACC (C). Blue closed squares represent men; red open circles represent women. ACC, anterior cingulate cortex; fALFF, fractional amplitude of low frequency fluctuations; L, left; PCC, posterior cingulate cortex; R, right. Spearman's correlations (ρ) were calculated.	94
Figure 17	Schematic representing how salt sensing in the SFO and OVLT affects the activity of several hypothalamic and medullary nuclei. The CVOs project to the SON and PVN of the hypothalamus. The SON primarily regulates the release of AVP from the posterior pituitary gland, while the PVN is largely responsible for regulating sympathetic outflow. The PVN has excitatory projections to the RVLM, the primary driver of sympathetic outflow. However, this response is modulated by the baroreceptor reflex as the NTS sends excitatory projections to the CVLM, which tonically inhibits the RVLM. Figure created in Biorender. AVP, arginine vasopressin; CVLM, caudal ventrolateral medulla; CVOs, circumventricular organs; NTS, nucleus tractus solitarius; OVLT, organum vasculosum of the lamina terminalis; PVN, paraventricular nucleus of the hypothalamus; RVLM, rostral ventrolateral medulla; SFO, subfornical organ; SNA, sympathetic nerve activity; SON, supraoptic nucleus of the hypothalamus.....	121
Figure 18	Regions of interest (ROIs) for the resting-state fMRI analysis. The name of each brain region is in the upper left with the slice location indicated in the lower left. The ROIs for the brainstem nuclei (CVLM, NTS, and RVLM) are depicted on the right side only since the ROIs on the left side are symmetrical. CVLM, caudal ventrolateral medulla; L, left; NTS, nucleus tractus solitarius; PVN, paraventricular nucleus of the hypothalamus; R, right; RVLM, rostral ventrolateral medulla; SON, supraoptic nucleus of the hypothalamus.....	122
Figure 19	Functional connectivity of the subfornical organ (SFO) with the left and right CVLM (A-B), NTS (C-D), and RVLM (E-F). Data are presented as mean \pm standard deviation. * $p < 0.05$ for baseline vs late phase. ART, aligned rank transformation; CVLM, caudal ventrolateral medulla; FC, functional connectivity; L, left; NTS, nucleus tractus solitarius; RM ANOVA, repeated measures analysis of variance; R, right; RVLM, rostral ventrolateral medulla.....	123

Figure 20	<p>Functional connectivity of the organum vasculosum of the lamina terminalis (OVLT) with the left and right CVLM (A-B), NTS (C-D), and RVLM (E-F). Data are presented as mean \pm standard deviation. ART, aligned rank transformation; CVLM, caudal ventrolateral medulla; FC, functional connectivity; L, left; NTS, nucleus tractus solitarius; R, right; RM ANOVA, repeated measures analysis of variance; RVLM, rostral ventrolateral medulla.....</p>	124
Figure 21	<p>Functional connectivity of the RVLM bilaterally. Data are presented as mean \pm standard deviation. L, left; R, right; RM ANOVA, repeated measures analysis of variance; RVLM, rostral ventrolateral medulla. .</p>	125
Figure 22	<p>Functional connectivity of the RVLM with the CVLM (A-B) and NTS (C-D). Data are presented as mean \pm standard deviation. *$p < 0.001$ for baseline vs late phase. ART, aligned rank transformation; CVLM, caudal ventrolateral medulla; FC, functional connectivity; L, left; NTS, nucleus tractus solitarius; R, right; RM ANOVA, repeated measures analysis of variance; RVLM, rostral ventrolateral medulla. .</p>	126
Figure 23	<p>Functional connectivity of the subfornical organ (SFO) with the PVN (A) and SON (B). Data are presented as mean \pm standard deviation. ART, aligned rank transformation; PVN, paraventricular nucleus of the hypothalamus; RM ANOVA, repeated measures analysis of variance; SON, supraoptic nucleus of the hypothalamus.....</p>	127
Figure 24	<p>Functional connectivity of the organum vasculosum of the lamina terminalis (OVLT) with the PVN (A) and SON (B). Data are presented as mean \pm standard deviation. PVN, paraventricular nucleus of the hypothalamus; RM ANOVA, repeated measures analysis of variance; SON, supraoptic nucleus of the hypothalamus.....</p>	127
Figure 25	<p>Functional connectivity of the PVN with the left and right CVLM (A-B), NTS (C-D), and RVLM (E-F). Data are presented as mean \pm standard deviation. ART, aligned rank transformation; CVLM, caudal ventrolateral medulla; FC, functional connectivity; L, left; NTS, nucleus tractus solitarius; PVN, paraventricular nucleus of the hypothalamus; R, right; RM ANOVA, repeated measures analysis of variance; RVLM, rostral ventrolateral medulla.....</p>	128

Figure 26	Fractional amplitude of low frequency fluctuations (fALFF) of the left and right CVLM (A-B), NTS (C-D), and RVLM (E-F). Data are displayed as mean \pm standard deviation. * $p < 0.001$ for baseline vs late phase. ART, aligned rank transformation; CVLM, caudal ventrolateral medulla; L, left; NTS, nucleus tractus solitarius; R, right; RM ANOVA, repeated measures analysis of variance; RVLM, rostral ventrolateral medulla.	129
Figure 27	Fractional amplitude of low frequency fluctuations (fALFF) of the PVN (A) and SON (B). Data are displayed as mean \pm standard deviation. * $p < 0.001$ for baseline vs late phase. ART, aligned rank transformation; PVN, paraventricular nucleus of the hypothalamus; RM ANOVA, repeated measures analysis of variance; SON, supraoptic nucleus of the hypothalamus.....	130
Figure 28	Correlations between serum progesterone and baseline fALFF in the right CVLM (A & B), left NTS (C & D), and left RVLM (E-F). Correlations are displayed for the entire cohort (left) and in only women (right). Women are red open circles; men are blue closed squares. CVLM, caudal ventrolateral medulla; fALFF, fractional amplitude of low frequency fluctuations; L, left; NTS, nucleus tractus solitarius; R, right; RVLM, rostral ventrolateral medulla. Pearson correlations (r) or Spearman's correlations (ρ) were used depending on whether the data were normally distributed.	131
Figure 29	Correlations between change in SBP pre- to post-infusion and change in fALFF in the SON from baseline to the late phase of the infusion. Correlations are presented in the entire cohort (A), in men only (B), and in women only (C). Women are red open circles; men are blue closed squares. fALFF, fractional amplitude of low frequency fluctuations; SBP, systolic blood pressure; SON, supraoptic nucleus of the hypothalamus. Pearson correlations (r) or Spearman's correlations (ρ) were used depending on whether the data were normally distributed.	132
Figure 30	The change in functional connectivity between the left RVLM and left NTS was positively correlated with the change in fALFF in the PVN (A) and in the left RVLM (B). Women are red open circles; men are blue closed squares. fALFF, fractional amplitude of low frequency fluctuations; L, left; NTS, nucleus tractus solitarius; PVN, paraventricular nucleus of the hypothalamus; RVLM, rostral ventrolateral medulla. Spearman's correlations (ρ) were used.	133

ABSTRACT

Central salt sensing in the circumventricular organs (CVOs) is critical in regulating neurohormonal responses to acute relative hypernatremia as occurs with high dietary salt intake. The CVOs, including the organum vasculosum lamina terminalis (OVLT) and subfornical organ (SFO), are capable of sensing changes in the salt concentration in the blood and mediate salt-induced changes in sympathetic nerve activity (SNA), vasopressin (AVP), thirst, and blood pressure (BP). Central salt sensing is also associated with the development of salt sensitive hypertension in rodents. Studies in humans demonstrate that acute relative hypernatremia alters the activity or functional connectivity of the CVOs. However, no studies have investigated whether there are sex differences in central neural activation during acute hypernatremia in humans, which could underly sex differences in neurohumoral responses to salt loading. Therefore, the purpose of this study was to investigate whether there are sex differences in the activation patterns of salt sensing and sympathoregulatory brain regions during acute hypernatremia. Thirty-two young healthy adults (17 men/15 women) underwent blood oxygenation level dependent (BOLD) functional magnetic resonance imaging (fMRI) at rest and during a 30-minute intravenous (IV) hypertonic saline infusion (3% NaCl). Women were not using hormonal contraception and were

tested during the follicular menstrual cycle phase. We calculated fractional amplitude of low frequency fluctuations (fALFF), which reflects the intensity of the spontaneous fluctuations in the BOLD signal in each brain region, and functional connectivity, which reflects the synchronization of low frequency fluctuations in the BOLD signal between our regions of interest. We hypothesized that acute hypernatremia would increase the fALFF in and functional connectivity between brain regions involved in sensing salt and increasing sympathetic outflow, while decreasing in nuclei that inhibit sympathetic outflow. We also hypothesized that these responses would be heightened in men. The main findings of this study were that acute relative hypernatremia increased fALFF in several brain regions associated with salt sensing and thirst, including the SFO, OVLT, anterior cingulate cortex (ACC), posterior cingulate cortex (PCC), insula, and thalamus, and in several sympathoregulatory brain regions, including the paraventricular nucleus (PVN), supraoptic nucleus (SON), rostral ventrolateral medulla (RVLM), nucleus tractus solitarius (NTS), and caudal ventrolateral medulla (CVLM). Overall, changes in fALFF were similar between men and women. This is consistent with the changes observed for serum sodium, thirst, SBP, and plasma AVP, all of which increased to a similar extent between the sexes. However, functional connectivity between the SFO and OVLT increased in men but decreased in women, indicating a sex-specific response. Interestingly, serum testosterone was positively correlated with the change in SFO-OVLT functional connectivity in men and women combined, suggesting that testosterone may impact this response. Collectively, these results demonstrate that, in response to acute relative

hypernatremia, these salt sensing and sympathoregulatory brain regions are activated similarly in both men and women tested during the follicular menstrual cycle phase (as assessed by fALFF); however, men seem to have a more synchronized neural response between the SFO and OVLT (as assessed via functional connectivity). This suggests that these regions are more tightly coupled in their neural response to acute hypernatremia in men. These findings set the stage for additional studies to investigate mechanisms of central salt sensing in humans, central salt sensing in the context of chronic salt loading, and sex differences across the lifespan.

Chapter 1

REVIEW OF THE LITERATURE

1.1 Hypertension, Cardiovascular Disease, and Dietary Salt Intake in Men and Women

1.1.1 Hypertension and Cardiovascular Disease in Men and Women

High blood pressure (BP) is one of the primary risk factors for a myriad of cardiovascular diseases including coronary heart disease, heart failure, and stroke (1, 2). This is of primary public health concern since about 120 million adults over 20 years old have high BP, equaling about 50% of the total United States population (1). Thus, BP-related diseases remain among the leading causes of morbidity and mortality (1, 3, 4). While high BP and BP-related diseases affect both men and women, hypertension affects men and women disproportionately across the lifespan. Men have a higher prevalence of hypertension compared to women until about the age of 65 after which women have a higher prevalence of hypertension. This shift reflects a greater age-related increase in BP in women after menopause, which is associated with the loss of the cardioprotective effects of female sex hormones (1, 5).

1.1.2 Salt Consumption, Hypertension, and Cardiovascular Disease

High dietary salt intake is associated with the pathogenesis of hypertension as well as numerous BP-dependent and -independent health effects, including effects on the heart, kidneys, vasculature, and brain (3, 6). Additionally, substantial evidence points to a relation between dietary salt intake (assessed directly by diet or indirectly via urinary sodium excretion) and BP (7–11), and reducing salt intake has been shown to significantly decrease BP in several large dietary studies (1, 12–14). Thus, most public health organizations encourage Americans to reduce dietary salt intake for its general BP-lowering effect (3, 15, 16).

1.2 Salt Sensitivity of Blood Pressure

1.2.1 Prevalence and Clinical Significance of Salt Sensitivity

While increasing dietary salt intake is generally associated with increased BP, BP responses to salt loading display substantial heterogeneity (17, 18). Approximately 25–50% of normotensive adults and 40–75% of hypertensive adults are typically classified as salt sensitive (SS), meaning BP is higher with salt loading compared to salt restriction, while the remainder are typically classified as salt resistant (SR), meaning BP is not elevated with salt loading compared to salt restriction (17, 19, 20). While traditionally the field has dichotomized participants as being either SR or SS, there is evidence that some individuals are inverse salt sensitive, or “counter-regulators,”

defined as those who have a paradoxical increase in BP on a low sodium diet or a decrease in BP on a high sodium diet. Across various groups, it appears that about 10-15% of the population exhibits inverse salt sensitivity (18, 21–24).

Variability in the prevalence of SS identified in previous studies likely results from differences in the salt loading or restriction protocol, the BP assessment technique, and/or the cutoff used to define SS BP (17, 19, 20). For example, some experiments utilize a rapid volume expansion/contraction protocol in which participants receive an intravenous (IV) saline infusion followed by a low salt diet and furosemide (17, 19). Other experiments use dietary protocols to characterize SS BP, measuring change in BP between low and high salt diets (19). In these dietary experiments, salt intake on both the low and high salt diets is highly variable across studies with salt intake on the high salt diet generally ranging from 100 to 300 mmol sodium/day (~2300 – 6900 mg sodium/day) and salt intake on the low salt diet ranging from 9 to 50 mmol sodium/day (~200 – 1150 mg sodium/day) (25). The arbitrary cutoff used to define SS BP also displays considerable variability across studies (19, 26). Some experiments utilize cutoffs based on percent changes in BP (e.g., a change in MAP > 5% in normotensive adults and a change in MAP > 10% in hypertensive adults) (27), while other studies use cutoffs based on absolute changes in BP (e.g., a change in MAP > 5 mmHg) (18, 28).

Given the variability in the methods used to assess SS BP, the reproducibility of SS BP has been questioned. A few studies have investigated the reproducibility of the rapid volume expansion/contraction protocol. For example, in 19 participants who completed this rapid protocol twice, Strazzullo et al. found a significant positive correlation between the BP responses with repeated testing ($\rho = 0.60$) (29).

Additionally, when performed twice within one year, Weinberger and Fineberg found a similar significant positive correlation between the change in MAP upon repeating this protocol ($r = 0.56$) (30). However, upon further examination of the study by Weinberger and Fineberg (30), it was demonstrated that four of the 28 subjects switched from SR to SS or vice versa upon repeated testing (25), and about half of the participants initially categorized as SS were classified as SR or “indeterminate” upon repeated testing, indicating poor reproducibility (28). A few experiments have also attempted to compare SS classification using a rapid volume expansion/contraction protocol to a dietary protocol. Looking across several studies, ~65-75% of participants were classified the same with both protocols (28). Thus, at an individual subject level, the ability to predict the BP response to a dietary protocol based on the BP response to a rapid IV protocol appears limited (31).

While rapid IV protocols for determining SS BP may have limited accuracy and reproducibility, “preferred” dietary protocols are generally thought to have better reproducibility. In a methodological review by Kurtz et al., the reproducibility of classifying participants as SS was reported as >90% when particular dietary protocol

characteristics (e.g., 1-week of low salt intake <50 mmol/d and high salt intake ~250 mmol/d) were utilized (28). For example, in a group of healthy men who underwent two dietary protocols to classify SS BP, Sharma et al. found good reproducibility in classifying participants as SS or SR as only one out of fifteen participants changed classifications upon repeated testing (32). In another study of 31 white, non-obese adults, Overlack et al. found that the BP response to the change in dietary salt intake differed in only 3 participants upon retesting; interestingly, this study classified participants as either SS, SR, or “counter-regulators” (i.e., inverse salt sensitive), suggesting that inverse salt sensitivity may also be a reproducible phenomenon (23). Draaijer et al. also found excellent reproducibility of SS testing in ten men with borderline hypertension as all participants were classified the same with repeated testing (33). Additionally, in a study by Gu et al., 450 Chinese adults completed a dietary protocol consisting of 7-day low salt and high salt diets twice, separated by about 4.5 years. The investigators found that these individuals’ BP responses were reproducible over this 4.5-year period (34). While some studies do not demonstrate good reproducibility of SS BP classifications with dietary protocols (35), it appears that SS testing can be reproducible when particular dietary protocol characteristics are followed (28).

The prevalence of SS also varies with demographic characteristics. Indeed, the factors associated with age-related increases in BP differ based on race and sex (36). Black adults tend to have a greater prevalence of SS than white adults (8, 37), and older

adults tend to be more SS than younger adults (30). Additionally, several studies suggest that women may be more SS than men across the lifespan (5, 19, 38–40). In fact, greater SS in women persists when stratifying participants based on hypertensive status or age (41). However, this apparent sex difference in the prevalence of SS BP is not without controversy as women are not more SS than men across all studies (42), and most dietary studies provide men and women with diets containing the same absolute sodium content without considering differences in sodium density associated with sex differences in caloric intake (8, 43). This is an important consideration since the association between absolute dietary sodium intake and BP varies with caloric intake such that those with lower caloric intake have larger changes in BP with increasing sodium intake (44). Thus, additional experiments should be conducted to determine whether this sex difference in SS BP is more a result of biological sex, sex hormones, or differences in caloric intake/sodium density between men and women.

The apparent sex difference in SS BP in humans also differs from what is seen in several animal models, since in several rodent models, male animals are more SS than female animals (5). First, in Dahl salt-sensitive rats, BP while consuming a high sodium diet is higher in male and ovariectomized female rats compared to non-ovariectomized female rats, suggesting a protective role of female sex hormones (45). Additionally, while ovariectomy exaggerates the change in BP in female animals, castration attenuates the increase in BP in male animals with high salt intake, suggesting that this sex difference is at least partially mediated by differences in male

and female sex hormones (46). Second, in the deoxycorticosterone acetate (DOCA)-salt hypertensive model, male animals have larger increases in BP than female animals (47). Third, male rats have larger increases in BP than female rats with chronic 28-day aldosterone/salt treatment (48). Lastly, although not a directly salt-sensitive model, male mice have greater increases in BP in response to chronic subcutaneous infusion of angiotensin II compared to female mice (49), and central infusion of an androgen receptor antagonist reduces the pressor response to angiotensin II in male animals (50). Adding to the complexity of understanding this apparent discrepancy between the rodent and human literature regarding sex differences, most intervention studies in rodent models are longer relative to their total lifespan (51, 52) compared to studies in humans, and the changes in BP observed in rodent models are typically larger than those seen in humans. Additional work is required to understand the apparent discrepancy between the rodent and human literature regarding sex differences in the prevalence and magnitude of SS BP.

Regardless of sex differences, SS BP has important clinical implications. SS BP has been identified as a cardiovascular risk factor (53) and is associated with an increased risk of mortality, independent of high BP (54, 55). Additionally, SS BP is associated with the development of hypertension (8, 19, 56). In fact, there is a J-shaped relation between the change in systolic BP with sodium loading and the development of hypertension, meaning that those with either large increases or decreases in BP with sodium loading have an increased incidence of hypertension (57). Thus, understanding

SS, whether there are sex differences, and its underlying physiological mechanisms is of utmost public health importance.

1.2.2 Mechanisms of Salt Sensitivity

The etiology of SS is multifactorial and involves several distinct yet overlapping physiological mechanisms. The effects of sodium on several systems, mechanisms underlying SS BP, and possible sex differences are explored below. This review highlights vascular, immune system, renal, and neural responses that may contribute to sodium-induced increases in BP.

1.2.2.1 Vascular Responses

High dietary sodium intake is associated with vascular dysfunction. First, elevated sodium intake decreases flow-mediated dilation (FMD), a measure of endothelial macrovascular function (58), and impairs cutaneous microvascular function assessed by measuring cutaneous vasodilation via Laser Doppler flowmetry (59). Second, high sodium intake is associated with increased arterial stiffness in both humans and animal models (60). Third, SS hypertension is associated with reduced large vessel compliance (8). Indeed, arterial compliance increases in inverse salt sensitive adults, decreases in SS adults, and changes minimally in SR adults while consuming a high sodium diet (61). Fourth, SS adults have impaired reductions in systemic vascular resistance with sodium loading compared to SR adults (62).

There are several mechanisms that might drive vascular dysfunction with sodium loading. These include differences in nitric oxide (NO) bioavailability, soluble guanylate cyclase signaling in vascular smooth muscle, sympathetic nerve activity (SNA), and various paracrine hormones (19). In support of an oxidative stress-related mechanism, local infusion of ascorbic acid, a nonspecific scavenger of reactive oxygen species (ROS); Tempol, a mimetic of superoxide dismutase which scavenges superoxide; or apocynin, which inhibits NADPH oxidase, each restore the impairment in cutaneous vasodilation associated with high salt intake (59). To further support this mechanism, free isoprostanes are elevated following sodium loading, and the excretion of NO metabolites is lower in SS hypertension (25), suggesting that decreased NO bioavailability and oxidative stress may play a role in SS hypertension.

Sodium loading may also impact the vasculature by altering adrenergic receptor activity. Specifically, in normotensive adults, high sodium intake upregulates α 2-adrenergic receptors and downregulates β 2-adrenergic receptors. Additionally, SS adults have fewer β 2-adrenergic receptors, and the number of β 2-adrenergic receptors correlates with the change in BP seen with changing sodium intake (8). Moreover, pressor responses to norepinephrine are larger in SS adults indicating that augmented vascular reactivity may contribute to SS BP (25).

There may also be sex differences in some of the above mechanisms. While consuming a high sodium diet decreases FMD in both men and women, men have a

lower FMD with high sodium intake compared to women, suggesting that women may be slightly protected from sodium-induced vascular dysfunction (6, 63). In another study, sex differences in the effects of sodium on NO-dependent vasodilation were assessed by measuring forearm blood flow in response to brachial artery administration of acetylcholine (ACh) with and without endothelial NO synthase (eNOS) inhibition by N^G-monomethyl-L-arginine. Although dietary sodium intake did not change the vasodilator response to ACh in men or women, there was less of a reduction in vasodilation with eNOS inhibition during the high sodium diet only in men, suggesting that the NO-dependent component of ACh-elicited vasodilation is lower after high sodium intake in men but not women (64). Additionally, young women have greater vascular β -adrenergic receptor function (65), which may contribute to the relative protection against the development of hypertension seen in young women.

1.2.2.2 Immune System Responses

The immune system and inflammatory responses to high sodium intake also play a significant role in determining BP responses to changes in sodium consumption (19). For instance, high sodium consumption increases the number of immune cells in the kidney in Dahl SS rats but not in SR rat strains, such as Sprague Dawley and SSBN13 rats (19, 66). Additionally, mutant Dahl SS rats with almost complete depletion of CD3⁺ T cells demonstrate reduced kidney damage and lower BP while consuming a high sodium diet compared to controls (67). Moreover, splenocyte transfer from Dahl

SS rats to Dahl SS rats deficient in T cells, causes BP to increase in T-cell deficient rats while the animals were fed a low sodium diet. Splenocyte transfer also causes exaggerated increases in BP with high sodium intake (19, 68). Furthermore, in male mice without lymphocytes due to a genetic deficiency, angiotensin II infusion produces less of an increase in BP compared to wild type mice, and adding back T-cells from a donor animal restores the pressor effects of angiotensin II (65). Lastly, CD8⁺ T cells increase the expression of the NaCl cotransporter in the distal convoluted tubule to elicit sodium reabsorption and a SS BP response (19, 69).

There may also be sex differences in immune responses associated with SS BP. For instance, there is an increase in proinflammatory T cells with DOCA-salt treatment in both male and female animals; however, female animals have a greater amount of T regulatory cells, which have anti-inflammatory properties and are linked with lower BP in female rats. Furthermore, decreasing T regulatory cells with anti-CD25 increases BP in female animals, eliminating the apparent sex difference (47).

Moreover, transfer of wild type male T-cells to intact female mice lacking lymphocytes produces a smaller pressor response to angiotensin II infusion compared to transfer to male mice lacking lymphocytes; and when T-cells from wild type female mice are given to male mice lacking lymphocytes, the pressor response to angiotensin II is reduced compared to when T-cells are donated from male mice (65).

1.2.2.3 Renal Responses

Salt sensitivity of BP has been historically linked to renal dysfunction, such that SS BP is hypothesized to be caused by an inability of the kidneys to adequately increase sodium excretion (8, 19). Indeed, chronic kidney disease, which involves altered renal sodium handling, is associated with SS hypertension (60, 70, 71). Additionally, SS animals and humans have fewer nephrons and a reduced glomerular surface area, which may impact their ability to attain sodium balance (8). Furthermore, in Dahl SS rats, natriuresis in response to increasing renal perfusion pressure is reduced compared to SR rats (19). Moreover, in black SS adults renal blood flow decreases when consuming a high sodium diet, while in SR adults, renal blood flow increases (8).

Salt sensitivity is also associated with differences in renin angiotensin aldosterone system (RAAS) hormone activity, which affects renal function. For example, SS adults have blunted changes in renin in response to salt depletion or salt loading (25, 42). The diminished suppression of renin during salt loading results in a failure to reduce angiotensin II and aldosterone, which ultimately causes sodium retention. According to Guyton's model, the failure of the above mechanisms to increase sodium excretion to counteract the elevated sodium intake results in an increase in BP to maintain normal sodium balance (25). In addition to RAAS hormones, SS men have lower plasma concentrations of atrial natriuretic factor after high sodium intake, which would also result in impaired sodium excretion (8).

While several studies suggest that augmented sodium retention, leading to an increase in cardiac output, is the main contributing cause of a SS BP response (8, 19), other studies demonstrate that normotensive SS adults do not retain more sodium, nor do they display larger increases in cardiac output compared to SR counterparts while consuming a high salt diet. Rather, SS adults display blunted reductions in systemic vascular resistance with salt loading compared to SR adults (72). This is supported by data in rodents indicating that high sodium intake elicits similar sodium retention in Dahl SS and SR rats (19, 73). Collectively, these data suggest that vascular dysfunction not augmented sodium retention may account for SS BP responses in most cases (72, 73).

Regardless, there appear to be sex differences in renal sodium handling that may differ across the menstrual cycle. Male animals tend to have greater sodium reabsorption in the proximal renal tubule, while female animals tend to have greater sodium reabsorption in the distal tubule segments (5). Additionally, in women during the follicular menstrual cycle phase, high sodium intake reduces sodium reabsorption in both the proximal and distal tubules; however, in the luteal phase, high sodium intake does not reduce sodium reabsorption in the proximal tubule but elicits renal vasodilation, which is not seen in the follicular phase (74). Thus, there are sex differences in renal sodium handling and some of these responses may differ across the menstrual cycle which may suggest a role of female sex hormones.

There are also sex differences in RAAS hormone responses to sodium loading. For instance, women have less of a reduction in plasma renin activity after salt loading compared to men (42). Additionally, women have a greater BP response to infusion of angiotensin II compared to men, which may be associated with greater release of aldosterone in women. This is supported by the findings that rat zona glomerulosa cells from female animals have greater aldosterone production compared to those from male animals at rest and in response to angiotensin II (41). However, studies in rodent models indicate that male sex or male sex hormones tend to promote renin, angiotensin-converting enzyme (ACE), and angiotensin II type 1 receptor (AT₁R) activity, leading to increases in BP, while female sex is associated with greater expression of ACE2, angiotensin-(1-7), the angiotensin II type II receptor (AT₂R), and the Mas receptor, leading to lower BP (5). This is supported in part by the finding that renal expression of AT₂R is greater in female mice compared to male mice (75). Additionally, in a study in which Sprague-Dawley rats were treated with angiotensin II for 10 days, BP increased significantly in only male animals and not female animals (76). Furthermore, female mice have less angiotensin II-induced sympathetic nervous system activation since ganglionic blockade during angiotensin II infusion elicits smaller reductions in BP in female mice (46).

1.2.2.4 Neural Responses

Abnormal activity of the sympathetic nervous system may also contribute to SS BP. This may be in part because of the effects of the sympathetic nervous system on renin

release/sodium reabsorption and vascular tone (5). Studies demonstrate that the nervous system responds to both acute and chronic salt loading. Generally, acute hypernatremia (or hyperosmolality) increases SNA and BP in both rodent models (77, 78) and humans (79–82). However, changes in SNA with salt loading are region specific. Acute hypernatremia via an IV hypertonic saline infusion in Sprague-Dawley rats increases lumbar SNA but reduces splanchnic and renal SNA (83). Similarly, infusion of NaCl into the lateral ventricle of male Sprague-Dawley rats elicits increases in lumbar SNA, adrenal SNA, and BP, while renal SNA decreases, and splanchnic SNA remains unchanged. Additionally, ganglionic blockade via chlorisondamine attenuates these responses (84). Part of this response may be baroreceptor-dependent, since animals with sinoaortic denervation display earlier increases in lumbar SNA and no change in splanchnic SNA (rather than a reduction in splanchnic SNA) in response to an IV hypertonic saline infusion (83). Additionally, acute sodium loading has been shown to increase pressor responses to exercise in both male Sprague-Dawley rats (85) and humans (82). This is potentially significant because autonomic reactivity is associated with SS BP (25).

Studies also indicate that the nervous system responds to chronic salt loading. First, some but not all studies indicate that plasma catecholamines remain elevated with sodium loading in SS hypertensive adults rather than decreasing as seen in SR hypertensive adults (8, 25, 86). Second, mathematical modeling demonstrates that a neurogenic computational model can accurately characterize SS hypertension (87).

Third, feeding Dahl SS rats a high sodium diet for 3-4 weeks leads to greater discharge of NaCl-sensitive neurons in the organum vasculosum of the lamina terminalis (OVLT) compared to Dahl SS rats fed a low sodium diet or Dahl SR rats; additionally, injecting a GABA agonist to inhibit OVLT neurons elicits larger reductions in renal and splanchnic SNA and BP in Dahl SS rats fed the high salt diet compared to those fed the low salt diet or Dahl SR rats (88). Fourth, sympathetic overactivity is associated with hypertension and SS BP in rodent models. For example, elevated sympathetic activity may be associated with SS BP in C57BL6/J mice. In this model, high salt feeding increased urinary excretion of epinephrine; however, there was not an effect for norepinephrine (89). Additionally, although not a SS model, elevated sympathetic activity is associated with the increase in BP seen in the spontaneously hypertensive rat model, a common model of hypertension and cardiovascular disease (90). Fifth, sodium loading augments BP reactivity. Elevated dietary salt intake affects the responsiveness of the sympathetic nervous system to stressors such as hypernatremia, insulin, and activation of sciatic afferents (77, 91). BP reactivity may be important since autonomic reactivity is associated with SS BP (25). Despite these findings, chronic (7-day) high sodium intake increases cardiovascular baroreflex sensitivity (cBRS). This finding is unexpected since elevated cBRS is associated with a reduced risk of cardiovascular disease; however, this may reflect a protective response to maintain BP in response to dehydration, in which plasma osmolality is elevated (72).

There are also sex differences in autonomic responses to sodium loading. First, female Dahl SS rats have lower BP compared to male animals and high sodium intake augments this difference, which may be partially explained by the lower sympathetic activity observed in female animals (93). Second, DOCA salt treatment in uninephrectomized rats elicits larger increases in BP in male rats, which is associated with a greater reduction in baroreflex sensitivity in male animals (94). Third, male DOCA-salt rats have higher catecholamine concentrations in the adrenal medulla than female animals and surgical removal of the adrenal medulla lowers BP in only male animals (95). Fourth, male mice have greater sympathetic responses to RAAS hormones. For instance, male mice have larger changes in BP and sympathetic activity with angiotensin II infusion compared to female mice (49). Fifth, treatment of Sprague Dawley rats with aldosterone and salt for 28 days increases BP to a greater extent in males than in females, which is likely driven by lower sympathetic outflow in female animals (48). Lastly, estradiol acts on the rostral ventrolateral medulla (RVLM) to inhibit angiotensin II- and aldosterone-induced increases in SNA and BP (65).

While few studies in humans have evaluated the impact of biological sex on sympathetic responses to sodium loading specifically, several studies indicate that there are sex differences in neural control of BP. Resting muscle sympathetic nerve activity (MSNA) is lower in young women, and young women may have greater baroreflex function compared to men (46, 96, 97). However, MSNA increases with age, and after the age of 50, MSNA is similar in men and women, indicating a steeper

age-related increase in MSNA in women (98). Additionally, although there is a direct relation between total peripheral resistance and MSNA and an inverse relation between cardiac output and MSNA in young men; these relations are absent in young women, suggesting that there may be sex differences in neural control of BP (96). Furthermore, young women have attenuated increases in BP and MSNA during stressors such as isometric handgrip exercise, post-exercise ischemia, and postural stress (head-up tilt testing) compared to young men (99, 100). Moreover, men have larger changes in blood oxygenation level dependent (BOLD) signal in the insula, anterior cingulate cortex, amygdala, and prefrontal cortex compared to women during lower body negative pressure, which may be associated with greater sympathetic responses in men (101).

1.3 Central Sodium Sensing: Implications for Fluid Balance and Blood Pressure Regulation

1.3.1 Central Sodium Sensing

The lamina terminalis is located on the anterior wall of the third ventricle and houses the primary central osmoreceptors (77, 102). The subfornical organ (SFO) and organum vasculosum of the lamina terminalis (OVLT), two circumventricular organs (CVOs), are two of the major structures that form the lamina terminalis (77). These regions are thought to be important sodium sensors since they have an extensive vascular supply and an incomplete blood-brain barrier. Therefore, the SFO and OVLT

are exposed to changes in the cerebrospinal fluid (CSF) and blood stream (77, 102). In addition to the SFO and OVLT, the median preoptic nucleus (MnPO) is thought to act as a site of integration, where signals converge from the SFO and OVLT, since the MnPO has a more complete blood brain barrier and thus may not be well suited for sodium sensing directly (102, 103).

Several lines of experimentation support the role of the CVOs in sodium-sensing. First, *in vitro* recordings demonstrate that the discharge of OVLT neurons increases with application of either hypertonic NaCl or mannitol, and hypertonic NaCl elicits a larger response in over half of OVLT neurons (104). Second, increasing the extracellular NaCl concentration increases the activity of OVLT neurons *in vitro* in a concentration-dependent manner (105). Third, *in vivo* recordings demonstrate that OVLT cell discharge increases with intracarotid injection or intracerebroventricular infusion of NaCl or sorbitol with greater responses to hypertonic NaCl (104). Fourth, an intravenous (IV) hypertonic saline infusion in male Wistar rats elicits neuronal activation (measured by Fos-like immunoreactivity) in several regions, including the SFO and OVLT, and lesioning the SFO or anteroventral third ventricle (AV3V) region attenuates activation in the MnPO (106). Fifth, intracerebroventricular infusion of 0.3 M Na artificial CSF increases BP in Wistar rats, and electrolytic lesion of the SFO reduces this BP response by 50-70% (107). The sensitivity of the CVOs to changes in sodium concentrations in the blood (and CSF) is clinically relevant, since high sodium consumption elevates CSF sodium concentrations (105); and in humans, a single high

salt meal increases plasma sodium concentration by just over 3 mmol/L (108). In addition to being sensitive to changes in sodium concentration, the lamina terminalis is also responsive to other circulating factors, such as the hormone angiotensin II, which also has implications for BP regulation (103).

While the OVLT and SFO are clearly important for central sodium sensing, the precise molecular mechanisms of sodium sensing are less clear and there are several candidate channels that might be involved. First, the N'-terminal variant of transient receptor vanilloid potential 1 (TPRV1) channel may be responsible for sensing changes in plasma osmolality and sodium concentration in the blood. This is supported by experiments demonstrating that knocking out TPRV eliminates hyperosmolality-induced increases in neuronal discharge. However, it is not clear whether TPRV1 knockout mice display altered thirst responses to sodium loading as would be expected if TPRV1 was involved in sodium sensing (77).

Second, the epithelial sodium channel (ENaC) has also been suggested as a sodium sensing mechanism. This is in part because treatment with benzamil (a potent antagonist of ENaC) blocks sympathetic and BP responses to acute hypernatremia, attenuates AVP release, and reduces the development of hypertension in several rodent models of SS hypertension (77).

Third, the Na_x channel expressed in glial cells has been postulated as another sodium-sensing mechanism. This is supported by work showing that Na_x -knock out mice fail to develop an aversion to saline during dehydration or infusion of a hypertonic sodium solution like wild type mice. Additionally, a clinical case study of a patient with essential hypernatremia has been reported in which the patient developed autoantibodies to Na_x . Experiments suggest that the Na_x channel is expressed in astrocytes and ependymal cells in the CVOs. When plasma or CSF sodium concentrations increase, as occurs with dehydration or a high sodium diet, Na_x channels open, resulting in an increase in intracellular sodium concentration and the subsequent activation of Na/K-ATPase. To provide ATP to Na/K-ATPase, anaerobic glycolysis is promoted, producing lactate. Lactate is then metabolized in GABAergic neurons to produce ATP, which closes an ATP-sensitive potassium channel. This results in the depolarization/activation of GABAergic neurons in the CVOs (102). While there is some evidence supporting this mechanism, other studies demonstrate that Na_x -knockout mice have normal AVP release in response to dehydration and intraperitoneal injection of hypertonic saline, casting doubt on this salt sensing mechanism (109).

Lastly, the Na-K-2Cl cotransporter (NKCC2) has been suggested to be involved in central sodium sensing. Rundgren et al. demonstrated that intracerebroventricular infusion of ethacrynic acid (an NKCC2 antagonist) in goats prevented changes in free water clearance and thirst to central NaCl loading (110). Additionally, in male

Sprague Dawley rats, NKCC2 and the Slc12a1 gene (encoding NKCC2) are expressed in the supraoptic nucleus of the hypothalamus (SON) and paraventricular nucleus of the hypothalamus (PVN); and their expression is upregulated by osmotic stress. Furthermore, administration of furosemide (an NKCC2 antagonist) *in vivo* reduces arginine vasopressin (AVP) release; and knocking down the Slc12a1 gene using a lentiviral vector elicits increases in urine production and plasma osmolality, suggesting that NKCC2 may be critical in regulating osmotic stability (111). Additional experimentation is required to determine the precise molecular mechanisms of sodium sensing in the brain and translate these findings into humans.

1.3.2 Implications for Fluid Balance

In response to elevations in plasma osmolality (or serum sodium concentration) as occur with dehydration or high dietary sodium intake, the CVOs trigger the release of AVP via projections to magnocellular neurons located in the PVN and SON of the hypothalamus, resulting in antidiuresis. This process helps maintain plasma osmolality within the homeostatic range (103).

Therefore, as expected, studies in humans demonstrate that hyperosmotic stimuli, such as a hypertonic saline infusion, increase thirst and plasma AVP in both young and older adults (112). However, the sensitivity of AVP release differs between men and women. Men have a higher sensitivity of AVP release (i.e., change in plasma AVP for a given change in plasma osmolality) than women (113, 114), suggesting that male sex

hormones increase the sensitivity of AVP release (115). Additionally, AVP release may differ across the menstrual cycle. The threshold for AVP release (plasma osmolality) is lower in women during the midluteal phase compared to women during the early follicular phase and men; however, this is balanced by a lower plasma osmolality in women during the midluteal phase compared to women during the early follicular phase and men (114). The role of estradiol in modulating AVP release has been further implicated by experiments in which premenopausal women were given a gonadotropin-releasing hormone analog to suppress endogenous estradiol and progesterone and provided with estradiol add-back. Estradiol add-back resulted in a lower threshold (plasma osmolality) for AVP release in these women (116). These findings align with those of previous work in which estradiol was administered to post-menopausal women (117). While estradiol has been implicated in modulating AVP release, progesterone does not seem to impact the regulation of AVP release (118). These findings regarding sex differences in AVP release are complemented by the finding that vasopressinergic neurons are larger in young men than in young women, which has been suggested to indicate that the activity of these neurons is higher in young men (119). Additionally, as will be discussed in more detail in section 1.3.4, estrogen and androgen receptors are expressed in the brain, including in the sodium-sensing CVOs and the SON and PVN of the hypothalamus (120, 121).

1.3.3 Implications for Blood Pressure Regulation

Central sodium sensing has significant implications for BP regulation since the CVOs mediate neurohumoral responses to alterations in sodium concentration via neural projections to several additional brain regions. The SFO and OVLT send neuronal projections to parvocellular neurons in the PVN, which modulates SNA and BP through downstream projections to medullary nuclei including the RVLM (65, 77).

This is supported by numerous studies. First, lesion of the AV3V region reduces the increase in BP seen in Dahl SS rats consuming a high sodium diet (122) and Sprague-Dawley rats with an OVLT lesion demonstrate an attenuated increase in BP with DOCA-salt treatment (123). Second, injection of NaCl into the internal carotid artery to target the forebrain vascular system increases renal SNA and BP, while electrolytic lesion of the OVLT attenuates this response (78). Third, *in vivo* experiments demonstrate that injection of hypertonic saline into the OVLT increases SNA and BP, while injection into adjacent regions does not elicit the same effect (105). Fourth, optogenetic stimulation of OVLT neurons in Sprague-Dawley rats elicits increases BP and HR, which are blocked by the administration of chlorisondamine, a ganglionic blocker; additionally, the activation of OVLT neurons increases SNA and the activity of RVLM neurons. Furthermore, 7-day chemogenetic stimulation of OVLT neurons increases fluid intake and BP due to increased neural activity (124). Fifth, high dietary sodium intake in male Sprague Dawley rats exaggerates SNA and BP responses to various stimuli, such as intracerebroventricular infusion of NaCl or electrical

stimulation of sciatic afferents; however, lesion of the lamina terminalis (AV3V region) blunts this effect (91). Sixth, feeding Dahl SS rats a high sodium diet for 3-4 weeks leads to greater discharge of NaCl-sensitive OVLN neurons compared to Dahl SS rats fed a low sodium diet or Dahl SR rats; additionally, injecting a GABA agonist to inhibit OVLN neurons elicits larger reductions in renal and splanchnic SNA and BP in Dahl SS rats fed the high salt diet compared to those fed the low salt diet or Dahl SR rats (88). Seventh, one study utilized RNA sequencing in Wistar Kyoto and spontaneously hypertensive rats to assess the effects of high sodium intake on the gene expression of several osmoregulatory and sympathoregulatory brain regions (such as the SFO, PVN, SON, nucleus tractus solitarius (NTS), and RVLM). Several genes, including genes for AVP in the SFO and SON, were upregulated or downregulated in one or both types of rats, suggesting that the aforementioned brain regions may play an important role in regulating responses to sodium loading (125). While both the OVLN and SFO are typically referred to as sodium sensing brain regions, one study demonstrates that lesioning the ventral lamina terminalis or OVLN alone but not the SFO alone prevents male Sprague Dawley rats from developing exaggerated cardiovascular responses when the RVLM is stimulated during high sodium intake, suggesting that the OVLN may have a more critical role in sodium sensing and cardiovascular regulation than the SFO (126). Together, these findings highlight the importance of the OVLN (and the SFO, but possibly to a lesser degree) in mediating BP responses to acute and chronic hypernatremic stimuli.

1.3.4 Sex Differences

There may also be sex differences in central sodium sensing and the regulation of sympathoregulatory brain regions. This is supported by studies indicating that estrogen and androgen receptors are expressed in several brain regions, including the sodium-sensing CVOs, and sympathoregulatory brain regions such as the PVN of the hypothalamus, and the NTS and RVLM in the brainstem (46, 65, 75, 120, 121, 127), suggesting that sex hormones may alter the activity of these brain regions. Indeed, in ovariectomized adult female Wistar rats, intracarotid injection of estradiol decreases the basal discharge of SFO neurons and the response of SFO neurons to intracarotid injection of hypertonic saline (128). Additionally, estrogen receptors are co-localized on neurons also expressing AT₁R, and estrogen has been shown to modulate the central effects of angiotensin II (46, 65). Indeed, intracerebroventricular infusion of estradiol in male and ovariectomized female mice reduces the effects of angiotensin II on BP, and blocking brain estrogen receptors prevents this effect (46, 75, 129). Additionally, estradiol treatment in ovariectomized female rats reduces AT₁R expression and binding affinity in the SFO, decreases the resting firing rate of SFO neurons, and attenuates the angiotensin II-induced change in firing rate (46). Furthermore, estradiol decreases the response of neurons in the area postrema to angiotensin II (46, 130), and estradiol microinjection into the NTS or RVLM of male or ovariectomized female rats decreases BP and improves baroreflex control of SNA (75).

The expression of estradiol receptor subtypes differs between different brain regions. Specifically, estradiol inhibits angiotensin II-induced activation of the SFO and area postrema through estrogen receptor- α (ER α) (46, 65); and through estrogen receptor- β (ER β), estradiol inhibits neurons in the PVN and RVLM to attenuate angiotensin II- or aldosterone-induced increases in sympathetic outflow and BP (46, 65, 131). This is supported by research demonstrating that knocking down ER α in the nervous system or in only the SFO elicits greater increases in BP with angiotensin II infusion; additionally, ganglionic blockade after the angiotensin II infusion elicits larger reductions in BP in the ER α knock-out mice, suggesting that estrogen may act centrally through ER α in the SFO to reduce angiotensin II-induced changes in SNA and BP (132). Additionally, using whole-cell recordings of RVLM neurons, estradiol decreases voltage-gated calcium currents (46). Moreover, knocking down ER β but not ER α in the PVN or RVLM of female animals with siRNA increases the effects of aldosterone on BP, suggesting that ER β in the PVN and RVLM is protective against aldosterone-induced increases in SNA and BP (46, 131).

There are multiple mechanisms through which estradiol may mediate its protective effects. One suggested mechanism is via estradiol-mediated inhibition of ROS production within the SFO (65, 75, 133) or elevated expression of neuronal NO synthase in the SFO and PVN of female animals (134). Additionally, estradiol may interact with kinase pathways to modulate RAAS hormone effects (75). Furthermore, estradiol may upregulate the protective arm of the RAAS. In a study in which a

subcutaneous sub-pressor dose of angiotensin II was administered prior to a 2-week pressor dose of angiotensin II, male and ovariectomized female rats developed an exaggerated hypertension that was blocked by pretreating rats with central administration of angiotensin-(1-7) or estrogen. Additionally, in non-ovariectomized females, sub-pressor treatment with angiotensin II led to a reduction in BP followed by a slight increase in BP with the pressor dose of angiotensin II, which was exaggerated with administration of an angiotensin-(1-7) receptor antagonist. Together, this suggests that estradiol may protect against the development of angiotensin II-induced hypertension through regulating brain RAAS activity (135).

1.3.5 Translational Research in Humans

Only a few translational research studies in humans have attempted to investigate this network of sodium-sensing brain regions. One study utilizing positron-emission tomography (PET) and BOLD functional magnetic resonance imaging (fMRI) found that an acute intravenous hypertonic saline infusion increases the activity of several brain regions, including the lamina terminalis, anterior cingulate, mid-cingulate, and insula (136). Other PET studies from this group have also shown activation of the anterior cingulate, middle temporal gyrus, and periaqueductal gray during acute hypernatremia elicited via a hypertonic saline infusion (137). Importantly, after participants are allowed to drink water to satiation, activation decreases in the anterior cingulate but remains elevated in the lamina terminalis (anterior wall of the third ventricle), suggesting that the anterior cingulate may be more involved in the

consciousness of thirst, whereas the lamina terminalis may be more involved with sensing plasma sodium concentrations (136).

Another study used an exercise-induced dehydration model to elicit acute relative hypernatremia to investigate the effects of hypernatremia on the functional connectivity of the ventral lamina terminalis (138). This study used arterial spin labeling (ASL) which is a perfusion-related neuroimaging technique that measures regional cerebral blood flow (rCBF) by magnetically labelling protons in water molecules in the blood and measuring the appearance of these labelled protons in the imaging plane (139). Farrell et al. found that rCBF in the ventral lamina terminalis was correlated with rCBF in the cerebellum, thalamus, orbitofrontal and prefrontal cortices, caudate nuclei, ventral striatum, and parahippocampi. The correlation also increased between rCBF in the lamina terminalis and rCBF in a few other brain regions, such as the right anterior cingulate cortex (ACC), prefrontal cortex, and left superior temporal gyrus, after exercise-induced dehydration (denoted “maximum thirst”), suggesting that the functional connectivity of the lamina terminalis changes with alterations in plasma osmolality (138). Additionally, our lab recently published a pilot study in which acute relative hypernatremia via an IV hypertonic saline infusion increased the functional connectivity between the SFO and OVLT; importantly, we observed no changes in functional connectivity between the SFO and OVLT in a volume control group (receiving an isotonic saline infusion) or a time control group (receiving no infusion) (140). Furthermore, in this study, the mean functional

connectivity maps for the CVOs were similar to the map in Farrell et al. (138, 140). Taken together, these studies suggest that the lamina terminalis plays a similar role in sodium sensing in humans as seen in animal models. However, none of these studies report activation of sympathoregulatory brain regions such as the PVN, RVLM, NTS, or CVLM in response to hypernatremia, nor do they report whether there are sex differences in these responses. Additionally, these studies have limitations, such as small sample size and the use of PET or ASL vs BOLD fMRI (see section 1.4 for a discussion of the advantages of BOLD fMRI).

Although not performed in the context of acute relative hypernatremia, studies in humans have used fMRI to investigate brainstem nuclei involved in autonomic cardiovascular control at rest and during various perturbations. Brainstem activity has been directly associated with sympathetic outflow by performing MSNA and BOLD fMRI concurrently. In this experimental context, MSNA is positively associated with BOLD activity in multiple brain regions, including the RVLM, hypothalamus, insula, posterior cingulate, and precuneus and negatively associated with BOLD activity in the CVLM, NTS, and periaqueductal gray (141–143). Additionally, brainstem activity has been associated with resting BP. BOLD signal in the ventrolateral medulla has been shown to be inversely related with resting BP (144), and rCBF in the RVLM, insula, dorsolateral pons, and cingulate cortices is correlated with resting BP in young normotensive adults. Furthermore, the functional connectivity between the ventrolateral prefrontal cortex and RVLM is greater in those with lower resting BP

(145). Moreover, structural analyses indicate that gray matter volume is higher in the RVLM and NTS in those with higher BP. This study also found that gray matter volume in the dorsomedial hypothalamus, anterior cingulate cortex, and posterior cingulate cortex is higher in those with lower MSNA (146). Lastly, MSNA burst incidence is strongly correlated with salience network connectivity in several areas, including parts of the insula, anterior cingulate cortex, thalamus, and cerebellum. This is potentially significant since the salience network contains brain regions that are activated by stimuli that acutely change sympathetic tone, such as cognitive tasks, pain, and autonomic challenges (147).

The activity of brain regions involved in cardiovascular control has also been investigated during various perturbations. For instance, isometric handgrip exercise and post-exercise ischemia activate medullary regions, corresponding to the NTS and RVLM (144, 148). Additionally, BOLD signal increases in the insula, thalamus, parietal cortex, and cerebellum during handgrip exercise, and the HR response to exercise is associated with reduced BOLD signal in the ventral medial prefrontal cortex (149). Furthermore, in a study in which participants underwent BOLD fMRI during isometric handgrip, maximal inspiration, and the Valsalva maneuver, the authors found that all tasks were associated with activation of the NTS and parabrachial nucleus; additionally, maximal inspiration and the Valsalva maneuver activated the periaqueductal gray, while isometric handgrip and maximal inspiration activated the raphe nuclei (150). Furthermore, increasing MSNA by inducing muscle

pain (infusing hypertonic saline into a muscle) increases BOLD activity in the RVLM, NTS, and periaqueductal gray (141). More specifically, when participants are separated based on their MSNA response to tonic muscle pain, BOLD signal increases in the dorsomedial hypothalamus and RVLM in those with increases in MSNA during tonic muscle pain but not in those with decreasing MSNA (151). Lastly, phenylephrine administration changes BOLD signal in multiple brainstem nuclei including the NTS, CVLM, RVLM, nucleus ambiguus, and nucleus obscurus, further supporting the role of these nuclei in BP regulation (152).

Taken together, these findings support the role of brainstem nuclei, including the RVLM, NTS, and CVLM in the regulation and generation of sympathetic outflow and suggest that other brain regions, including the insula, hypothalamus and periaqueductal gray may also be associated with MSNA (153). While multiple studies have identified several sympathoregulatory brain regions in humans, few studies have assessed sex differences in brain activation related to autonomic cardiovascular control. In one study, men and women displayed differences in forebrain BOLD fMRI responses to isometric handgrip exercise (154). However, to our knowledge, no studies have assessed whether there are sex differences in activation of these sympathoregulatory brain regions during sodium loading.

1.4 Blood Oxygenation Level Dependent Functional Magnetic Resonance Imaging (BOLD fMRI)

1.4.1 Introduction to MRI

MRI and its underlying principles developed rapidly during the 20th century (139, 155, 156). One of the main phenomena that makes MRI possible is magnetic resonance, the principle that atomic nuclei can absorb energy from a magnetic field if the magnetic field oscillates at a particular frequency. Hydrogen atoms are the most commonly imaged type of atom with MRI because they are the most abundant in the human body and possess nuclear magnetic resonance properties, specifically magnetic moment and angular momentum (139, 157, 158). Hydrogen has an intrinsic property of spin (155, 157). Thus, since the proton in hydrogen possesses a positive charge, its spin causes the generation of an electrical current, which creates a small magnetic field and causes it to experience torque in an external magnetic field. The spin also creates angular momentum (139, 157). When not under the influence of an external magnetic field, hydrogen atoms spin around random axes, and the net magnetization is close to zero (139, 158). However, when placed in an external static magnetic field, hydrogen atoms reorient to rotate around the axis of the static magnetic field, in a process called precession. This alignment of hydrogen atoms creates a net magnetization in the direction of the static magnetic field (referred to as longitudinal magnetization) (139, 157–160).

Each type of atom precesses at a particular frequency (known as the Larmor frequency), which is determined by the product of the gyromagnetic ratio, a constant value for each type of nucleus, and the static magnetic field strength (139, 156–158). By applying radiofrequency energy at the Larmor frequency (i.e., an oscillating magnetic field at an angle to the main magnetic field), the hydrogen atoms become excited, and the net magnetization tips from the longitudinal into the transverse plane, creating transverse magnetization (139, 155, 157, 159, 160). Once the oscillating magnetic field is removed, hydrogen atoms gradually return to precessing around the axis of the main magnetic field and release radiofrequency energy, which is the signal received and used to generate MRI images (139, 158). Most MRI images depend on measuring the recovery rate of the longitudinal magnetization (known as T_1) or the decay of the transverse magnetization (T_2) after excitation, which varies depending on the tissue type (e.g., gray matter vs white matter vs CSF) (139, 155, 157–160). In the 1970s, this basic understanding of physics was translated into the creation of the first MRI images of biological tissues, and in the 1990s, BOLD fMRI emerged as a functional neuroimaging technique (139, 156, 159).

1.4.2 Introduction to BOLD fMRI

BOLD fMRI relies on the coupling of neuronal activity with cerebral blood flow and oxygenation (161, 162) and crucially depends on the magnetic properties of hemoglobin. Oxyhemoglobin is diamagnetic and therefore has a negligible effect on the surrounding magnetic field; however, deoxyhemoglobin is paramagnetic and alters

the surrounding magnetic field (139, 160). When something paramagnetic, such as deoxyhemoglobin, distorts the magnetic field, surrounding protons begin to precess at different frequencies because of differences in magnetic field strength. This causes the transverse magnetization to decay more rapidly. Thus, by measuring the rate of the decay in transverse magnetization (or the time constant, T_2^* , as is done with BOLD fMRI) it is possible to determine the proportions of oxy- and deoxy-hemoglobin in a region (139). Neuronal activity increases blood flow and oxygen in excess of the demands (160–162), thereby flushing out deoxyhemoglobin. Thus, increases in neuronal activity decrease the effects of deoxyhemoglobin on the decay of transverse magnetization, leading to an increase in BOLD signal (139). In summary, changes in BOLD signal reflect changes in brain blood flow and oxygenation (161–163).

Because of its hemodynamic origins, the BOLD signal has a “sluggish” time course. Following the onset of a stimulus, the BOLD signal initially decreases, reflecting an immediate increase in local deoxyhemoglobin. Following a brief (2-3 second) delay, the BOLD signal increases, plateaus at around 6-12 seconds, and returns to baseline often with a post-stimulus undershoot. This is supported by the findings that compared to electrophysiological recordings of neural activity, BOLD signal increases about 2 seconds after the onset of neuronal activity, and the signal plateaus about 7 seconds after the onset of neuronal activity (160, 163, 164). The delay in the BOLD signal reflects a lag in the hemodynamic response since there is a delay between the onset of

neuronal activity and regional vasodilation to increase blood flow and oxygen supply (163).

Many research studies across several fields have used BOLD fMRI to investigate brain activation in response to different tasks (e.g., cognitive, visual, or motor tasks). The two primary task-based experimental designs are block and event-related designs. For block designs, participants are presented with a series of alternating stimuli or tasks for short periods. Typically, a task-based block is contrasted with another condition or a control block (160, 163). For block designs, it is typically assumed that the BOLD signal returns to baseline during the resting/control block (139). Block duration is most commonly 15-30 seconds, and the order of the blocks is often counterbalanced across subjects (163). If the block duration is too short (e.g., 2 seconds), the BOLD signal cannot return to baseline between task and control blocks, thus reducing the change in the BOLD signal and statistical power. Alternatively, if the block duration is particularly long (e.g., greater than 3 minutes), it can be more difficult to determine whether the BOLD signal change is a result of the task or low-frequency noise, since BOLD signal has the most noise at low frequencies (e.g., scanner drift) (139).

For event-related designs, brief (i.e., 0.5 to 8 seconds) events are presented in a random order separated by an inter-stimulus interval (i.e., no stimulus for about 0.5 to 20 seconds) to allow the participant to return to baseline (163). If event-related designs

have a large inter-stimulus interval (e.g., >15 seconds), the experiment can be inefficient since the frequency of events is low; however, if the inter-stimulus interval is very short (e.g., 2 seconds), the BOLD signal can exhibit a plateau or saturation where it is no longer possible to determine the event-related effects. More frequently, jittering is used so the interstimulus interval is variable but on average about 4-6 seconds (139).

Event-related designs enable the characterization of the hemodynamic response with more temporal detail than block designs; however, block designs have greater statistical power to detect changes in activation since the amplitude of the activation is greater with block designs (~2-3%) compared to event-related designs (<1%) (139, 163). Since the change in the BOLD signal with most tasks is small (i.e., no more than a few percent change from baseline), it is necessary to perform many trials/repetitions to ensure adequate power to detect significant changes in brain activation (139). For example, with a block design, increasing the number of blocks from 1 to 5 blocks in a sample of 17-23 subjects increases the power from 16-27% (1 block) to 54-75% (5 blocks); and further increasing the number of blocks continues to increase power (165). Additionally, in an event-related experiment in which participants viewed a checkerboard for 500 milliseconds, increasing the number of trials increased the size of the activation; and at least 25 trials were necessary to stably estimate the fMRI hemodynamic response (166). Thus, it is essential with task-based experiments to have many repetitions of the stimulus.

The utility of BOLD fMRI is supported by several studies comparing BOLD fMRI with other neuronal recording techniques. For instance, in one study, simultaneous BOLD fMRI and electrophysiological measurements were recorded from Wistar rats during electric forepaw stimulation. The authors found that the BOLD signal had an approximately linear relation to electrophysiological activity in the somatosensory cortex (167). Another study compared brain activity in brain area V5 in humans measured via BOLD fMRI to single-cell responses in V5 of macaque monkeys during a moving visual stimulus and demonstrated that BOLD signal was directly proportional to average neuronal firing rate (168). Additionally, simultaneous BOLD fMRI and electrophysiological recordings in the visual cortex of monkeys have been performed while the animals were viewing a rotating checkerboard pattern. In this study, the authors concluded that BOLD fMRI signal represents the underlying neural responses since there was an approximately linear relation between neural and BOLD fMRI responses. Furthermore, BOLD fMRI was better correlated with local field potentials, which represents local neuronal input signal and processing, rather than multi-unit activity, which reflects predominantly local neural output. This suggests that BOLD fMRI predominately represents local neuronal input and processing (161, 164). Thus, BOLD fMRI is regarded as a robust indirect indicator of neuronal activity (163).

Although there are many available neuroimaging techniques, BOLD fMRI possesses several distinct advantages over most other imaging modalities. For instance, although

EEG has better temporal resolution (on the order of milliseconds) compared to BOLD fMRI (slightly less than one second at best), BOLD fMRI has better spatial resolution compared to EEG. BOLD fMRI can have a spatial resolution of one millimeter or better, whereas EEG typically has a spatial resolution around a few to several centimeters (139, 169). BOLD fMRI also enables imaging of deeper subcortical brain structures that are more difficult to image with surface-based techniques such as EEG which depends on changes in electrical activity at the scalp (170). Additionally, BOLD fMRI provides better spatial and temporal resolution compared to PET imaging. Compared to the temporal resolution of BOLD fMRI (about one second), PET has a temporal resolution on the order of tens of seconds; and the spatial resolution of PET (around one centimeter) is worse than that of BOLD fMRI (about one millimeter). BOLD fMRI is also less invasive (i.e., does not require radiation exposure or radioactive contrasts) compared to PET imaging (139, 170, 171). Furthermore, compared to ASL, BOLD fMRI has higher temporal signal-to-noise ratio (172). Moreover, in resting state fMRI analyses, BOLD fMRI is most commonly used and the connectivity between most brain networks is higher using BOLD fMRI compared to ASL (172, 173). In one study in which eight resting-state brain networks were created (including the sensorimotor, auditory, primary visual, default-mode, salience, and executive control networks) using a seed-based functional connectivity approach, the resting-state networks were similar for BOLD fMRI and ASL. However, functional connectivity tended to be higher using BOLD fMRI compared to ASL (172). Likewise, another study using a seed-based connectivity approach found that

functional connectivity assessed using ASL and BOLD fMRI produced similar results, but functional connectivity assessed with ASL had a reduced intensity compared to BOLD fMRI (173). Thus, based on the current literature, BOLD fMRI might be superior to ASL for resting-state fMRI experiments.

1.4.3 Resting-State fMRI

Resting-state fMRI involves measuring brain activity in the absence of an explicit task or external stimulation. With resting-state fMRI, the primary focus is on low-frequency fluctuations in the BOLD signal (i.e., with a frequency less than 0.1 Hz), which are thought to represent spontaneous brain activity (163, 174, 175). Interest in resting-state fMRI began in the 1990's as one of the first resting-state fMRI studies assessed the functional connectivity of part of the motor cortex associated with hand movement at rest and during a bilateral finger tapping task. In this study, the low-frequency fluctuations in the BOLD signal in regions of the motor cortex were correlated within and between hemispheres for both resting-state and task scans with higher correlations in the task data (175). Resting-state experiments have grown in popularity since then due to increased interest in understanding spontaneous brain activity and resting state brain networks, which are reliably produced across scanning sessions and between different subjects (163, 174).

Resting-state scans between five and seven minutes in length are typically recommended; however, longer scans (~13 minutes) have been suggested to provide

greater reliability (163, 176). This is supported by a study in which functional connectivity analyses were performed on scans ranging in length from 2-12 minutes. In this study, the strength of the functional connectivity within and between a few networks (including the default mode network and attention network) stabilized above scan lengths of about 5 minutes (176). General recommendations for resting-state fMRI can also include instructing participants to keep their eyes open and fixated on a fixation cross. In support of using an eyes-open state, functional connectivity of the default mode network and attention network is stronger in eyes-open than eyes-closed conditions but not different between eyes-open fixated and eyes-open non-fixated conditions. Although there are no differences in this study regarding the presence or absence of eye fixation, fixation is generally recommended because it minimizes any possible effects of eye motion (163, 176).

Resting-state fMRI possesses several distinct advantages over traditional task-based experimental designs. First, resting-state experiments do not require participants to complete a task, so they can be conducted in participants unable to perform a task-based experiment, due to factors such as age, physical condition, or mental status (174). Second, resting-state experiments can be used to investigate brain activation during conditions that do not fit standard task-based experimental designs (e.g., sleep) (177). Third, resting-state studies allow many networks to be identified simultaneously rather than needing a task for each brain region/network of interest (174).

One of the most common approaches for resting-state fMRI analysis is independent component analysis (ICA), which is a data-driven analysis approach that can be used to separate the fMRI data into a set of spatially or temporally independent components (163). This technique has been used to identify resting state networks, or components (i.e., brain regions with synchronized BOLD activity). Networks identified include the default mode network, salience network, executive control network, visual networks, auditory network, and sensorimotor network (176, 178). Additionally, ICA identifies these networks with moderate to high test-retest reliability. One study assessed the test-retest reliability of ICA, particularly temporal concatenation group ICA, within a session and between sessions 5-16 months apart. The number of components generated was fixed to 20 components and the networks identified included motor and auditory brain regions, vision networks, fronto-parietal networks, an executive and attentional network, and the default mode network. Importantly, these components were identified with moderate to high reliability within and between scanning sessions (179). ICA also has potential clinical relevance since the resting-state networks identified by ICA have been suggested to be markers of different neurodegenerative diseases and psychiatric illnesses (180). For instance, Alzheimer's disease, epilepsy, schizophrenia, and depression are all associated with altered resting state networks (179). One of the primary advantages of ICA is that it does not require many a priori assumptions (such as a starting region of interest); however, it requires the researcher to carefully distinguish between components representing physiological signal and

noise (174), and ICA generally does not easily demonstrate connections between different brain networks (178).

The other most common approach for resting-state fMRI analysis is seed-based functional connectivity (180). Functional connectivity reflects the synchronization/correlation of low frequency fluctuations in the BOLD signal between different brain regions/voxels. With these correlational analyses, activity in a predefined region of interest is compared with that of another region of interest or to the rest of the brain in a voxel-by-voxel manner (163). Thus, one of the disadvantages of this approach is that it requires the selection of an a priori region of interest (174). Regions that have correlated activity patterns can be identified to build resting state brain networks (163). The correlation of the activity between two brain regions suggests that they participate in the same function (178). The utility of functional connectivity analyses is supported by the findings that functional connectivity is reliable across subjects, sessions, and separate subject groups, and correlations detected with this approach are largely (although not entirely) constrained by anatomy (176). One study assessed the test-retest reliability of resting-state fMRI between scans in a single session and separate sessions at least 5 months apart. Using a seed-based functional connectivity approach, the test-retest reliability ranged from modest to high, and reliability was greater when there were significant compared to non-significant correlations, positive correlations compared to negative correlations, and brain regions in the default mode network compared to other networks (e.g., task

positive network) (181). Additionally, in a 1-year longitudinal study, in which healthy participants underwent 9 scan sessions, the intraclass correlation coefficient for connectivity strength between 16 nodes of the default mode network was greater than 0.6 for over 70% of the connectivity values, suggesting high reproducibility (182). Moreover, ICA and seed-based correlational methods demonstrate similar results, suggesting that both approaches reflect similar features of resting state fMRI data (176).

Additional less common but growing analysis approaches include Regional Homogeneity analysis (ReHo) and amplitude of low frequency fluctuations (ALFF) or fractional ALFF (fALFF). ReHo uses Kendall's coefficient of concordance to determine the similarity of the time series of each voxel to that of its adjacent voxels, thus representing the synchronization of neighboring voxels (163, 183). ALFF or fALFF is an indicator of signal magnitude in each voxel, reflecting the intensity of the spontaneous fluctuations in BOLD signal on a voxel-by-voxel basis (163, 184), which is thought to be proportional to local neural activity (178). ALFF is calculated by taking the square root of the power spectrum of low frequency fluctuations (0.01-0.08 Hz) (185), whereas fALFF represents the ratio of the power spectrum in the low-frequency range to the complete frequency range (184). fALFF may be preferable to ALFF since fALFF reduces the influence of physiological noise and has improved sensitivity in determining brain activity over ALFF (163, 184). Similar to ICA, both ReHo and ALFF/fALFF can be calculated without the selection of an a priori region

of interest. Additionally, ALFF or fALFF and ReHo are often used as complementary measures because they reflect different properties of spontaneous activity (i.e., signal amplitude for ALFF and fALFF and local synchrony for ReHo) (163). The use of fALFF and ReHo to investigate BOLD signal on a voxel-by-voxel basis is supported by the findings that fALFF and ReHo are associated with metabolic information gathered through PET imaging. Specifically, fALFF is strongly associated with the metabolic rate of glucose and oxygen, blood flow, and blood volume and ReHo is strongly associated with the metabolic rate of glucose and oxygen and slightly associated with blood flow and blood volume (186).

1.5 Summary

This literature review highlights several key points related to salt sensitivity of blood pressure, central sodium sensing, and whether there are differences between men and women. First, the prevalence of hypertension differs between men and women across the lifespan such that hypertension is more prevalent in younger men compared to younger women but is also more prevalent in older women compared to older men (1). Second, dietary sodium intake is positively associated with BP (7–10, 12, 13). However, BP responses to sodium loading are heterogenous (17, 18) with about 25–50% of normotensive adults and about 40–75% of hypertensive adults typically classified as SS (17, 19, 20). Third, several studies indicate that women are more SS than men across the lifespan (19, 38–41). However, this is not unequivocal (42) and many dietary studies provide men and women with diets containing the same absolute

sodium content without considering differences in sodium density associated with sex differences in caloric intake (8, 43). Additionally, in most rodent models, male animals are more SS than female animals (45–49). Fourth, the etiology of SS is complex but includes altered neural activity (8, 25, 77, 78, 80, 81, 83, 84, 86–90). Fifth, the CVOs, namely the SFO and OVLT, are sensitive to changes in sodium concentration in the CSF and blood stream and mediate downstream changes in sympathetic activity and BP (77, 78, 88, 102, 104, 105, 122–124). Sixth, there may be sex differences in central sodium sensing since 1) sex hormone receptors are expressed in the brain, including in the CVOs and sympathoregulatory brain regions (46, 75, 120, 121, 127); 2) estradiol decreases the basal discharge of SFO neurons and the responsiveness of these neurons to intracarotid injection of hypertonic saline (128), and 3) men have a higher sensitivity of AVP release than women (113, 114). Seventh, only a few studies in humans have attempted to investigate the brain regions involved in sodium sensing; however, studies have shown that acute relative hypernatremia may increase the activity of several brain regions, including the lamina terminalis (136), and acute hypernatremia also increases the correlation of rCBF in the lamina terminalis with rCBF in several cortical brain regions (138). Additionally, our lab recently published a pilot study in which acute relative hypernatremia increased the functional connectivity between the SFO and OVLT (140). Eighth, studies in humans have used fMRI to identify several brainstem nuclei and cortical brain regions implicated in the regulation of sympathetic outflow and BP (141, 142, 144, 148–150, 152). However, to our knowledge, no publications have reported whether there are sex

differences in the activation of sodium sensing and sympathoregulatory brain regions during sodium loading in humans.

Chapter 2

SEX DIFFERENCES IN THE ACTIVATION OF SALT SENSING BRAIN REGIONS DURING ACUTE HYPERNATREMIA

2.1 Introduction

Blood pressure (BP)-related diseases remain a major public health challenge in both men and women (1, 4). However, the prevalence of hypertension is higher in men compared to women until about 65 years of age, after which the prevalence is greater in women. This shift is likely associated with menopause and the loss of the cardioprotective effects of female sex hormones (1, 2, 5). One possible reason for the high incidence of hypertension in adults may be excessive salt consumption (187), since dietary salt intake is associated with BP (1, 7, 11–13, 15, 16). Additionally, sex differences in salt sensitivity of BP (i.e., the change in BP with a change in salt load) have been identified between male and female rodents (45, 47) and men and women (25, 39, 43). Therefore, investigating the mechanisms underlying sex differences in responses to salt may be important in advancing our understanding of differences in the prevalence of hypertension between men and women.

While several physiological mechanisms mediate the effects of dietary salt on the cardiovascular system, including vascular, immune, renal, and neural responses (19, 25), this study focuses on neural mechanisms related to salt sensing in the brain (140). Central salt sensing, which occurs primarily in the circumventricular organs (CVOs) is critical in mediating neurohumoral responses to hypernatremia as occurs with high salt intake (77, 78, 88, 102, 104, 105, 122–124). The CVOs include the organum vasculosum of the lamina terminalis (OVLT) and subfornical organ (SFO), which are anatomically suited to sensing changes in the salt concentration in the blood since they possess an extensive vascular supply and an incomplete blood brain barrier (77, 102). This is also supported by the findings that 1) NaCl excites OVLT neurons *in vitro* (105), 2) OVLT cell discharge increases with intracarotid injection or intracerebroventricular infusion of NaCl *in vivo* (104), and 3) intravenous (IV) hypertonic saline infusion in male Wistar rats elicits neuronal activation in the SFO and OVLT (106). Additionally, in rodents, the CVOs have been shown to mediate salt-induced changes in vasopressin (AVP), thirst, sympathetic nervous system activity (SNA), and BP (77, 78, 103, 105), and salt-sensing in the CVOs has been associated with the development of salt sensitive hypertension (88). Furthermore, the sensitivity of the CVOs to changes in the salt concentration in the blood is clinically relevant, since a single high salt meal increases plasma sodium concentration by just over 3 mmol/L in humans (108).

Only a few studies have investigated central salt sensing in humans. In one study of young healthy adults, an IV hypertonic saline infusion elicited activation in the anterior cingulate cortex, middle temporal gyrus, and periaqueductal gray measured by positron emission tomography (PET) (137). Another study in young healthy adults found that blood oxygen level dependent (BOLD) functional magnetic resonance imaging (fMRI) signal increased in several brain regions during an IV hypertonic saline infusion including the anterior wall of the third ventricle (i.e., lamina terminalis), anterior cingulate, and insula. Furthermore, activation in the lamina terminalis remained elevated immediately following fluid ingestion, suggesting that the lamina terminalis is involved in sensing sodium/osmolality and not thirst sensations (136). Another study in young healthy adults using pulsed arterial spin labeling found that hypernatremia caused by exercise-induced dehydration increased functional connectivity between the lamina terminalis and several other brain regions (138). Additionally, our pilot study in young healthy adults using BOLD fMRI demonstrated that acute hypernatremia via an IV hypertonic saline infusion increased functional connectivity between the SFO and OVLT during the last 15 minutes of the 30-minute hypertonic saline infusion. We also found that baseline SFO-OVLT functional connectivity was positively correlated with baseline serum sodium, suggesting a physiological relation between serum sodium concentration and SFO-OVLT functional connectivity (140). However, to our knowledge no studies in humans have determined whether there are sex differences in central salt sensing.

Therefore, the purpose of this study was to assess whether there are differences in central salt sensing between men and women. Similar to our pilot study (140), we conducted resting-state fMRI scans at rest and during a 30-minute IV hypertonic saline infusion. We assessed the functional connectivity (i.e., the correlation of the BOLD signal time course between two brain regions) between the SFO and OVLT. We also assessed the functional connectivity of the SFO and OVLT with several additional brain regions implicated in central salt sensing or processing thirst, including the anterior cingulate cortex (ACC), insula, and sensory subdivision of the thalamus. As a complementary measure, we calculated fractional amplitude of low frequency fluctuations (fALFF). fALFF measures the ratio of the power spectrum in the low-frequency range (0.008 – 0.10 Hz) to the entire detectable frequency range within a specific brain region, reflecting the intensity of the spontaneous fluctuations in the BOLD signal in each brain region (163, 184). We hypothesized that acute relative hypernatremia (via an IV hypertonic saline infusion) would increase the functional connectivity between and fALFF in our regions of interest (ROIs), which are all associated with salt sensing and/or perception of thirst. We also hypothesized that men would have greater responses since 1) in salt sensitive rodent models, male animals display larger changes in arterial BP compared to female animals (45, 47), 2) men have greater AVP release in response to an IV hypertonic saline infusion compared to women (114), 3) sex hormone receptors are expressed in the CVOs (46, 75, 120, 121, 127), and 4) in rodents, estradiol decreases the basal discharge of SFO

neurons and the response of SFO neurons to intracarotid injection of hypertonic saline (128).

2.2 Methods

2.2.1 Subjects

Seventeen healthy young men and fifteen healthy premenopausal women (18-34 years) participated in this research study. Participants were recruited primarily via internal classifieds ads, flyers posted locally, and targeted social media ads. Verbal and written informed consent were obtained from all participants prior to participating in the study. Participants were excluded from the study if they exhibited hypertension (BP $\geq 130/\geq 80$ mmHg at their screening visit), current tobacco use, pregnancy, or clinical signs and symptoms of cardiovascular disease, diabetes, kidney disease, pulmonary disease, or liver disease. Participants had BMI between 18.5 and 30.2 kg/m². We excluded participants unable to undergo an MRI scan as determined by guidelines set by the Center for Biomedical and Brain Imaging at the University of Delaware, including individuals with ferromagnetic implants, claustrophobia, or neurological and psychiatric disorders. Individuals were also excluded if they were currently taking anxiety and/or depression medications, and women were excluded if they were using any form of hormonal contraception.

2.2.2 Experimental Protocol

The experimental design can be seen in **Figure 1**. Participants completed three visits. During the first visit, participants provided informed consent and completed a preliminary MRI screening to make sure it was safe for them to undergo our MRI protocol. Following consenting and the preliminary screening, participants completed a physical screening at the Nurse Managed Primary Care Center (NMPCC) at the University of Delaware, including height, weight, resting electrocardiogram (ECG), BP, a complete metabolic panel, a complete blood count, a lipid panel, HbA1c, and medical history. The MRI and hypertonic saline infusion visit (visit 3) occurred at the Center for Biomedical and Brain Imaging at the University of Delaware. Women completed their MRI testing during the follicular phase of their menstrual cycle (i.e., the first 12 days after the start of bleeding).

The approach for the MRI data collection is seen in **Figure 2**. Upon arrival, participants provided a spot urine sample to assess urine specific gravity and in women, to verify pregnancy status. Following at least 5 minutes of quiet supine rest, brachial artery BP was measured at baseline in triplicate using the auscultatory method. A baseline thirst rating was also performed using a Likert scale. Participants were asked to put a mark on a 10 cm horizontal line, indicating their thirst level, ranging from “not at all” (0 cm) to “maximal thirst” (10 cm). Participants had an IV catheter placed into an antecubital vein in their left or right arm. The catheter was used for infusing hypertonic saline and drawing blood samples pre- and post-infusion.

Before drawing blood samples, the IV line was flushed with isotonic saline followed by the collection of “waste” blood to minimize contamination of blood samples with hypertonic saline. This approach was successfully implemented in a pilot study in our laboratory (140).

Blood samples were obtained pre- and post-infusion to assess changes in serum electrolytes (EasyElectrolyte Analyzer; Medica, Bedford, MA), plasma osmolality (3D3 Osmometer; Advanced Instruments, Norwood, MA), hematocrit (Clay Adams Brand, Readacrit Centrifuge; Becton Dickinson, Sparks, MD), hemoglobin (Hb 201+ model; HemoCue, Lake Forest, CA), and plasma AVP. EDTA plasma samples were stored at -80°C and sent to the Wake Forest School of Medicine Biomarker Analytical Core to analyze plasma AVP using an Invitrogen Arg8-Vasopressin competitive enzyme-linked immunosorbent assay (ELISA) kit. This assay had an analytical sensitivity of 0.88 pg/mL and an assay range of 1.6-1000 pg/mL. Additional serum samples were stored to measure baseline sex hormone concentrations (sex hormone concentrations were measured in all subjects at baseline, except for one subject who had sex hormone concentrations assessed from a post-infusion blood sample). Sex hormones were analyzed by RAD fertility, a member of the CCRM Fertility Network. Samples were analyzed with an ADVIA Centaur CP Immunoassay System (Siemens Healthcare Diagnostics, Tarrytown, NY) using chemiluminescent acridinium ester technology (188). Serum progesterone was less than the detectable limit of the assay

in 4 participants; in these cases, serum progesterone was recorded as the minimum (0.050 ng/mL).

Once participants were situated in the MRI scanner, an anatomical T1 scan and ~10-minute baseline resting state BOLD fMRI scan were conducted. After the baseline scans, hypertonic saline (3% NaCl) was infused at $0.15 \text{ ml} \cdot \text{kg}^{-1} \cdot \text{min}^{-1}$ through the IV catheter for 30 minutes while participants were in the MRI scanner. A registered nurse performed the hypertonic saline infusion and blood draws. The infusion pump and stand stayed in the MRI control room (outside of the MRI room) and were connected to participants with long, MR compatible tubing. During this 30-min infusion, there was an additional 30-minute BOLD fMRI scan. Our analysis focused on the late phase (15-30 min) of the infusion, since our previous pilot data indicates that the functional connectivity between the SFO and OVLT starts to increase significantly above baseline starting at ~13 minutes into this same hypertonic saline infusion protocol (189). Additional BP measurements, a thirst rating, and a blood draw were completed following this scan and infusion.

2.2.3 MRI Acquisition

We used a 3T MRI Siemens Prisma Scanner and 64-channel head coil to obtain all brain images at the Center for Biomedical and Brain Imaging. Padding was placed around the participant's neck and head and arms to minimize head motion and contact

with the MRI bore. Participants were also instructed to keep both their head and the rest of their body as still as possible.

All participants underwent a T1-weighted anatomical scan [repetition time (TR) = 2080 ms; echo time (TE) = 4.6 ms; field of view = 210 x 210 mm; voxel size = 0.7 mm³; slice thickness = 0.7 mm] followed by two functional BOLD fMRI scans (baseline & infusion). Functional scans were acquired using a multi-band gradient-echo echo-planar imaging (EPI) sequence [TR = 829 ms; TE = 40 ms; flip angle = 52°; field of view = 208 x 208 mm; voxel size = 2.0 mm³; slice thickness = 2.0 mm]. During functional scans, participants were instructed to keep their eyes open and fixated on a white cross (on a black screen) as is recommended to minimize the effects of eye motion and ensure the reliability and consistency of our results (190). These sequences are identical to those validated in our laboratory's pilot study (140).

2.2.4 MRI Analysis

The preprocessing steps described here were also utilized in our group's pilot study (140). Functional MRI images were processed and analyzed using MRICroGL, AFNI (Analysis of Functional NeuroImages) and FSL (FMRIB Software Library). Initially, the 30-minute infusion fMRI scans were split into an early phase (0-15 minutes) and late phase (15-30 minutes) using AFNI. Only the late phase scans were analyzed. Scans were also deobliqued and resampled to RPI (right, posterior, inferior) orientation. The remainder of the preprocessing included: 1) de-spiking of the resting-

state fMRI scans to eliminate outliers in the time series, 2) slice-timing correction of the fMRI scans to correct for slight differences in the acquisition of 2D slices within each 3D brain volume, 3) 3D rigid motion correction to a reference frame to correct for head motion in the resting-state data (we removed time points with head motion > 0.5 mm), 4) cleaning the fMRI data using ANATICOR (accounting for the 6 motion parameters, white matter, and CSF signal), 5) band-pass filtering (0.008 to 0.10 Hz) to focus the analysis on low frequency fluctuations in the resting-state BOLD fMRI signal (190), 6) skull-stripping of the T1-anatomical scan using FSL, 7) co-registration (i.e., alignment) of the T1-anatomical and functional scans, 8) normalization of all scans to the 1mm MNI152 template, and 9) spatial smoothing of the resting-state data using a Gaussian kernel of full-width half maximum (FWHM) = 4mm. These smoothing dimensions align with recommendations to choose a Gaussian kernel of FWHM double the voxel size (which was 2 mm³ for this study) (163). All scans were pre-processed the same way for both functional connectivity and fALFF analyses except for bandpass filtering, which was omitted for the fALFF analysis, since that analysis requires the entire frequency range (184).

The ROIs for this study were defined as follows. The SFO and OVLT were each defined as a 2-mm radius sphere based on previous studies (**Figure 3A**) (138, 140, 189, 191). The Montreal Neurological Institute (MNI) coordinates corresponding to the center of each ROI were as follows: SFO: x = 0 mm, y = 2 mm, z = -6 mm and OVLT: x = 0 mm, y = 2 mm, z = -12 mm. The location of these seeds has been

verified using Duvernoy's Atlas of the Human Brainstem and Cerebellum (192) and these ROIs are consistent with those used in a pilot study conducted in our lab (140). We also analyzed the left and right ACC and insula, which were extracted from the Automated Anatomical Labeling Atlas 3, AAL3 (193), and the sensory subdivision of the thalamus, based on the Oxford Thalamic Connectivity Atlas (194–196) (**Figure 3A**). These brain regions have been implicated in central salt sensing/thirst in previous studies (136–138). As control ROIs, we assessed the posterior cingulate cortex (PCC), which was also extracted from the AAL3 atlas (193), and the hand area of the primary motor cortex (M1), which was defined as a 4-mm radius sphere based on coordinates identified by Buckner et al. (197) (**Figure 3B**). The PCC is part of the default mode network and was not hypothesized to have changes in functional connectivity or fALFF during the hypertonic saline infusion, since it is primarily involved in “internal mentation” and not directly involved in central salt sensing (198). The PCC was also used as a control ROI for our pilot study, in which we found no significant changes in functional connectivity between the SFO and PCC with the infusion as hypothesized (140). We chose the hand area of M1 as our second control ROI since the experimental protocol does not include any motor tasks involving the hands and it was not hypothesized to be involved in sodium sensing. All ROIs are depicted in **Figure 3**.

Following pre-processing, we calculated functional connectivity and fALFF. These are complementary analysis approaches since functional connectivity reflects the synchronization of the low frequency fluctuations in the BOLD signal between our

ROIs and fALFF reflects the intensity of the spontaneous fluctuations in the BOLD signal in each brain region (163, 184). First, we conducted seed-to-seed functional connectivity analyses to assess the functional connectivity between our ROIs. We assessed functional connectivity between the SFO and OVLT. We also calculated the functional connectivity of these two CVOs with additional ROIs, including the left and right ACC and insula, and the sensory subdivision of the thalamus. Functional connectivity was also calculated between the SFO/OVLT and the control ROIs in which we hypothesized there would be no significant changes (i.e., PCC and M1 hand area). Pearson correlations were computed between the ROIs for the seed-to-seed functional connectivity analysis. Pearson correlations were converted to Z-scores using a Fisher's transform which were statistically analyzed, as in our pilot study (140).

We also calculated fALFF for all our ROIs as a complementary analysis. fALFF is a newer approach to resting state fMRI analysis, which we calculated as the ratio of the power spectrum in the low-frequency range (0.008 – 0.10 Hz) to the complete frequency range (184). fALFF is regarded as an indicator of signal magnitude on a voxel-by-voxel basis, reflecting the intensity of the spontaneous fluctuations in BOLD signal in each voxel (163, 184). fALFF is also thought to be proportional to local neural activity (178). The use of fALFF to investigate BOLD signal on a voxel-by-voxel basis is supported by the findings that fALFF is strongly associated with the metabolic rate of glucose and oxygen, blood flow, and blood volume as assessed via

PET imaging (186). Thus, we assessed fALFF in each region of interest (ROI) as a marker of how BOLD signal magnitude changes with acute relative hypernatremia.

2.2.5 Statistical Analysis

Statistics were conducted with IBM SPSS Statistics 28.0 and GraphPad Prism 8.0. Normality was verified using the Shapiro-Wilk test. Normally distributed baseline characteristics were compared between groups (men and women) using independent 2-tailed t-tests. Alternatively, Mann-Whitney U tests were conducted on non-normally distributed data. 2x2 (time*sex) repeated measures analysis of variance (ANOVA) models were used to compare changes in thirst, BP, and biochemical data (e.g., plasma osmolality, serum sodium) pre- to post-infusion in men and women. 2x2 (time*sex) repeated measures ANOVAs were also used to assess changes in functional connectivity from baseline to the late phase (15-30min) of the infusion in men and women. If data were non-normally distributed, aligned rank transformations (ARTs) were conducted prior to performing 2x2 (time*sex) repeated measures ANOVAs. ARTs were completed using ARTool2 (version 2.2.2) (199, 200). Significant time*sex interactions were followed with pairwise post-hoc comparisons. Effect sizes were calculated as partial η^2 . Since some of the data were analyzed using ARTs, some of the effect sizes apply to the ranked data; these cases are identified in the text with the abbreviation, “ART.” Pearson and Spearman’s correlations were also utilized to assess the relation between functional connectivity, fALFF, and participant screening characteristics and biochemical data.

Power was calculated using GPower3.0. Power calculations based on our preliminary data ($\eta^2 = 0.059$; $f = 0.25$) indicated that a sample size of $n=28$ would provide us with $>80\%$ power to detect a small to medium effect size of $f=0.25$ with $\alpha=0.05$. This assumed that we had an even split of men and women and a moderate correlation among repeated measures ($r\approx 0.5$). The data we present here includes 32 participants, exceeding the sample size estimated by the power analysis by 4 participants.

2.3 Results

2.3.1 Participant Characteristics

Participant characteristics for all 32 participants (17 men and 15 women) who completed this study are presented in **Table 1**. The cohort exhibits diversity as 13 participants ($<50\%$) identified as white. On average, women had slightly lower age, height, body mass, BMI, SBP, and triglycerides compared to men (all: $p<0.050$); women also had slightly higher HDL cholesterol compared to men ($p=0.010$). However, there were no significant differences between men and women in DBP, total cholesterol, LDL cholesterol, or blood glucose (all: $p>0.050$).

2.3.2 Blood Pressure, Thirst, and Biochemical Data Pre- and Post-Infusion

Changes in blood pressure, thirst, and biochemical data with the hypertonic saline infusion are presented in **Table 2**. Urine specific gravity was consistent with data from normally hydrated participants in our lab (201, 202), and there were not significant

differences between men and women ($p=0.519$). As expected, we observed robust pre- to post-infusion increases in plasma osmolality (main effect of time: $p<0.001$, partial $\eta^2 = 0.913$, $N=29$), serum sodium (main effect of time: $p<0.001$, partial $\eta^2 = 0.901$, $N=30$), and serum chloride (main effect of time: $p<0.001$, partial $\eta^2 = 0.937$, $N=30$), demonstrating the effectiveness of our protocol in eliciting acute relative hypernatremia. Of note, there were no main effects of sex or phase*sex interactions for these variables (all: $p>0.100$). Hematocrit decreased (main effect of time: $p<0.001$, partial $\eta^2 = 0.610$, $N=27$) and was significantly lower in women (main effect of sex: $p<0.001$, partial $\eta^2 = 0.535$, $N=27$). Hemoglobin exhibited a significant time*sex interaction (time*sex interaction: $p=0.018$, partial $\eta^2 = 0.213$, $N=26$); however, hemoglobin decreased pre- to post-infusion in both men ($p<0.001$) and women ($p=0.020$) and was significantly lower in women both pre- ($p=0.001$) and post-infusion ($p=0.002$). SBP increased significantly pre- to post-infusion (ART: main effect of time: $p=0.038$, partial $\eta^2 = 0.174$, $N=25$); however, there were no significant changes pre- to post-infusion for DBP (main effect of time: $p=0.616$, partial $\eta^2 = 0.011$, $N=25$) or MAP (ART: main effect of time: $p=0.173$, partial $\eta^2 = 0.079$, $N=25$). As anticipated, DBP and MAP were significantly lower in women compared to men (DBP: main effect of sex: $p=0.009$, partial $\eta^2 = 0.261$, $N=25$; MAP: ART: main effect of sex: $p=0.017$, partial $\eta^2 = 0.225$, $N=25$) and SBP exhibited a trend of being lower in women (ART: main effect of sex: $p=0.081$, partial $\eta^2 = 0.126$, $N=25$). Thirst (as assessed on a Likert scale) increased significantly pre- to post-infusion (ART: main effect of time: $p<0.001$, partial $\eta^2 = 0.366$, $N=30$). Lastly, plasma AVP increased pre-

to post-infusion to a similar extent between men and women (ART: main effect of time: $p=0.012$, partial $\eta^2 = 0.218$; main effect of sex: $p=0.790$, partial $\eta^2 = 0.003$; time*sex interaction: $p=0.729$, partial $\eta^2 = 0.005$, $N=28$; **Figure 4**).

Average sex hormone concentrations are presented in **Table 3**. As expected, serum testosterone was higher in men compared to women ($p<0.001$); and FSH, LH, and progesterone were all higher in women compared to men ($p<0.050$). However, estradiol and progesterone were still relatively low in women, as expected for women tested in the follicular phase of their menstrual cycle (203–205).

2.3.3 Head Motion

Average TR-TR head motion is presented in **Figure 5**. Head motion was minimal in all participants (<0.20 mm) and there were no significant differences between men and women or between baseline and the late phase of the infusion (ART: main effect of phase: $p=0.292$, partial $\eta^2 = 0.037$; main effect of sex: $p=0.183$, partial $\eta^2 = 0.058$; phase*sex interaction: $p=0.573$, partial $\eta^2 = 0.011$, $N=32$).

2.3.4 Functional Connectivity

First, we assessed the functional connectivity between the CVOs. Functional connectivity between the SFO and OVLT displayed a significant phase*sex interaction (phase*sex interaction: $p<0.001$, partial $\eta^2 = 0.317$, $N=32$), such that

functional connectivity increased in men ($p=0.043$) but decreased in women ($p=0.004$) from baseline to the late phase of the infusion (**Figure 6**).

In addition, we assessed the functional connectivity of the SFO and OVLT with several additional cortical and subcortical brain regions involved in salt sensing or perception of thirst (**Figures 7 and 8**). Functional connectivity between the SFO and right ACC decreased significantly from baseline to the late phase of the infusion (main effect of phase: $p=0.029$, partial $\eta^2 = 0.150$, $N=32$); however, there were no sex differences (main effect of sex: $p=0.508$, partial $\eta^2 = 0.015$; phase*sex interaction: $p=0.636$, partial $\eta^2 = 0.008$; **Figure 7B**) and no significant effects were found between the SFO and the left ACC (main effect of phase: $p=0.198$, partial $\eta^2 = 0.055$; main effect of sex: $p=0.369$, partial $\eta^2 = 0.027$; phase*sex interaction: $p=0.827$, partial $\eta^2 = 0.002$, $N=32$, **Figure 7A**). Additionally, functional connectivity did not change significantly and there were not significant sex differences in the functional connectivity of the SFO with the sensory thalamus or left or right insula (all: $p>0.150$, **Figure 7C-E**). There were also no significant effects for functional connectivity of the OVLT with the left or right ACC, sensory thalamus, or left or right insula (all: $p>0.050$, **Figure 8**).

Lastly, we assessed the functional connectivity of the SFO and OVLT with the control ROIs, in which we hypothesized there would not be significant changes in functional connectivity. As hypothesized, there were no significant effects for the functional

connectivity of the SFO or OVLT with the left or right PCC or left or right M1 hand area (all: $p > 0.050$, **Figure 9**).

2.3.5 fALFF

As a complementary fMRI index, we calculated fALFF. fALFF increased from baseline to the late phase of the infusion in the SFO (main effect of time: $p < 0.001$, partial $\eta^2 = 0.336$, $N=32$) and OVLT (ART: main effect of time: $p < 0.001$, partial $\eta^2 = 0.479$, $N=32$) to a similar extent in men and women (both: phase*sex: $p > 0.500$, sex: $p > 0.800$, **Figure 10**). fALFF also increased in the left ACC (ART: main effect of time: $p < 0.001$, partial $\eta^2 = 0.373$, $N=32$), right ACC (ART: main effect of time: $p < 0.001$, partial $\eta^2 = 0.462$, $N=32$), left insula (main effect of time: $p < 0.001$, partial $\eta^2 = 0.536$, $N=32$), right insula (main effect of time: $p < 0.001$, partial $\eta^2 = 0.543$, $N=32$), and sensory subdivision of the thalamus (ART: main effect of time: $p < 0.001$, partial $\eta^2 = 0.560$, $N=32$); however, these responses were not significantly different between men and women (all: phase*sex interactions: $p > 0.050$, main effects of sex: $p > 0.100$, **Figure 11**). For our control ROIs, fALFF increased in the left PCC (main effect of time: $p < 0.001$, partial $\eta^2 = 0.421$, $N=32$) and right PCC (ART: main effect of time: $p = 0.001$, partial $\eta^2 = 0.300$, $N=32$) with similar responses in men and women (both: phase*sex: $p > 0.600$, sex: $p > 0.800$, **Figure 12A-B**); however, as expected, there were no significant changes in fALFF in the left M1 hand area (ART: main effect of time: $p = 0.083$, partial $\eta^2 = 0.097$, $N=32$, **Figure 12C**) or right M1 hand area (main effect of time: $p = 0.139$, partial $\eta^2 = 0.072$, $N=32$, **Figure 12D**).

2.3.6 Correlations

We conducted exploratory correlational analyses to assess the relation between our fMRI outcomes (i.e., functional connectivity and fALFF) and participant screening characteristics and biochemical data. First, we assessed the relation between sex hormone concentrations, menstrual cycle day, and our fMRI outcomes. Serum testosterone was positively correlated with the change in SFO-OVLT functional connectivity from baseline to the late phase of the infusion in men and women combined ($\rho=0.385$, $p=0.033$, $N=31$, **Figure 13A**); however, this relation was absent when only men were analyzed ($\rho=-0.156$, $p=0.565$, $N=16$, **Figure 13B**). Additionally, the day of the menstrual cycle on which women were tested was negatively correlated with baseline SFO-OVLT functional connectivity ($\rho=-0.540$, $p=0.038$, $N=15$, **Figure 14A**), suggesting that women tested later in the follicular phase of their menstrual cycle displayed lower baseline SFO-OVLT functional connectivity; however, baseline SFO-OVLT functional connectivity was not significantly correlated with either serum estradiol ($\rho=0.046$, $p=0.869$, $N=15$, **Figure 14B**) or serum progesterone ($r=0.094$, $p=0.739$, $N=15$, **Figure 14C**) in women. There were no significant correlations for serum estradiol or progesterone with SFO-OVLT functional connectivity or fALFF in these brain regions in either women alone or in the entire cohort (all: $p>0.050$, data not shown).

Additionally, participants' age was significantly associated with the change in SFO-OVLT functional connectivity. In the entire cohort (men and women combined), age

was positively correlated with the change in SFO-OVLT functional connectivity from baseline to the late phase of the infusion ($r=0.488$, $p=0.005$, $N=32$, **Figure 15A**). This response appears to be driven by women as this correlation persisted in only women ($r=0.606$, $p=0.017$, $N=15$, **Figure 15B**) but not in only men ($r=-0.087$, $p=0.739$, $N=17$, **Figure 15C**).

Lastly, since fALFF increased in the left and right PCC, we included the PCC, which was originally one of our control ROIs, in our exploratory correlational analyses. We found that the change in thirst pre- to post-infusion was positively correlated with the change in fALFF in the right PCC from baseline to the late phase of the infusion ($\rho=0.614$, $p<0.001$, $N=30$, **Figure 16A**). There were also trends for positive correlations between the change in thirst and the change in fALFF in the left PCC ($\rho=0.309$, $p=0.096$, $N=30$, **Figure 16B**) and left ACC ($\rho=0.356$, $p=0.054$, $N=30$, **Figure 16C**).

2.4 Discussion

In this study of young, healthy adults we assessed whether there are sex differences in the change in functional connectivity and/or fALFF of brain regions involved in salt sensing during acute relative hypernatremia. Generally, we hypothesized that our IV hypertonic saline infusion protocol would elicit an increase in the functional connectivity and fALFF of our ROIs, which have been implicated in salt sensing or perception of thirst. We also hypothesized that men would have greater responses.

The main findings of this study were as follows: 1) there was a significant interaction for SFO-OVLT functional connectivity, as functional connectivity increased in men but decreased in women from baseline to the late phase of the infusion; 2) the change in SFO-OVLT functional connectivity was positively correlated with serum testosterone, suggesting that testosterone may play a role in this sex-specific response; 3) age was positively correlated with the change in SFO-OVLT functional connectivity; 4) functional connectivity between the SFO and right ACC decreased from baseline to the late phase of the infusion in men and women; and 5) fALFF increased from baseline to the late phase of the infusion in the SFO, OVLT, ACC, insula, and sensory subdivision of the thalamus as well as in the PCC, which we originally chose as a control ROI. We also found that the change in fALFF in the PCC was positively correlated with change in thirst with acute relative hypernatremia.

We assessed functional connectivity of these brain regions to investigate how the synchronization of the low frequency fluctuations in the BOLD signal between our ROIs might change with acute relative hypernatremia. We recently demonstrated that the functional connectivity between the SFO and OVLT increases with acute relative hypernatremia in young healthy adults (140), so we hypothesized that SFO-OVLT functional connectivity would increase in men and women with men demonstrating a greater response. Our primary finding was that there was a significant phase*sex interaction for functional connectivity between the SFO and OVLT, as functional connectivity increased in men but decreased in women. This suggests that men may

rely more heavily on SFO-OVLT connectivity to detect and process changes in the salt concentration in the blood as occurred with this protocol. This finding partially aligns with our hypothesis since men displayed a greater increase in functional connectivity compared to women; however, we initially hypothesized that women would also have an increase in SFO-OVLT functional connectivity, not a reduction. While functional connectivity decreased in women, it is important to note that SFO-OVLT functional connectivity only decreased to a z-score of ~ 0.15 during the late phase from a z-score of ~ 0.27 at baseline, so SFO-OVLT functional connectivity was not completely abolished in women during the late phase. Additionally, women had a slightly higher baseline SFO-OVLT functional connectivity compared to men, albeit not statistically significant; thus, it is possible that there may be a ceiling effect, in which the higher baseline functional connectivity predisposed women to display a reduction in functional connectivity. Altogether, this finding suggests that there may be sex differences in the synchronization of the SFO and OVLT with acute relative hypernatremia.

Additionally, we found that acute relative hypernatremia decreased functional connectivity between the SFO and right ACC with a similar effect in both men and women. This finding is in opposition to another study in which acute relative hypernatremia increased the correlation of regional cerebral blood flow between the ventral lamina terminalis and the right ACC (138). However, in our lab's pilot study, we found that functional connectivity between the OVLT and a cluster in the ACC

was lower during the late phase of the infusion (140), similar to the findings in the present study. This discrepancy could be related to differences in methodology, such as the protocol to achieve hypernatremia (exercise induced dehydration (138) vs hypertonic saline infusion (140)), the use of arterial spin labeling (138) vs BOLD fMRI (140), and different seeds/ROIs for the CVOs. While speculative, the reduction in functional connectivity between the SFO and right ACC observed here may reflect a shift in sodium sensing in which communication is directed to key interoceptive brain regions (such as the SFO and OVLT) preferentially over higher-order brain regions, like the ACC, involved with interpreting and acting on interoceptive signals (140).

As a complementary measure, we calculated fALFF for our ROIs. fALFF reflects the intensity of the spontaneous fluctuations in the BOLD signal in each voxel (163, 184) and is thought to be proportional to local neural activity (178). Since we would anticipate that activity in the CVOs, ACC, insula, and sensory thalamus would increase with acute relative hypernatremia, our findings that fALFF increased in the SFO, OVLT, ACC, insula, and sensory subdivision of the thalamus align with our hypothesis. This is also consistent with previous work demonstrating that hypernatremia (via an IV hypertonic saline infusion) elicits activation of the anterior wall of the third ventricle (i.e., lamina terminalis), ACC, insula, and part of the thalamus (136). These brain regions are also implicated in salt sensing/perception of thirst in a few other studies (137, 138, 140). While fALFF increased in these brain

regions as expected, the responses were not significantly different between men and women, contrary to our hypothesis. The lack of sex differences in fALFF reflect the similar responses we observed for other physiological parameters, such as plasma osmolality, serum sodium, plasma AVP, SBP, and thirst. Given these variables changed to a similar extent in men and women, it may not be surprising that there were not sex differences in change in fALFF. One possibility for why these responses were similar between men and women may be that women were tested during the follicular menstrual cycle phase, when circulating concentrations of female sex hormones are relatively low. If potential sex differences are driven by sex hormones, it is possible that if women were tested during the luteal phase, when circulating sex hormone concentrations are higher, sex differences may have been more apparent.

While we originally chose the PCC as a control ROI, hypothesizing no significant changes, fALFF increased in the left and right PCC from baseline to the late phase of the infusion. Our motivation to choose the PCC as a control ROI was based on 1) its primary role in “internal mentation” as a major hub of the default mode network, not being directly involved in central salt sensing (198), and 2) our pilot study in which functional connectivity between the SFO and PCC did not change significantly with this same protocol (140). We hypothesize that the changes in fALFF observed here may be related to the role of the PCC in thirst, since previous studies demonstrate that the PCC may be involved in thirst. One study using PET found that the PCC was activated in response to a 25-minute IV hypertonic saline infusion (136). Another

study using ASL found that an exercise-induced dehydration protocol also led to activation in the PCC (138). Indeed, in the present study, the change in fALFF in the PCC was positively correlated with the change in thirst (**Figure 16**). This supports the involvement of the PCC in the emotional/cognitive dimensions of thirst, such as the awareness of the urge to drink. While fALFF increased in the PCC, there were no significant effects on fALFF in the M1 hand area. This suggests that the changes in fALFF observed are not global changes distributed universally across the entire brain, strengthening the results observed for fALFF in the sodium sensing brain regions.

In an exploratory analysis, we assessed whether our fMRI outcomes correlated with serum sex hormone concentrations. A study in ovariectomized adult female Wistar rats demonstrated that estradiol decreases the basal discharge of SFO neurons and the response of SFO neurons to intracarotid injection of hypertonic saline (128); thus, we hypothesized that higher serum estradiol concentration would be associated with lower functional connectivity and fALFF of the CVOs and less of a response to our perturbation. While menstrual cycle day was negatively correlated with baseline SFO-OVLT functional connectivity, we did not find any significant correlations between our fMRI outcomes and serum estradiol or progesterone. It is unclear why women tested later in their menstrual cycle, but not female sex hormone concentrations were correlated with SFO-OVLT functional connectivity. It may be that a combination of sex hormones (rather than estradiol or progesterone alone) accounts for this effect or a separate underlying mechanism may be involved. The lack of significant correlations

with female sex hormones may also be partly because women were tested in the follicular phase when serum estradiol and progesterone are still relatively low. It is possible that significant associations would have been detected if women were tested across the entire menstrual cycle and participants had a larger range for serum estradiol and progesterone. While significant correlations were absent for female sex hormones, serum testosterone was positively correlated with the change in SFO-OVLT functional connectivity from baseline to the late phase of the infusion in men and women combined, suggesting that testosterone may be associated with the heightened synchrony between the CVOs in men during the late phase of the infusion. This is consistent with our hypothesis and aligns with existing research demonstrating that testosterone may contribute to salt sensitivity of BP in rodents (46, 206, 207).

In addition to sex hormone concentrations, we assessed the relation between age and our fMRI outcomes. In men and women together, age was positively correlated with the change in SFO-OVLT functional connectivity from baseline to the late phase of the infusion. This response appears to be driven by women as this correlation persisted in only women but not in only men. These correlations suggest that adults who are older tend to have a greater change in SFO-OVLT functional connectivity with salt loading. This finding requires validation in a cohort with a wider age range; however, it appears to be consistent with the literature suggesting that older adults are more salt sensitive than younger adults (30).

This study has several strengths, including 1) a highly controlled stimulus to minimize variability (3% NaCl for 30 min at rate of $0.15 \text{ ml} \cdot \text{kg}^{-1} \cdot \text{min}^{-1}$), 2) verification of the effectiveness of our perturbation by assessing changes in serum electrolytes, plasma osmolality, and plasma AVP, and 3) testing women who were not using hormonal contraception in the follicular phase of their menstrual cycle to control for sex hormone-mediated variability among women. Additionally, we utilized two complementary measures (functional connectivity and fALFF) to investigate activation of the above salt sensing brain regions in humans. There are multiple ways that brain activity can change with a perturbation, including a change in the magnitude of the activity, the extent of the activation, and/or how the brain region communicates with other areas. By combining fALFF and functional connectivity, we were able to assess the intensity/magnitude of the spontaneous fluctuations in the BOLD signal in each individual brain region (fALFF) (163, 184) and the synchronization of low frequency fluctuations in the BOLD signal between our ROIs (functional connectivity). Lastly, we included two control ROIs (PCC and M1 hand area), both of which displayed no significant effects for functional connectivity, and there were no significant effects on fALFF in the M1 hand area. This suggests that changes in functional connectivity and fALFF are not distributed universally across the entire brain, strengthening the results observed in the sodium sensing brain regions.

While our study has several strengths, we also recognize a few limitations. First, this study was not designed to differentiate between salt- vs osmo-sensing; however, in

rodents, OVLT neurons have been shown to respond more robustly to hypertonic saline than hypertonic mannitol/sorbitol, suggesting a primarily salt-sensing mechanism (104). Additionally, we are unable to identify the molecular mechanisms of salt sensing in this experiment. Several molecular mechanisms of central salt sensing have been suggested, including the N²-terminal variant of transient receptor vanilloid potential 1 (nTRPV1) channel (208, 209), the epithelial sodium channel (ENaC) (210–212), a glial NaX channel (213, 214), and the Na-K-2Cl cotransporter (NKCC2) (110, 215); the importance of each of these mechanisms requires further investigation. Second, while we recognize the importance of testing women across the menstrual cycle, we tested women who were not using hormonal contraceptives during the follicular phase based on previous studies showing that sex hormones affect osmotic regulation across the menstrual cycle (114) and recommendations for testing women in research (216). Thus, future studies are warranted to investigate whether there are differences in salt sensing during acute hypernatremia across the menstrual cycle and whether hormonal contraception may affect these responses. A detailed discussion of the technical limitations associated with this approach can be found in our group's previous publication (140).

2.5 Conclusion

In this study of young, healthy adults, we found that acute relative hypernatremia elicited changes in the activation patterns of several salt sensing brain regions. In this cohort, men and women displayed similar physiological responses to acute

hypernatremia, including similar changes in SBP, serum sodium, plasma AVP, and thirst. Consistent with this lack of sex differences, functional connectivity decreased between the SFO and right ACC and fALFF increased in the SFO, OVLT, ACC, PCC, insula, and sensory subdivision of the thalamus with similar responses between men and women. However, functional connectivity between the SFO and OVLT increased in men but decreased in women with salt loading, indicating a sex-specific response. Interestingly, serum testosterone was positively correlated with the change in SFO-OVLT functional connectivity, suggesting that testosterone may play a role. Altogether, these results bolster existing evidence that several brain regions are involved in salt sensing and/or perception of thirst in humans. Additionally, although most responses were similar between men and women, we demonstrate that there may be sex differences in the synchronization of the SFO and OVLT during acute hypernatremia. These findings set the stage for additional work to investigate mechanisms of central salt sensing in humans and potential sex differences across the lifespan.

Table 1 Participant screening characteristics.

	Overall (N=32)	Men (N=17)	Women (N=15)	P-value (men vs women)
Race, N (%)				
White	13 (40.6%)	6 (35.3%)	7 (46.7%)	
Black	6 (18.8%)	5 (29.4%)	1 (6.7%)	
Asian	8 (25.0%)	4 (23.5%)	4 (26.7%)	
American Indian	1 (3.1%)	1 (5.9%)	0 (0.0%)	
> 1 race/other/not reported	4 (12.5%)	1 (5.9%)	3 (20.0%)	
Age, yr	27±4	29±3	24±4*	0.003
Height, cm	171.0±8.3	175.6±6.0	165.8±7.3*	<0.001
Mass, kg	70.3±12.3	77.2±11.1	62.5±8.4*	<0.001
BMI, kg·m ⁻²	23.9±2.8	25.0±2.8	22.7±2.2*	0.018
SBP, mmHg	106±8	111±5	101±8*	<0.001
DBP, mmHg	67±6	69±6	65±4	0.071
Total Cholesterol, mg/dL	172±27	174±29	169±25	0.570
HDL Cholesterol, mg/dL	57±10	53±6	63±11*	0.010
LDL Cholesterol, mg/dL	98±24	103±27	91±19	0.141
Triglycerides, mg/dL	78±33	88±38	66±22*	0.027
Glucose, mg/dL	93±7	94±8	90±4	0.153

*p<0.05 vs men. Data are represented as mean ± standard deviation. BMI, body mass index; DBP, diastolic blood pressure; HDL, high density lipoprotein; LDL, low density lipoprotein; SBP, systolic blood pressure. Independent 2-tailed t-tests or Mann-Whitney U tests were used.

Table 2 Blood pressure, thirst, and biochemical data pre- and post-hypertonic saline infusion.

	Overall		Men		Women		P-value		
	Pre	Post	Pre	Post	Pre	Post	Time	Sex	Time*Sex
SBP, mmHg (N=25, 12 W/13 M)	114±10	117±11*	118±7	120±8*	109±11	113±13*	0.038	0.081	0.538
DBP, mmHg (N=25, 12 W/13 M)	66±8	67±7	70±5	69±7	61±8 [†]	64±7 [†]	0.616	0.009	0.169
MAP, mmHg (N=25, 12 W/13 M)	82±8	83±8	86±4	86±7	77±9 [†]	80±8 [†]	0.173	0.017	0.248
Thirst, cm (N=30, 15 W/15 M)	4.3±2.1	6.0±2.3*	4.6±1.9	6.0±2.5*	4.0±2.4	6.0±2.1*	<0.001	0.705	0.610
USG (N=27, 13 W/14 M)	1.016±0.009	N/A	1.018±0.009	N/A	1.015±0.009	N/A	N/A	0.519	N/A
Hct, % (N=27, 11 W/16 M)	42±4	40±4*	45±4	42±3*	38±2 [†]	36±3* [†]	<0.001	<0.001	0.303
Hb, g/dL (N=26, 10 W/16 M)	13.3±1.9	12.6±1.6*	14.2±1.8	13.3±1.5*	11.9±1.0 [†]	11.5±0.8* [†]	<0.001	0.002	0.018
Plasma Osm, mOsm/kg H ₂ O (N=29, 14 W/15 M)	287±3	293±3*	288±2	294±2*	286±4	292±3*	<0.001	0.143	0.852
Serum Na, mmol/L (N=30, 14 W/16 M)	138.4±2.0	141.5±1.8*	138.2±1.7	141.4±2.0*	138.5±2.4	141.7±1.7*	<0.001	0.661	0.964
Serum K, mmol/L (N=29, 13 W/16 M)	4.13±0.32	4.27±0.37*	4.16±0.33	4.33±0.37*	4.08±0.31	4.20±0.37*	0.006	0.336	0.225
Serum Cl, mmol/L (N=30, 14 W/16 M)	106.3±2.4	111.9±2.3*	105.8±2.8	111.2±2.9*	106.9±1.7	112.6±1.2*	<0.001	0.125	0.701
Plasma AVP, pg/ml (N=28, 12 W/16 M)	22.4±9.7	28.3±13.6*	22.5±9.8	27.1±13.8*	22.3±9.9	29.8±13.8*	0.012	0.790	0.729

*p<0.05 vs pre-infusion, [†]p<0.05 vs men. Data are represented as mean ± standard deviation. AVP, arginine vasopressin; Cl, Chloride; DBP, diastolic blood pressure; Hb, hemoglobin; Hct, hematocrit; K, potassium; M, men; MAP, mean arterial pressure; Na, sodium; Osm, osmolality; SBP, systolic blood pressure; USG, urine specific gravity; W, women. 2x2 repeated measures ANOVAs were used, except for USG, which utilized a Mann-Whitney U test.

Table 3 Serum sex hormone concentrations on the day of the MRI and infusion visit.

	Overall (n=31)	Men (n=16)	Women (n=15)	p-value
Estradiol, pg/mL	39.94±20.66	32.77±9.97	47.59±26.20	0.188
FSH, mIU/mL	5.08±2.16	3.78±1.57	6.47±1.84 [†]	<0.001
LH, mIU/mL	5.32±2.00	4.56±1.06	6.12±2.45 [†]	0.035
Progesterone, ng/mL	0.194±0.108	0.151±0.101	0.239±0.099 [†]	0.022
Testosterone, ng/dL	290.5±280.6	536.7±154.2	27.9±11.8 [†]	<0.001

[†]p<0.05 vs men. Data are represented as mean ± standard deviation. FSH, follicle-stimulating hormone; LH, luteinizing hormone. Independent 2-tailed t-tests or Mann-Whitney U tests were used.

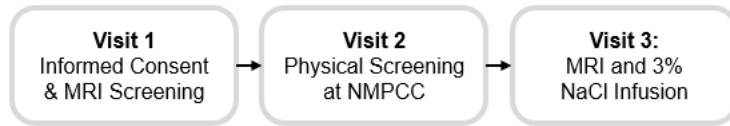


Figure 1 Experimental design. Participants completed 3 visits, including 1) an informed consent and preliminary MRI screening, 2) a physical screening at the nurse managed primary care center (NMPCC), and 3) the MRI and hypertonic saline (3% NaCl) infusion data collection. All women completed the MRI and infusion visit within the first 12 days of their menstrual cycle. MRI, magnetic resonance imaging.

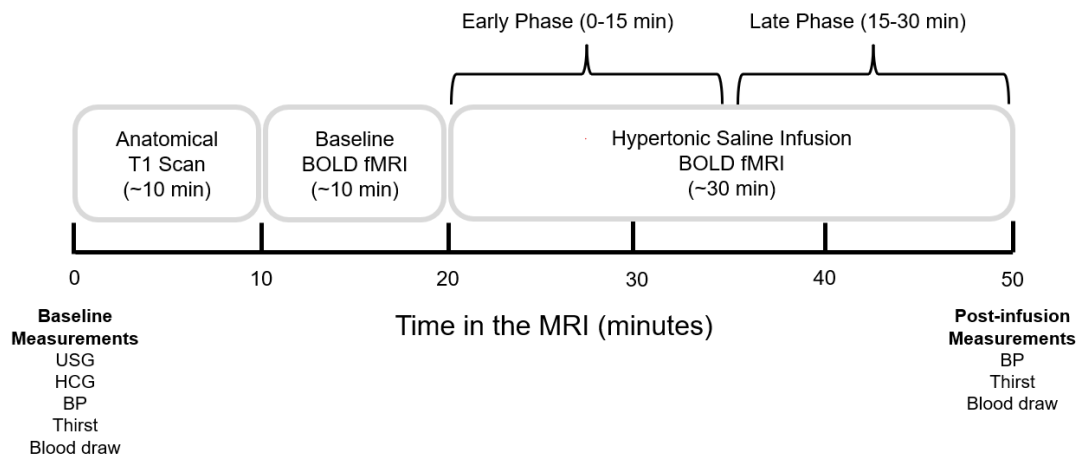
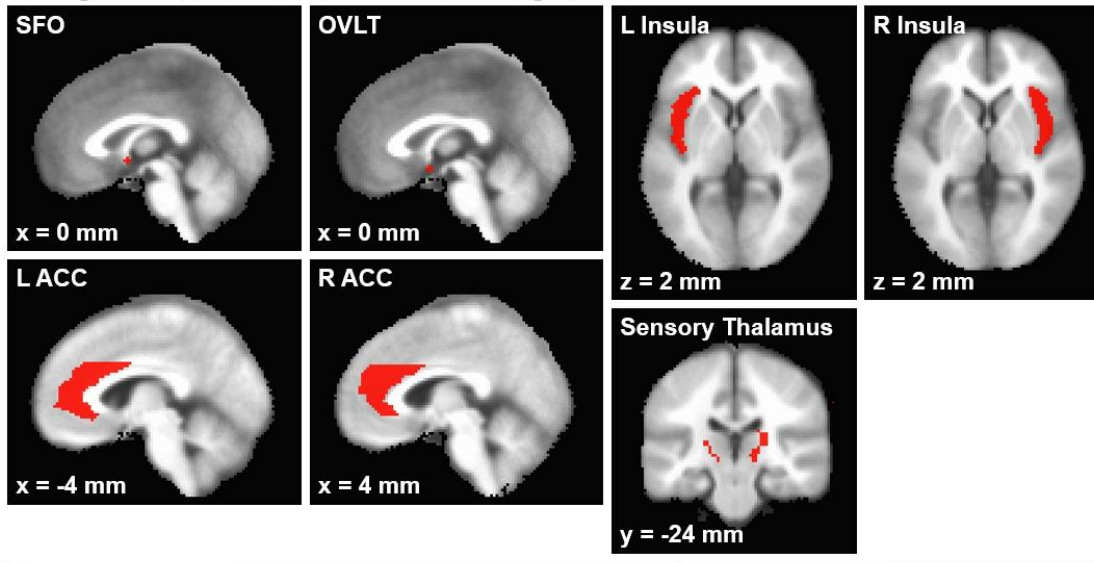


Figure 2 MRI and hypertonic saline infusion protocol. Participants provided a spot urine sample at baseline to assess urine specific gravity (USG), and a human chorionic gonadotropin (HCG) pregnancy test was performed for all women. Baseline blood pressure (BP), thirst, and blood samples were also obtained. Participants underwent a T1-weighted anatomical scan and BOLD fMRI scan at baseline, followed by a 30-minute BOLD fMRI scan during an IV hypertonic saline infusion. BP, thirst, and blood samples were obtained following the infusion. BOLD fMRI, blood oxygen level dependent functional magnetic resonance imaging; BP, blood pressure; IV, intravenous.

A. Regions of Interest Involved in Salt Sensing and Thirst



B. Control Regions of Interest

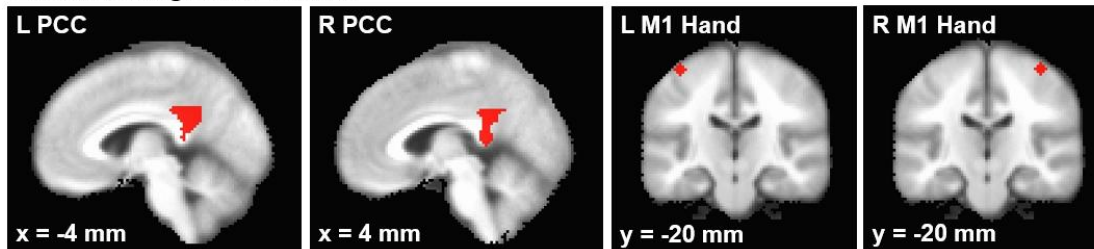


Figure 3 Regions of interest for the resting state fMRI analysis: regions of interest involved in salt sensing and thirst (A) and control regions of interest (B). The name of each brain region is in the upper left with the slice position indicated in the lower left. ACC, anterior cingulate cortex; fMRI, functional magnetic resonance imaging; L, left; M1, primary motor cortex; OVLT, organum vasculosum of the lamina terminalis; PCC, posterior cingulate cortex; R, right; SFO, subfornical organ.

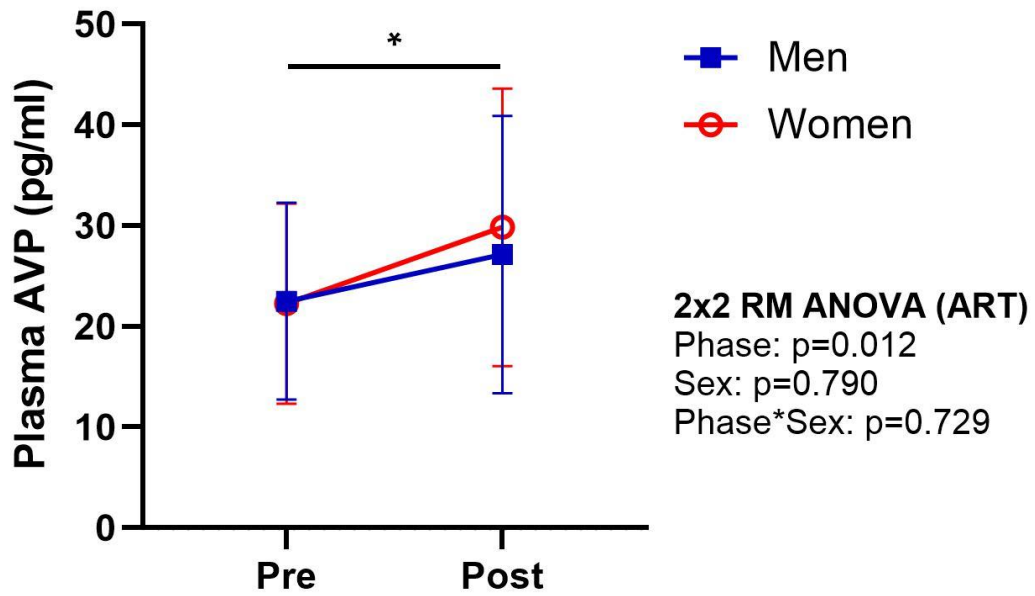


Figure 4 Plasma AVP increases pre- to post-infusion. Data are presented as mean \pm standard deviation. * $p < 0.05$ pre- vs post-infusion. ART, aligned rank transformation; AVP, arginine vasopressin; RM ANOVA, repeated measures analysis of variance.

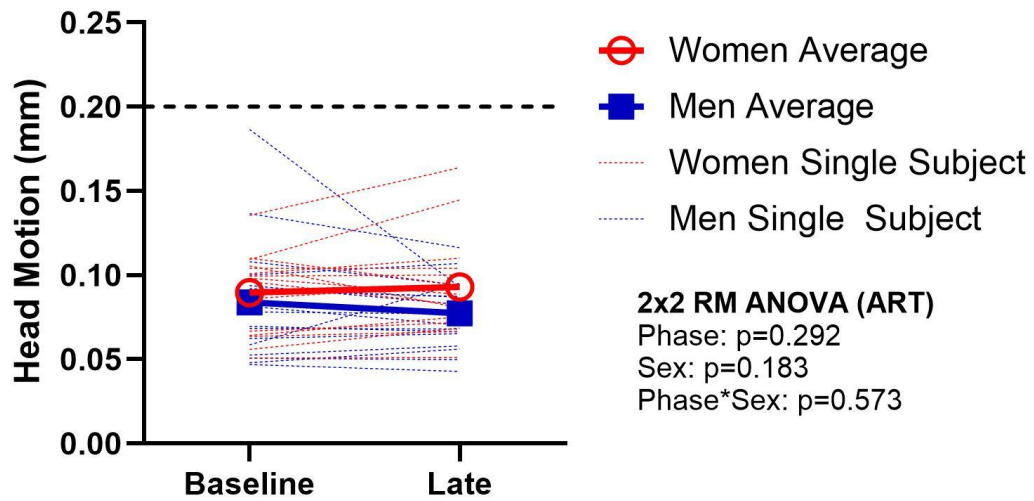


Figure 5 Average TR-to-TR head motion during baseline and the late phase (15-30 minutes) of the hypertonic saline infusion. Head motion was minimal (<0.20 mm) in all participants and there were no significant differences between the phases or sexes. The average response for men is represented by the blue solid squares/line; the average response for women is represented as the red open circles/line. Individual subject responses are shown as blue (men) or red (women) dashed lines. ART, aligned rank transformation; RM ANOVA, repeated measures analysis of variance.

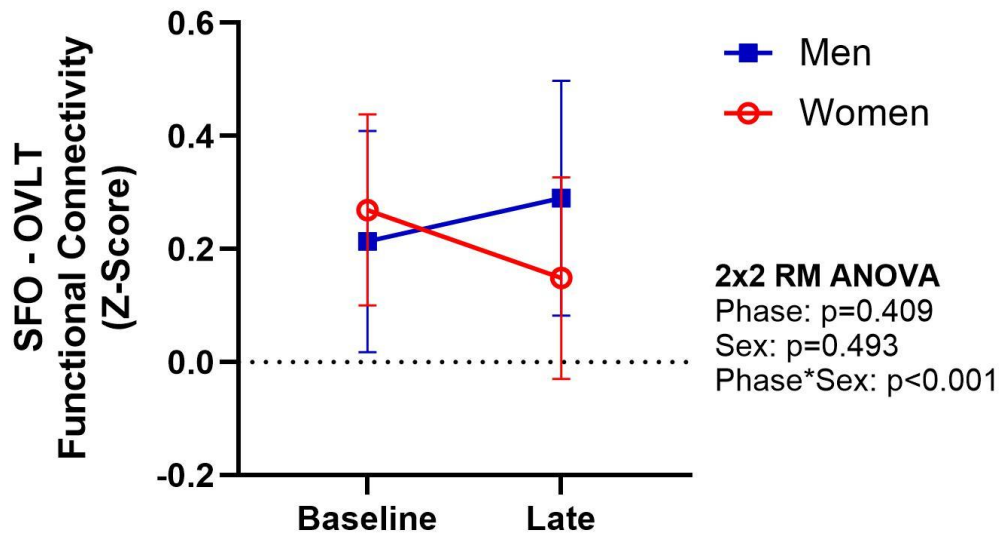


Figure 6 Functional connectivity between the subfornical organ (SFO) and organum vasculosum of the lamina terminalis (OVLT). There is a significant phase*sex interaction and post-hoc testing reveals that functional connectivity increased in men ($p=0.043$) but decreased in women ($p=0.004$) from baseline to the late phase of the infusion. Data are presented as mean \pm standard deviation. RM ANOVA, repeated measures analysis of variance.

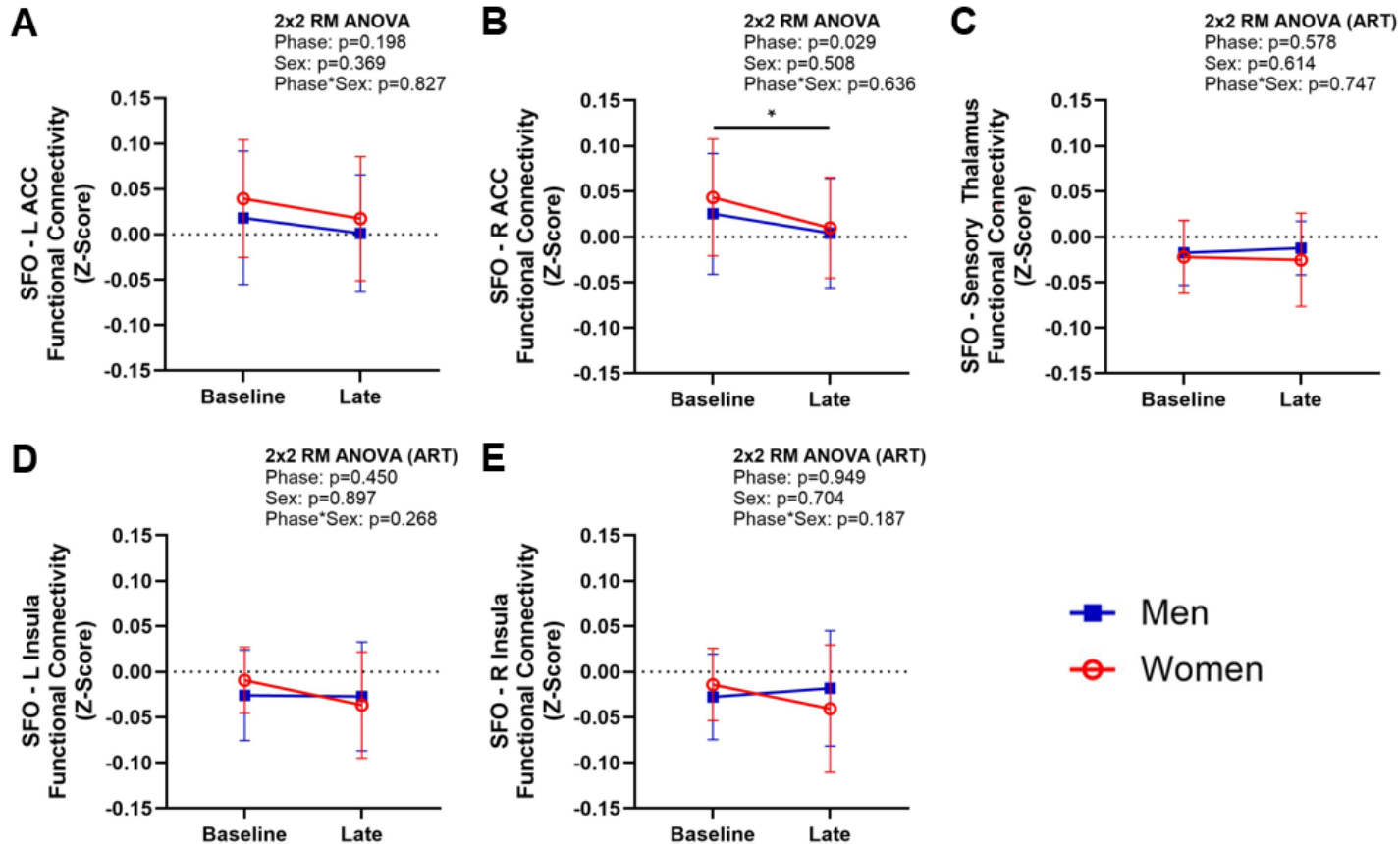


Figure 7 Functional connectivity between the subformal organ (SFO) and additional regions of interest including the left (L) and right (R) anterior cingulate cortex (ACC) (A & B), sensory thalamus (C), and L and R insula (D & E). Data are presented as mean \pm standard deviation. * $p < 0.05$ for baseline vs late phase. ART, aligned rank transformation; RM ANOVA, repeated measures analysis of variance.

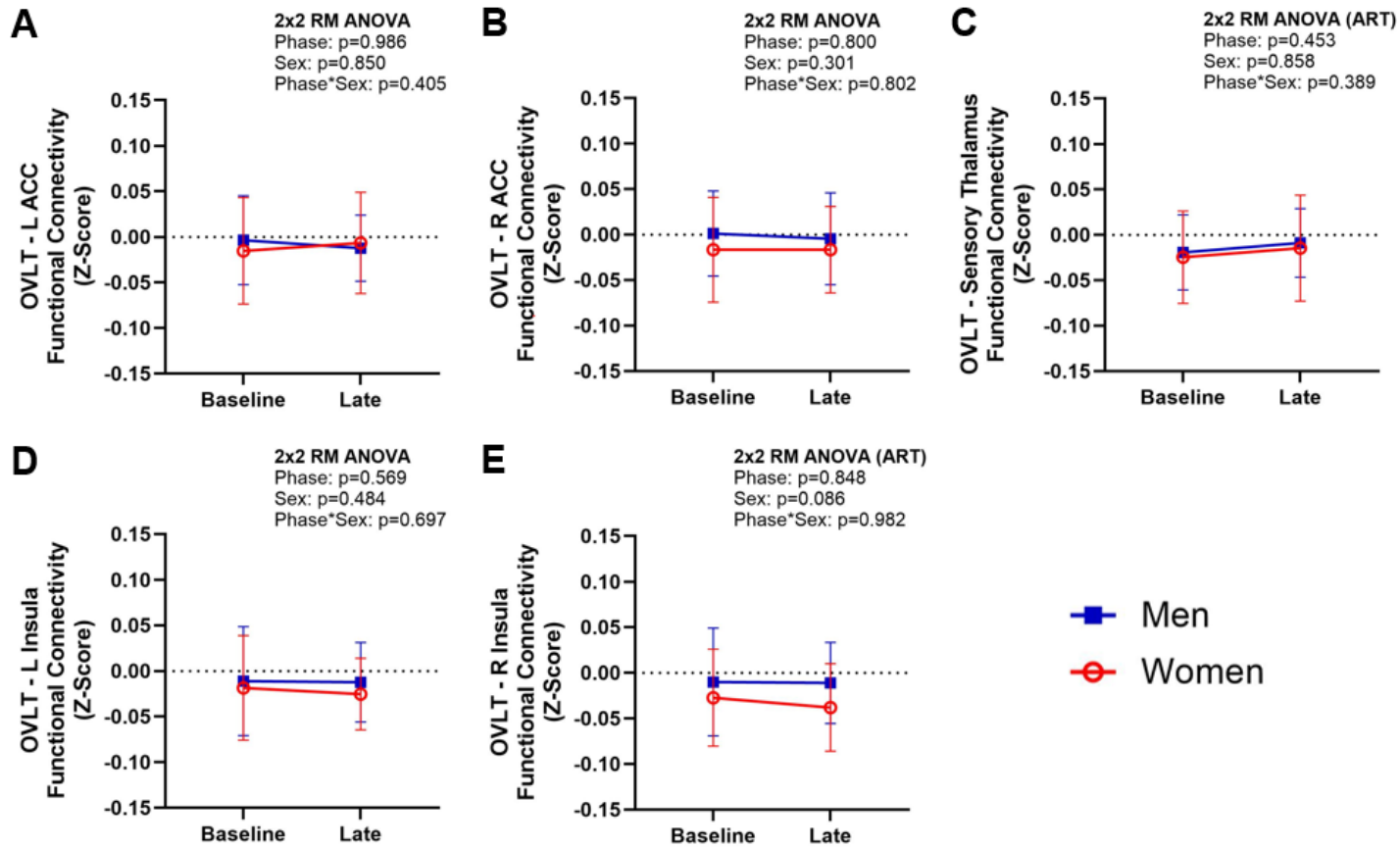


Figure 8 Functional connectivity between the organum vasculosum of the lamina terminalis (OVLT) and additional cortical or subcortical regions of interest, including the left (L) and right (R) anterior cingulate cortex (ACC) (A & B), sensory thalamus (C), and L and R insula (D & E). Data are presented as mean \pm standard deviation. ART, aligned rank transformation; RM ANOVA, repeated measures analysis of variance.

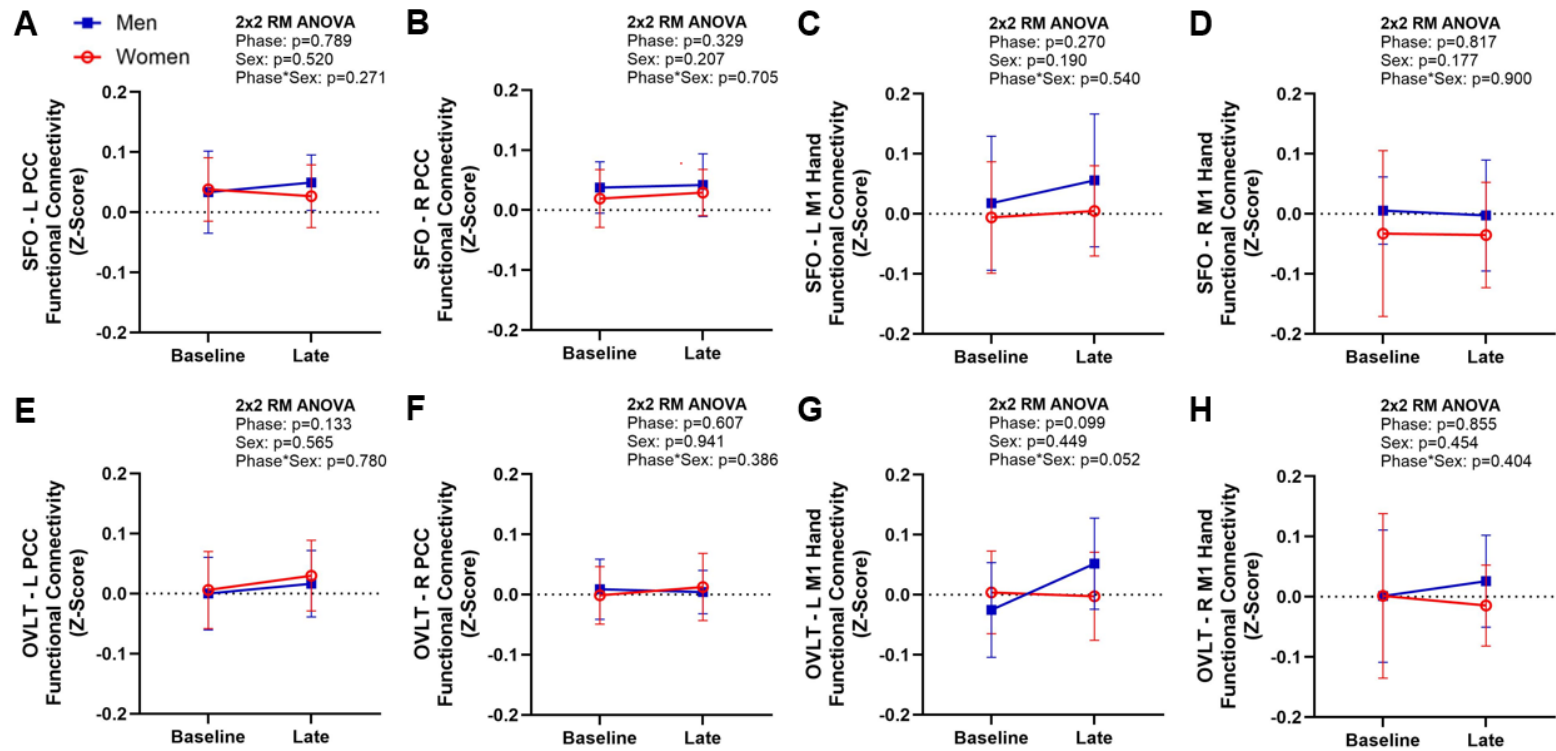


Figure 9 Functional connectivity between the CVOs and our control regions of interest, including the subformal organ (SFO) with the left (L) and right (R) PCC (A & B) and L and R M1 hand area (C & D), as well as the organum vasculosum of the lamina terminalis (OVLT) with the L and R PCC (E & F) and L and R M1 hand area (G & H). Data are presented as mean \pm standard deviation. CVOs, circumventricular organs; M1, primary motor cortex; PCC, posterior cingulate cortex; RM ANOVA, repeated measures analysis of variance.

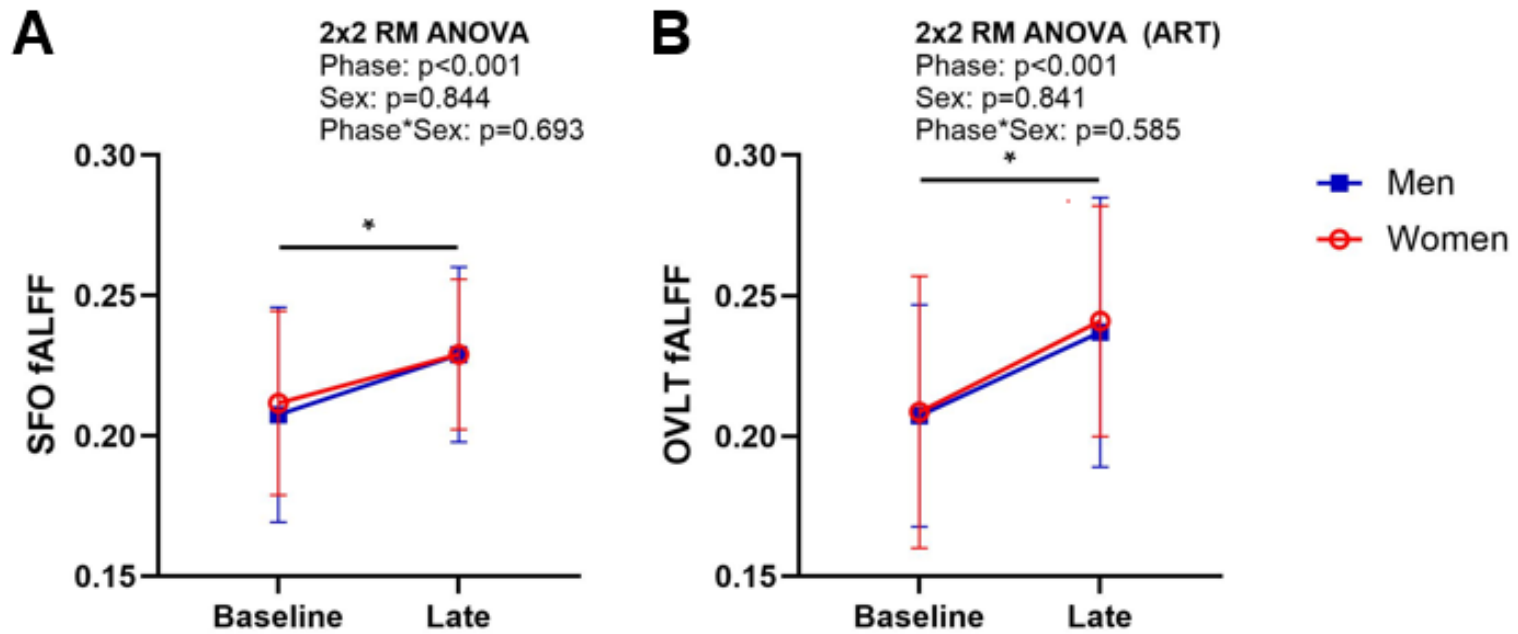


Figure 10 Fractional amplitude of low frequency fluctuations (fALFF) of the subformical organ (SFO) (A) and organum vasculosum of the lamina terminalis (OVLT) (B). Data are presented as mean \pm standard deviation. * $p < 0.001$ for baseline vs late phase. ART, aligned rank transformation; RM ANOVA, repeated measures analysis of variance.

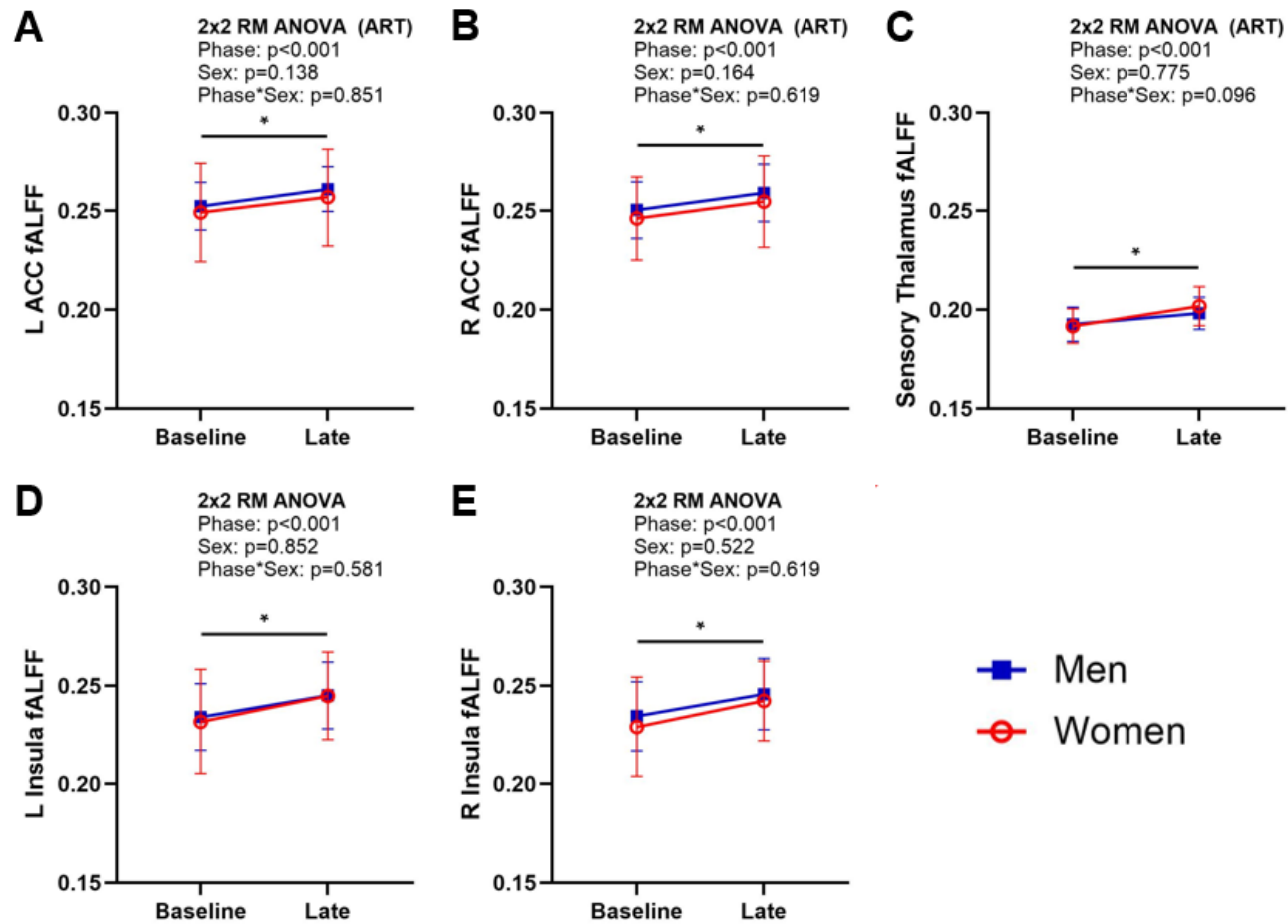


Figure 11 Fractional amplitude of low frequency fluctuations (fALFF) of additional regions of interest. fALFF was calculated for the left (L) and right (R) anterior cingulate cortex (ACC) (A & B), sensory thalamus (C), and L and R insula (D & E). Data are presented as mean \pm standard deviation. * $p < 0.001$ for baseline vs late phase. ART, aligned rank transformation; RM ANOVA, repeated measures analysis of variance.

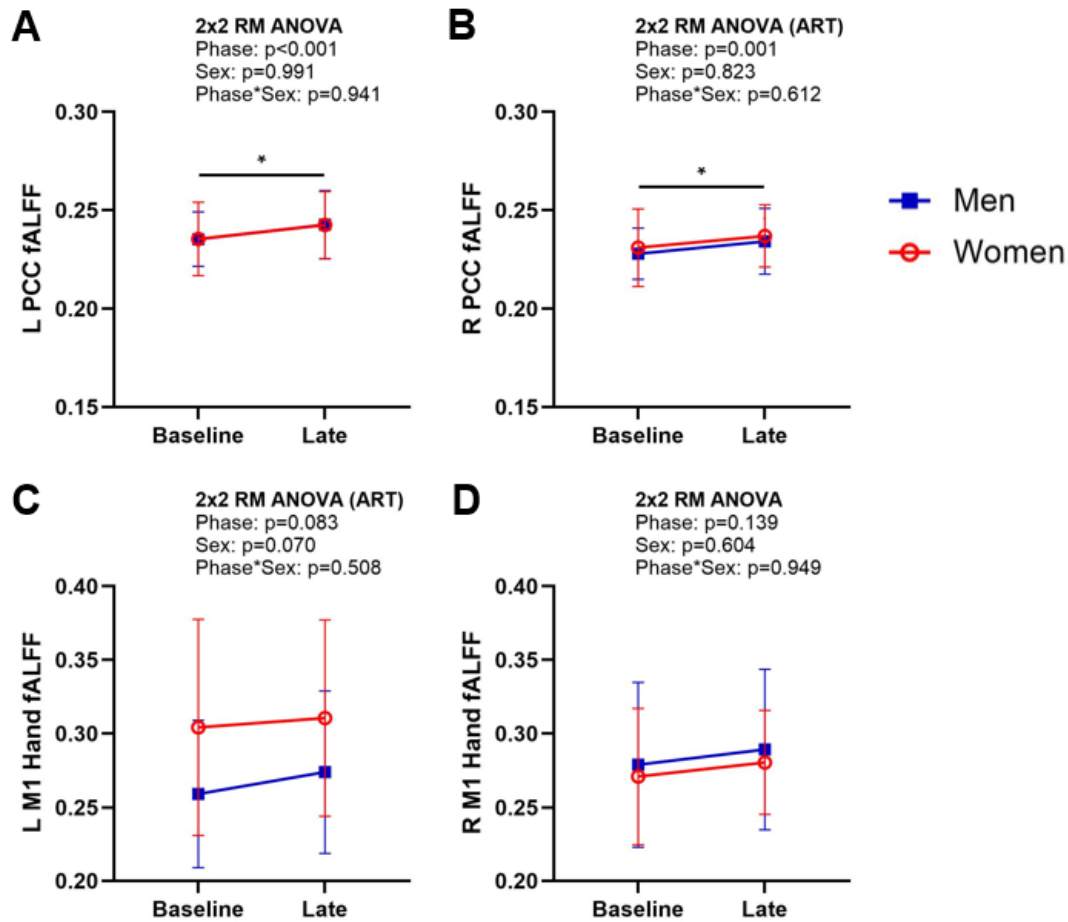


Figure 12 Fractional amplitude of low frequency fluctuations (fALFF) of control regions of interest, including the left (L) and right (R) PCC (A & B) and L and R M1 hand area (C & D). Data are presented as mean \pm standard deviation. * $p < 0.005$ for baseline vs late phase. ART, aligned rank transformation; M1, primary motor cortex; PCC, posterior cingulate cortex; RM ANOVA, repeated measures analysis of variance.

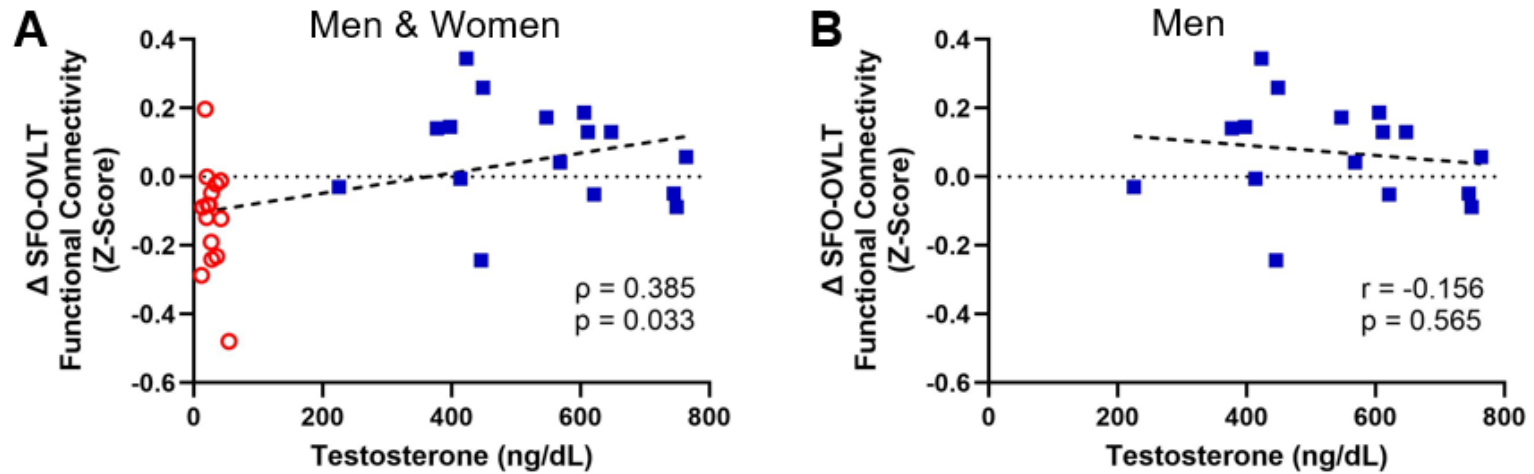


Figure 13 Correlations between serum testosterone and the change in SFO-OVLT functional connectivity with acute relative hypernatremia. Results are presented for the entire cohort (A) and for men separately (B). Blue closed squares represent men; red open circles represent women. OVLT, organum vasculosum of the lamina terminalis; SFO, subfornical organ. Pearson (r) or Spearman's (ρ) correlations were calculated.

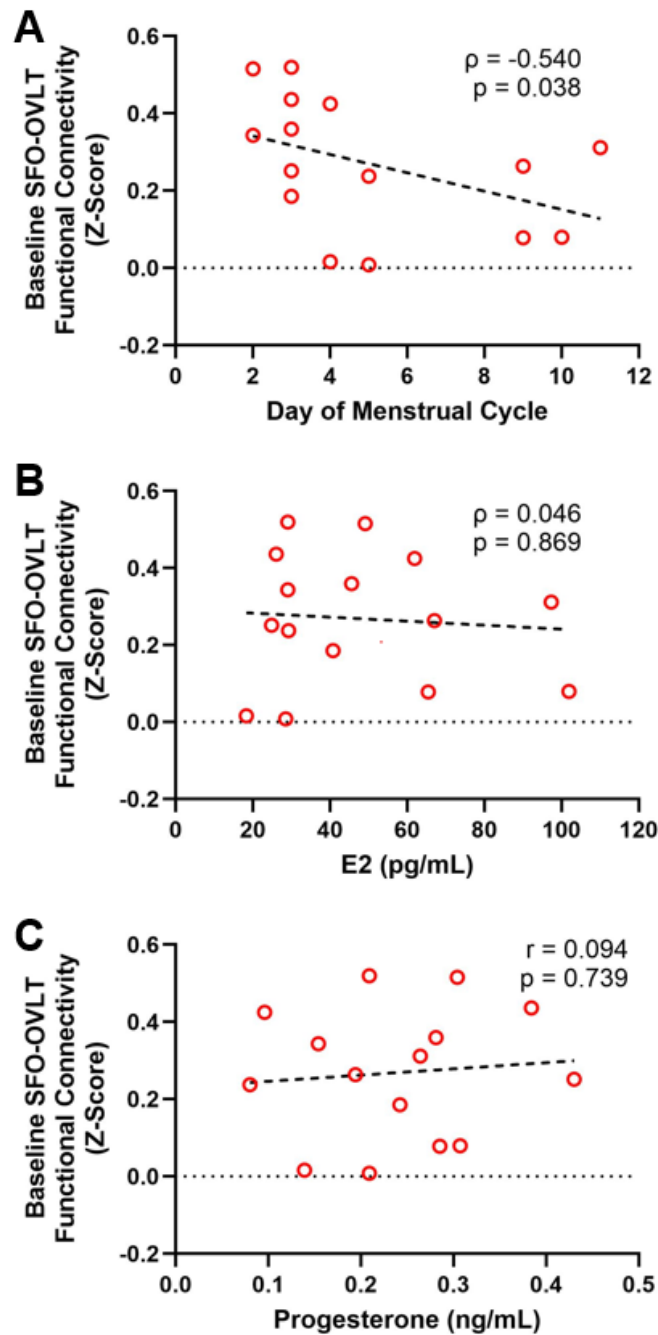


Figure 14 Correlations between baseline SFO-OVLT functional connectivity and the day of the menstrual cycle on which women were tested (A), serum estradiol (B), and serum progesterone (C) in women. Pearson (r) or Spearman's correlations (ρ) were calculated. E2, estradiol; OVLT, organum vasculosum of the lamina terminalis; SFO, subfornical organ.

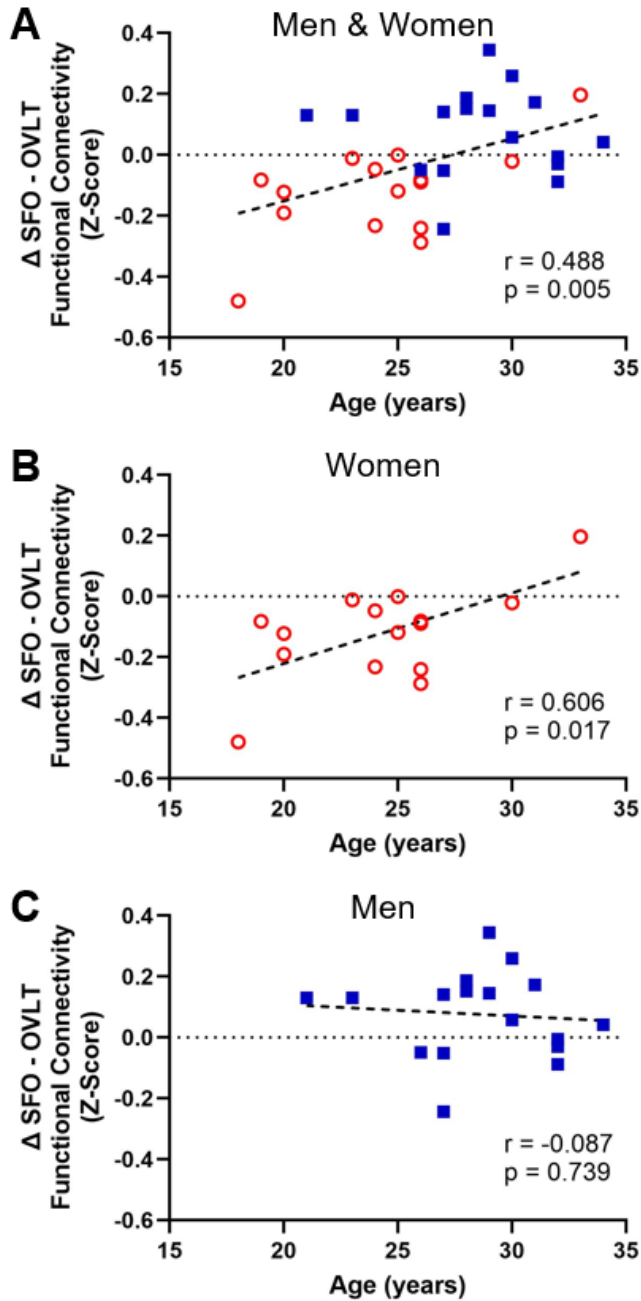


Figure 15 Correlations between age and the change in functional connectivity between the subfornical organ (SFO) and organum vasculosum of the lamina terminalis (OVLT) in the entire cohort (A), women alone (B), and men alone (C). Blue closed squares represent men; red open circles represent women. Pearson correlations (r) were used.

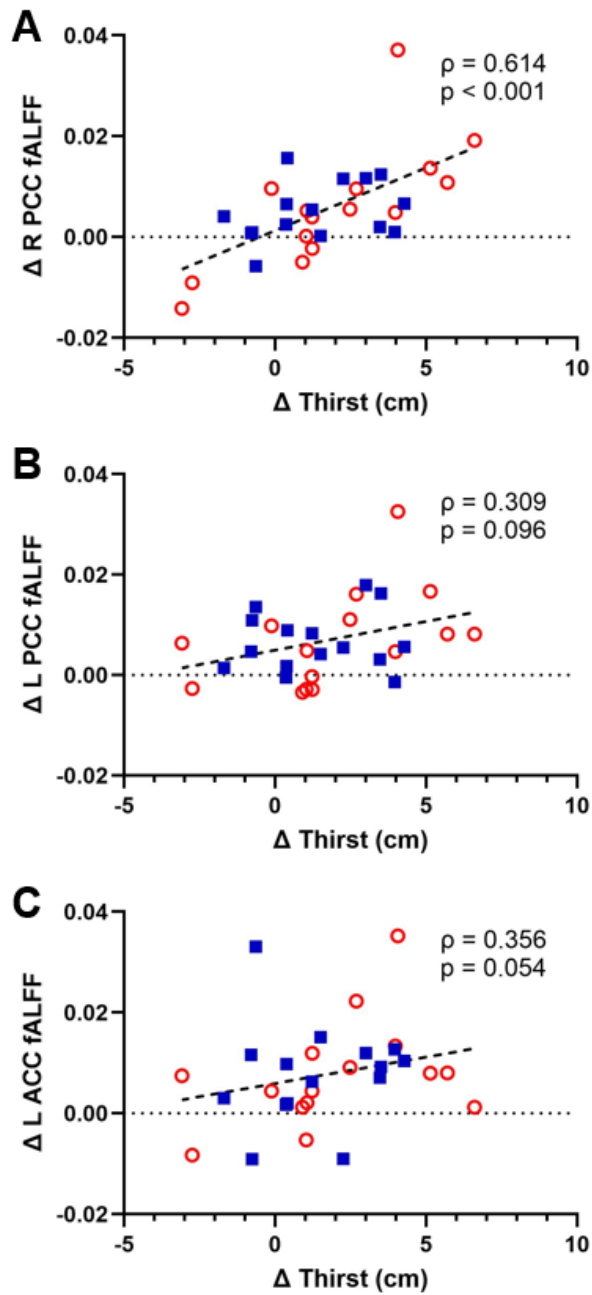


Figure 16 Correlations between the change in thirst and the change in fALFF in the right and left PCC (A & B) and in the left ACC (C). Blue closed squares represent men; red open circles represent women. ACC, anterior cingulate cortex; fALFF, fractional amplitude of low frequency fluctuations; L, left; PCC, posterior cingulate cortex; R, right. Spearman's correlations (ρ) were calculated.

Chapter 3

SEX DIFFERENCES IN THE ACTIVATION OF SYMPATHOREGULATORY BRAIN REGIONS DURING ACUTE HYPERNATREMIA

3.1 Introduction

While blood pressure (BP)-related diseases remain a major public health challenge in both sexes (1, 4), men have a higher prevalence of hypertension compared to women until about age 65, after which the prevalence is greater in women, reflecting a greater age-related increase in BP in women after menopause (1, 2, 5). The high prevalence of hypertension in adults may be partly because adults consume more salt than recommended (187) since elevated salt intake is associated with increased BP (1, 7, 11–13, 15, 16). Additionally, while not all consistent, several studies suggest that there are sex differences in salt sensitivity of BP in humans (19, 38–41) and rodents (45–49). Thus, investigating the mechanisms underlying sex differences in responses to salt may be important in understanding disparities in the prevalence of hypertension between men and women.

One mechanism that is thought to contribute to salt sensitivity of BP is an altered neurogenic response to salt loading, since the nervous system responds to both acute

and chronic salt loading (8, 25, 77, 80, 81, 87, 89, 90). Acute hypernatremia increases sympathetic nerve activity (SNA) and BP in both rodent models (77, 78) and humans (79–82). However, changes in SNA with salt loading are region specific. Intravenous (IV) hypertonic saline infusion in Sprague-Dawley rats increases lumbar SNA but reduces splanchnic and renal SNA (83). Similarly, infusion of saline into the lateral ventricle of male Sprague-Dawley rats increases lumbar SNA, adrenal SNA, and BP, while renal SNA decreases, and splanchnic SNA remains unchanged (84). Part of this response may be baroreceptor-dependent, since animals with sinoaortic denervation display earlier increases in lumbar SNA and no change in splanchnic SNA (rather than a reduction in splanchnic SNA) with IV hypertonic saline infusion (83). Additionally, Dahl salt sensitive rats fed a high salt diet for 3-4 weeks have a greater discharge of salt-sensitive organum vasculosum of the lamina terminalis (OVLT) neurons compared to Dahl salt sensitive rats fed a low salt diet or Dahl salt resistant rats; furthermore, injecting a gamma-aminobutyric acid (GABA) agonist to inhibit OVLT neurons elicits larger reductions in renal and splanchnic SNA and BP in Dahl salt sensitive rats fed the high salt diet. This suggests that chronic salt loading increases SNA and therefore arterial BP via the OVLT in this model of SS hypertension (88). Collectively, these experiments suggest that there may be a neurogenic component to salt sensitivity of BP.

There are also sex differences in autonomic responses to salt loading. First, female Dahl salt sensitive rats have lower BP compared to male animals with high salt intake,

which may be partially explained by lower sympathetic activity in female animals (93). Second, deoxycorticosterone acetate (DOCA) salt treatment elicits larger increases in BP in male rats, which is associated with a greater reduction in baroreflex sensitivity in male animals (94). Third, male DOCA-salt rats have higher catecholamine concentrations in the adrenal medulla than female animals and surgical removal of the adrenal medulla lowers BP in only male animals (95). Fourth, treatment of Sprague Dawley rats with aldosterone and salt for 28 days increases BP to a greater extent in males than in females, which is likely driven by lower sympathetic outflow in female animals (48). Thus, in salt sensitive rodent models, male animals have greater changes in BP, which can be attributed to differences in neural control of BP.

The above sympathetic responses are largely mediated via the baroreceptors and associated brainstem nuclei, including the nucleus tractus solitarius (NTS), caudal ventrolateral medulla (CVLM), and rostral ventrolateral medulla (RVLM) (**Figure 17**) (141). These brainstem nuclei have been identified using functional magnetic resonance imaging (fMRI). Macefield and Henderson conducted a novel study in which they performed concurrent muscle sympathetic nerve activity (MSNA) and blood oxygen level dependent (BOLD) fMRI. They found that MSNA bursts were associated with increased BOLD activity in the RVLM, hypothalamus, insula, and precuneus and reduced BOLD activity in the CVLM and NTS (141, 153). Additionally, maximal inspiratory breath hold, which increases MSNA, increases

BOLD activity in the RVLM while decreasing BOLD activity in the NTS and CVLM (141); and isometric handgrip exercise and post-exercise ischemia increase BOLD activity in the NTS and RVLM (141, 144, 148, 150).

Importantly, the activity of these medullary nuclei is impacted by projections from the salt sensing circumventricular organs (CVOs), as the CVOs have been shown to mediate salt-induced changes in SNA in preclinical models (**Figure 17**) (77, 124). Data from our laboratory in humans shows that hypernatremia via an IV hypertonic saline infusion increases MSNA and BP in young, healthy adults (79, 80). We also recently demonstrated that acute hypernatremia via an IV hypertonic saline infusion increases functional connectivity between the SFO and OVLT during the last 15 minutes of a 30-minute hypertonic saline infusion in young healthy adults using BOLD fMRI (140). However, no studies have investigated whether there are sex differences in the activation of these MSNA- and BP-regulating brain nuclei in response to acute hypernatremia in humans.

Therefore, the purpose of this study was to assess whether there are sex differences in the change in functional connectivity and fractional amplitude of low frequency fluctuations (fALFF) of MSNA- and BP-regulating nuclei in response to acute relative hypernatremia. Functional connectivity is a measure of the correlation of the BOLD signal time course between two brain regions, whereas fALFF measures the ratio of the power spectrum in the low-frequency range (0.008 – 0.10 Hz) to the entire

detectable frequency range within a specific brain region, reflecting the intensity of the spontaneous fluctuations in BOLD signal in each brain region (163, 184). We hypothesized that acute hypernatremia would increase functional connectivity between and fALFF in brain regions responsible for increasing sympathetic outflow/BP (paraventricular nucleus of the hypothalamus (PVN), supraoptic nucleus of the hypothalamus (SON), RVLM, SFO, and OVLT), while decreasing in inhibitory brain regions (CVLM and NTS). We also hypothesized that these responses would be greater in men compared to women. Identification of sex differences in the activation of sympathoregulatory brain networks during hypernatremia could have significant implications for understanding sex differences in the effects of dietary salt on BP regulation.

3.2 Methods

3.2.1 Subjects

Seventeen healthy young men and fifteen healthy premenopausal women (18-34 years) participated in this research study. The same participants included in the analysis in chapter 2 are included here. Verbal and written informed consent were obtained from all participants prior to participating in the study. Participants were excluded from the study if they exhibited high BP ($\geq 130/\geq 80$ mmHg at their screening visit), current tobacco use, pregnancy, or clinical signs and symptoms of cardiovascular disease, diabetes, kidney disease, pulmonary disease, or liver disease.

Participants had BMI between 18.5 and 30.2 kg/m². We excluded participants unable to undergo an MRI scan as determined by guidelines set by the Center for Biomedical and Brain Imaging at the University of Delaware, including individuals with ferromagnetic implants, claustrophobia, or neurological and psychiatric disorders. Individuals were also excluded if they were currently taking anxiety and/or depression medications, and women were excluded if they were using any form of hormonal contraception.

3.2.2 Experimental Protocol

The experimental design can be seen in **Figure 1**. Participants completed three visits (as in chapter 2). During the first visit, participants provided informed consent and completed a preliminary MRI screening. Next, participants completed a physical screening at the Nurse Managed Primary Care Center (NMPCC) at the University of Delaware, including height, weight, resting electrocardiogram (ECG), BP, a complete metabolic panel, a complete blood count, a lipid panel, HbA1c, and medical history. The MRI and hypertonic saline infusion visit (visit 3) occurred at the Center for Biomedical and Brain Imaging at the University of Delaware. Women completed their MRI testing during the follicular phase of their menstrual cycle (i.e., the first 12 days after the start of bleeding).

The approach for the MRI data collection is the same as in chapter 2 (**Figure 2**). Upon arrival, participants provided a spot urine sample to assess urine specific gravity and in

women, to verify pregnancy status. Following at least 5 minutes of quiet supine rest, brachial artery BP was measured at baseline in triplicate using the auscultatory method. A baseline thirst rating was also performed using a Likert scale. Participants were asked to put a mark on a 10 cm horizontal line, indicating their thirst level, ranging from “not at all” (0 cm) to “maximal thirst” (10 cm). Participants had an IV catheter placed into an antecubital vein in their left or right arm. The catheter was used for infusing hypertonic saline and drawing blood samples pre- and post-infusion. Before drawing blood samples, the IV line was flushed with isotonic saline followed by the collection of “waste” blood to minimize contamination of blood samples with hypertonic saline. This approach was successfully implemented in a pilot study in our laboratory (140).

Blood samples were obtained pre- and post-infusion to assess changes in serum electrolytes (EasyElectrolyte Analyzer; Medica, Bedford, MA), plasma osmolality (3D3 Osmometer; Advanced Instruments, Norwood, MA), hematocrit (Clay Adams Brand, Readacrit Centrifuge; Becton Dickinson, Sparks, MD), hemoglobin (Hb 201+ model; HemoCue, Lake Forest, CA), and plasma AVP. EDTA plasma samples were stored at -80°C and sent to the Wake Forest School of Medicine Biomarker Analytical Core to analyze plasma AVP using an Invitrogen Arg8-Vasopressin competitive enzyme-linked immunosorbent assay (ELISA) kit. This assay had an analytical sensitivity of 0.88 pg/mL and an assay range of 1.6-1000 pg/mL. Additional serum samples were stored to measure baseline sex hormone concentrations (sex hormone

concentrations were measured in all subjects at baseline, except for one subject who had sex hormone concentrations assessed from a post-infusion blood sample). Sex hormones were analyzed by RAD fertility, a member of the CCRM Fertility Network. Samples were analyzed with an ADVIA Centaur CP Immunoassay System (Siemens Healthcare Diagnostics, Tarrytown, NY) using chemiluminescent acridinium ester technology (188). For 4 participants, in whom serum progesterone was less than the detectable limit of the assay, serum progesterone was recorded as the minimum (0.050 ng/mL).

Once participants were situated in the MRI scanner, an anatomical T1 scan and an ~10-minute baseline resting state BOLD fMRI scan were conducted. After the baseline scans, hypertonic saline (3% NaCl) was infused through the IV catheter for 30 minutes (rate: $0.15 \text{ ml} \cdot \text{kg}^{-1} \cdot \text{min}^{-1}$) while participants were in the MRI scanner. A registered nurse performed the hypertonic saline infusion and blood draws. During this 30-min infusion, there was an additional 30-minute BOLD fMRI scan. Our analysis focused on the late phase (15-30 min) of the infusion, since our previous pilot data indicates that the functional connectivity between the SFO and OVLT starts to increase significantly above baseline starting at ~13 minutes into this same hypertonic saline infusion protocol (189). Additional blood pressure measurements and a blood draw were completed following this scan and infusion. The same data analyzed in chapter two were used to perform the analyses here.

3.2.3 MRI Acquisition

As in chapter 2, we used a 3T MRI Siemens Prisma Scanner and 64-channel head coil at the Center for Biomedical and Brain Imaging to obtain all brain images. Padding was placed around the participant's neck and head and arms to minimize head motion and contact with the MRI bore. Participants were also instructed to keep both their head and the rest of their body relaxed and as still as possible.

All participants underwent a T1-weighted anatomical scan [repetition time (TR) = 2080 ms; echo time (TE) = 4.6 ms; field of view = 210 x 210 mm; voxel size = 0.7 mm³; slice thickness = 0.7 mm] followed by two functional BOLD fMRI scans (baseline & infusion). Functional scans were acquired using a multi-band gradient-echo echo-planar imaging (EPI) sequence [TR = 829 ms; TE = 40 ms; flip angle = 52°; field of view = 208 x 208 mm; voxel size = 2.0 mm³; slice thickness = 2.0 mm]. During functional scans, participants were instructed to keep their eyes open and fixated on a white cross (on a black screen) as is recommended to minimize the effects of eye motion and ensure reliability and consistency of results (190). These sequences are identical to those validated in our laboratory's pilot study (140).

3.2.4 MRI Analysis

As in chapter 2, the preprocessing steps described here were also utilized in our group's pilot study (140). Functional MRI images were processed and analyzed using MRICroGL, AFNI (Analysis of Functional NeuroImages) and FSL (FMRIB Software

Library). Initially, the 30-minute infusion fMRI scans were split into an early phase (0-15 minutes) and late phase (15-30 minutes). This study focuses on only the late phase of the 30-minute infusion. Scans were also deobliqued and resampled to RPI (right, posterior, inferior) orientation. The remainder of the preprocessing included: 1) de-spiking of the resting-state fMRI data to remove outliers, 2) slice-timing correction of the resting state fMRI data to correct for slight differences in the acquisition of 2D slices within each 3D brain volume, 3) 3D rigid motion correction to a reference frame to correct for head motion in the resting-state data (we removed time points with head motion > 0.5 mm), 4) cleaning the BOLD fMRI data using ANATICOR (which accounted for the 6 motion parameters, white matter, and CSF signal), 5) band-pass filtering (0.008 to 0.10 Hz) to focus the analysis on low frequency fluctuations in the resting-state BOLD fMRI signal (190), 6) skull-stripping of the T1-anatomical scan using FSL, 7) co-registration (i.e., alignment) of the T1-anatomical and functional scans, 8) normalization of all scans to the 1mm MNI152 template, and 9) spatial smoothing of the resting-state data using a Gaussian kernel of full-width half maximum (FWHM) = 4mm. This kernel size aligns with recommendations to smooth with a Gaussian kernel of FWHM double the voxel size (which was 2 mm isotropic for this study) (163). All scans were pre-processed the same way for both functional connectivity and fALFF analyses except for bandpass filtering, which was omitted for the fALFF analysis because the fALFF analysis requires the entire frequency range (184).

Our regions of interest (ROIs) included the PVN, SON, CVLM, NTS, and RVLM. The PVN and SON were defined as 2-mm radius spheres centered around MNI coordinates identified using a combination of histology and MRI (217), and the CVLM, NTS, and RVLM were defined on the left and right sides as 2-mm radius spheres centered around MNI coordinates identified in a previous study (152); the brainstem ROIs were created symmetrically on the left and right sides (**Figure 18**). The MNI coordinates for the center of each ROI are presented in **Table 4**.

Following pre-processing and the creation of our ROIs, we conducted seed-to-seed functional connectivity analyses to assess the functional connectivity between our ROIs. We also assessed the functional connectivity of these brain regions with the SFO and OVLT, which were also defined as 2-mm radius spheres based on previous studies (138, 140, 189, 191, 192). Pearson correlations were computed between the ROIs for the seed-to-seed functional connectivity analysis. Pearson correlations were converted to Z-scores using a Fisher's transform which were statistically analyzed.

As a complementary analysis, we also assessed fALFF in each of our ROIs. These are complementary analysis approaches since functional connectivity reflects the synchronization of low frequency fluctuations in the BOLD signal between our ROIs and fALFF reflects the intensity/magnitude of the spontaneous fluctuations in the BOLD signal in each brain region (163, 184). fALFF was calculated as the ratio of the

power spectrum in the low-frequency range (0.008 – 0.10 Hz) to the complete frequency range (184).

3.2.5 Statistical Analysis

Statistics were conducted with IBM SPSS Statistics 28.0 and GraphPad Prism 8.0. Normality was verified using the Shapiro-Wilk test. Normally distributed baseline characteristics were compared between groups (men and women) using independent 2-tailed t-tests. Alternatively, Mann-Whitney U tests were conducted on non-normally distributed data. 2x2 (time*sex) repeated measures analysis of variance (ANOVA) models were used to compare changes in BP and biochemical data (e.g., plasma osmolality, serum sodium) pre- to post-infusion in men and women. 2x2 (time*sex) repeated measures ANOVAs were also used to assess changes in functional connectivity and fALFF from baseline to the late phase (15-30min) of the infusion in men and women. If data were non-normally distributed, aligned rank transformations (ARTs) were conducted prior to performing 2x2 (time*sex) repeated measures ANOVAs. ARTs were completed using ARTool2 (version 2.2.2) (199, 200). Significant time*sex interactions were followed with pairwise post-hoc comparisons. Effect sizes were calculated as partial η^2 . Since some of the data were analyzed using ARTs, some of the effect sizes apply to the ranked data; these cases are identified in the text with the abbreviation, “ART.” Pearson and Spearman’s correlations were also utilized to assess the relation between functional connectivity, fALFF, and participant screening characteristics and biochemical data.

Power was calculated using GPower3.0. Power calculations based on our preliminary data ($\eta^2 = 0.059$; $f = 0.25$) indicated that a sample size of $n=28$ would provide us with $>80\%$ power to detect a small to medium effect size of $f=0.25$ with $\alpha=0.05$. This assumed that we have an even split of men and women and there is a moderate correlation among repeated measures ($r\approx 0.5$). The data we present here includes 32 participants, exceeding the sample size estimated by the power analysis by 4 participants.

3.3 Results

3.3.1 Participant Characteristics

As described in chapter 2, participant characteristics for all 32 participants (17 men and 15 women) are displayed in **Table 1**. The cohort is diverse as only 13 participants ($<50\%$) identified as white. Women had slightly lower age, height, body mass, BMI, SBP, and triglycerides compared to men (all: $p<0.050$); women also had slightly higher HDL cholesterol ($p=0.010$). However, DBP, total cholesterol, LDL cholesterol, and blood glucose were similar between men and women (all: $p>0.050$).

3.3.2 Blood Pressure, Thirst, and Biochemical Data Pre- and Post-Infusion

As described in chapter 2, changes in BP, thirst, and biochemical data are presented in **Table 2**. There were robust pre-to post-infusion increases in plasma osmolality (main effect of time: $p<0.001$, partial $\eta^2 = 0.913$, $N=29$), serum sodium (main effect of time:

$p < 0.001$, partial $\eta^2 = 0.901$, $N=30$), and serum chloride (main effect of time: $p < 0.001$, partial $\eta^2 = 0.937$, $N=30$), demonstrating the effectiveness of our protocol in eliciting acute relative hypernatremia. Hematocrit decreased pre- to post-infusion (main effect of time: $p < 0.001$, partial $\eta^2 = 0.610$, $N=27$) and was significantly lower in women (main effect of sex: $p < 0.001$, partial $\eta^2 = 0.535$, $N=27$). Hemoglobin exhibited a significant time*sex interaction (time*sex interaction: $p=0.018$, partial $\eta^2 = 0.213$, $N=26$). However, hemoglobin also decreased pre- to post-infusion in both men ($p < 0.001$) and women ($p=0.020$) and was significantly lower in women both pre- ($p=0.001$) and post-infusion ($p=0.002$), as expected. SBP increased pre- to post-infusion (ART: main effect of time: $p=0.038$, partial $\eta^2 = 0.174$, $N=25$); however, there were no significant changes in DBP (main effect of time: $p=0.616$, partial $\eta^2 = 0.011$, $N=25$) or MAP (ART: main effect of time: $p=0.173$, partial $\eta^2 = 0.079$, $N=25$). As anticipated, DBP and MAP were significantly lower in women compared to men (DBP: main effect of sex: $p=0.009$, partial $\eta^2 = 0.261$, $N=25$; MAP: ART: main effect of sex: $p=0.017$, partial $\eta^2 = 0.225$, $N=25$) and SBP exhibited a trend of being lower in women (ART: main effect of sex: $p=0.081$, partial $\eta^2 = 0.126$, $N=25$). Thirst (as assessed on a Likert scale) increased significantly pre- to post-infusion (ART: main effect of time: $p < 0.001$, partial $\eta^2 = 0.366$, $N=30$). Lastly, plasma AVP increased from pre- to post-infusion to a similar extent between men and women (ART: main effect of time: $p=0.012$, partial $\eta^2 = 0.218$; main effect of sex: $p=0.790$, partial $\eta^2 = 0.003$; time*sex interaction: $p=0.729$, partial $\eta^2 = 0.005$, $N=28$; **Figure 4**).

Average sex hormone concentrations are presented in **Table 3**. As expected, serum testosterone was higher in men ($p < 0.001$); and FSH, LH, and progesterone were all higher in women ($p < 0.050$). However, estradiol and progesterone are still relatively low in women, as expected for women tested in the follicular menstrual cycle phase (203–205).

3.3.3 Head Motion

As discussed in chapter 2, average TR-TR head motion was minimal in all participants (< 0.20 mm) and similar between men and women and between baseline and the late phase of the infusion (ART: main effect of phase: $p = 0.292$, partial $\eta^2 = 0.037$; main effect of sex: $p = 0.183$, partial $\eta^2 = 0.058$; phase*sex interaction: $p = 0.573$, partial $\eta^2 = 0.011$, $N = 32$, **Figure 5**).

3.3.4 Functional Connectivity

We assessed the functional connectivity between the CVOs and several sympathoregulatory brainstem nuclei. Functional connectivity increased between the SFO and left CVLM from baseline to the late phase of the infusion (main effect of time: $p = 0.032$, partial $\eta^2 = 0.144$, $N = 32$, **Figure 19A**); however, there were no significant effects for functional connectivity of the SFO with the right CVLM, left or right NTS, or left or right RVLM (all: $p > 0.100$, **Figure 19B-F**). There were also no significant effects for functional connectivity of the OVLT with the left or right CVLM, NTS, or RVLM (all: $p > 0.050$, **Figure 20**).

We also assessed the functional connectivity between these sympathoregulatory brainstem nuclei. There was a trend for the bilateral functional connectivity of the RVLM to increase from baseline to the late phase of the infusion (main effect of phase: $p=0.078$, partial $\eta^2 = 0.100$, $N=32$, **Figure 21**). Additionally, our protocol significantly increased functional connectivity between the left RVLM and left NTS from baseline to the late phase of the infusion (ART: main effect of phase: $p<0.001$, partial $\eta^2 = 0.325$, $N=32$, **Figure 22C**). However, there were no other significant effects of phase/time or sex or phase*sex interactions for functional connectivity of the RVLM with the CVLM or NTS (all: $p>0.100$, **Figure 22**).

In addition to assessing the above brainstem nuclei, we also calculated functional connectivity for two hypothalamic nuclei, the PVN and SON. We found no significant effects for the functional connectivity of the SFO and OVLT with the PVN or SON (all: $p>0.200$, **Figures 23-24**). Additionally, there were no significant effects for the functional connectivity of the PVN with the left or right CVLM, NTS, or RVLM (all: $p>0.100$, **Figure 25**).

3.3.5 fALFF

Since functional connectivity reflects the synchronization of low frequency fluctuations in the BOLD signal between our ROIs, we utilized fALFF as a complementary approach to assess the intensity/magnitude of the spontaneous fluctuations in the BOLD signal in each individual brain region (163, 184). fALFF

increased from baseline to the late phase of the infusion in all the sympathoregulatory nuclei we assessed, including the left CVLM (ART: main effect of phase: $p < 0.001$, partial $\eta^2 = 0.525$, $N=32$, **Figure 26A**), right CVLM (ART: main effect of phase: $p < 0.001$, partial $\eta^2 = 0.489$, $N=32$, **Figure 26B**), left NTS (ART: main effect of phase: $p < 0.001$, partial $\eta^2 = 0.559$, $N=32$, **Figure 26C**), right NTS (ART: main effect of phase: $p < 0.001$, partial $\eta^2 = 0.437$, $N=32$, **Figure 26D**), left RVLM (ART: main effect of phase: $p < 0.001$, partial $\eta^2 = 0.531$, $N=32$, **Figure 26E**), and right RVLM (ART: main effect of phase: $p < 0.001$, partial $\eta^2 = 0.466$, $N=32$, **Figure 26F**), as well as the PVN (ART: main effect of phase: $p < 0.001$, partial $\eta^2 = 0.379$, $N=32$, **Figure 27A**) and SON (main effect of phase: $p < 0.001$, partial $\eta^2 = 0.318$, $N=32$, **Figure 27B**). While fALFF increased in all these areas there were no significant main effects of sex or phase*sex interactions (all: $p > 0.100$).

3.3.6 Correlations

As in chapter two, we performed exploratory analyses investigating whether any of the fMRI outcomes (i.e., functional connectivity or fALFF) were associated with any participant screening characteristics or biochemical data. First, we found that there were no significant correlations with serum estradiol or testosterone ($p > 0.05$, data not shown). However, in the entire cohort (men and women combined), there were significant negative correlations between serum progesterone and baseline fALFF in the right CVLM ($\rho = -0.382$, $p = 0.034$, $N=31$, **Figure 28A**), left NTS ($\rho = -0.467$, $p = 0.008$, $N=31$, **Figure 28C**), and left RVLM ($\rho = -0.393$, $p = 0.029$, $N=31$, **Figure**

28E). These correlations also persisted when men were removed from the analysis and correlations were calculated in only women (all: $p < 0.05$, $N = 15$, **Figure 28B, D, F**).

Additionally, the change in SBP pre- to post-infusion was positively correlated with the change in fALFF in the SON in men ($\rho = 0.570$, $p = 0.042$, $N = 13$, **Figure 29B**).

There was also a trend for a positive correlation between change in SBP and change in fALFF in the SON in the entire cohort ($\rho = 0.390$, $p = 0.054$, $N = 25$, **Figure 29A**).

Although this correlation was still positive in women, it was not statistically significant ($r = 0.322$, $p = 0.308$, $N = 12$, **Figure 29C**). Lastly, the change in left RVLM – left NTS functional connectivity was positively correlated with the change in fALFF in the PVN ($\rho = 0.390$, $p = 0.027$, $N = 32$, **Figure 30A**) and left RVLM ($\rho = 0.477$, $p = 0.006$, $N = 32$, **Figure 30B**).

3.4 Discussion

In this study of young, healthy adults, we assessed whether there are sex differences in the effects of acute relative hypernatremia on the functional connectivity and fALFF of MSNA- and BP-regulating nuclei, including the PVN, SON, NTS, CVLM, and RVLM. Generally, we hypothesized that acute hypernatremia would increase the fALFF of and functional connectivity between nuclei involved in increasing sympathetic outflow and BP (i.e., PVN, SON, and RVLM), while decreasing in areas that inhibit sympathetic outflow and BP (i.e., CVLM and NTS). We also hypothesized that these responses would be greater in men compared to women.

The main findings of this study were as follows: 1) acute relative hypernatremia increased functional connectivity between the SFO and left CVLM and between the left RVLM and left NTS, 2) there was a trend for the bilateral functional connectivity of the RVLM to increase with our salt loading protocol, and 3) acute hypernatremia increased fALFF in the CVLM, NTS, RVLM, PVN, and SON. Overall, the responses were similar between men and women. We also found that serum progesterone was negatively correlated with fALFF at baseline in the right CVLM, left NTS, and left RVLM; the change in SBP pre- to post-infusion was positively correlated with the change in fALFF in the SON; and the change in left RVLM – left NTS functional connectivity was positively correlated with the change in fALFF in the PVN and left RVLM.

As hypothesized, acute relative hypernatremia increased fALFF in the PVN and left and right RVLM. There was also a trend for the bilateral functional connectivity of the RVLM to increase, as hypothesized. Since the RVLM is one of the primary drivers of sympathetic outflow, and the PVN sends excitatory projections to the RVLM to increase sympathetic outflow (**Figure 17**) (65, 77), these findings are consistent with studies demonstrating that acute hypernatremia increases SNA and BP in both rodents (77, 78) and humans (79–82). This is also consistent with studies demonstrating that BOLD signal in the RVLM is positively associated with MSNA (141) and that the RVLM is activated in response to perturbations that increase MSNA, such as isometric

handgrip exercise (148), maximal inspiratory breath hold (141), and bolus injection of phenylephrine (152).

fALFF also increased in the SON from baseline to the late phase of the infusion. This aligns with our hypothesis, since the SON contains magnocellular neurons responsible for the release of AVP from the posterior pituitary (**Figure 17**) (103), and our protocol significantly increased plasma AVP (**Figure 4**). Interestingly, the change in fALFF in the SON was positively correlated with the change in SBP with acute relative hypernatremia (**Figure 29**). This is expected since both fALFF in the SON (**Figure 27B**) and SBP (**Table 2**) increased with the hypertonic saline infusion protocol, and AVP, which is regulated in part by the SON, elicits fluid retention and vasoconstriction, which can increase BP (115). Thus, fALFF increased in the PVN, SON, and RVLM as hypothesized.

While fALFF increased in these brain regions as hypothesized, fALFF also increased in the NTS and CVLM with acute hypernatremia (rather than decreasing as originally hypothesized). Additionally, functional connectivity increased between the SFO and left CVLM and between the left RVLM and left NTS, contrary to our hypothesis. We initially hypothesized that fALFF and functional connectivity would decrease in these brain regions, since acute hypernatremia increases SNA and BP in both rodents (77, 78) and humans (79–82), and the NTS and CVLM exert an inhibitory effect on the RVLM, the main nuclei responsible for driving sympathetic outflow (153).

We have conceived a few plausible explanations for these unexpected findings. First, changes in SNA with acute salt loading are region specific. IV hypertonic saline infusion in Sprague-Dawley rats increases lumbar SNA but reduces splanchnic and renal SNA (83). Similarly, infusion of saline into the lateral ventricle of male Sprague-Dawley rats elicits increases in lumbar SNA, adrenal SNA, and BP, while renal SNA decreases, and splanchnic SNA remains unchanged; in this same study, single-unit recordings of neurons in the RVLM revealed that RVLM neurons responded heterogeneously as well; ~46% of neurons were excited, 37% inhibited, and 17% displayed no change (84). Thus, since we defined our ROIs as 2-mm radius spheres, we may be sampling a small subset of neurons in the CVLM and NTS that are excited with salt loading, while this may not characterize all neurons in these nuclei. Second, part of these SNA responses to salt loading may be baroreceptor-dependent, since animals with sinoaortic denervation display earlier increases in lumbar SNA and no change in splanchnic SNA (rather than a reduction) with IV hypertonic saline infusion compared to intact animals (83). Thus, it is possible that the baroreceptor reflex may impact changes in regional SNA via increases in the activity of the NTS and CVLM.

In addition, the finding that fALFF increased in the NTS may align with a few other studies demonstrating that BOLD signal intensity also increases in the NTS with physiological perturbations such as isometric handgrip exercise (150), post-exercise ischemia (148), and the Valsalva maneuver (141, 150). Previous studies have also shown that in addition to inhibiting the RVLM via the CVLM (153), the NTS may

have direct projections to the RVLM, some of which are excitatory (218, 219).

Therefore, the increases in fALFF in the NTS and functional connectivity between the left NTS and left RVLM may reflect direct excitatory projections between these nuclei. In support of this hypothesis, we found that the change in functional connectivity between the left RVLM and left NTS was positively correlated with the change in fALFF in the PVN and left RVLM (**Figure 30**). Since the PVN and RVLM are sympathoexcitatory, the increase in left RVLM – left NTS functional connectivity observed in this cohort may reflect direct projections associated with increased sympathetic outflow.

We found that changes in functional connectivity and fALFF during acute relative hypernatremia in this cohort were relatively similar between men and women, contrary to our hypothesis that men would have greater responses. While these differences were hypothesized based on the literature (48, 93–95, 114); in this cohort, the overall physiological responses to the hypertonic saline infusion (i.e., changes in serum sodium, thirst, SBP, and plasma AVP) were similar between men and women. Thus, the lack of sex differences in the fMRI responses parallels the lack of hemodynamic and biochemical differences observed between men and women. It is also possible that the analysis techniques used in this study (e.g., fALFF which measures spontaneous fluctuations in the BOLD signal) may not be sensitive enough to detect sex differences in underlying neural activity.

While no significant sex differences were observed, serum progesterone was negatively correlated with baseline fALFF in the right CVLM, left NTS, and left RVLM (**Figure 28**). Although these correlations are statistically significant, we recognize that the women included in this cohort were all tested during the follicular menstrual cycle phase when sex hormone concentrations were relatively low, giving a small range for serum progesterone and estradiol. Thus, part of the reason no sex differences or associations with serum estradiol were observed in this cohort could be that women were tested during the follicular phase of their menstrual cycle, when sex hormone concentrations are relatively low. Thus, additional studies need to be conducted to determine if there are differences in these responses across the menstrual cycle, providing a greater spread of female sex hormone concentrations, and if women tested during the luteal phase (high hormone phase) differ compared to men.

This study has several strengths, including 1) a highly controlled stimulus, 2) verification of the effectiveness of our stimulus by assessing changes in serum electrolytes, plasma osmolality, BP, thirst, and plasma AVP, 3) testing women who were not using hormonal contraception in the follicular phase of their menstrual cycle to control for sex hormone-mediated variability among women, and 4) measurement of sex hormone concentrations in men and women. Additionally, we utilized two complementary measures (fALFF and functional connectivity) to investigate the activation of the above sympathoregulatory brain regions in humans. By combining fALFF and functional connectivity, we were able to assess changes in the intensity of

the spontaneous fluctuations in BOLD signal in each brain region (fALFF) (163, 184) and the synchronization of the low frequency fluctuations in the BOLD signal between our ROIs (functional connectivity). Lastly, in chapter two, we included two control ROIs (PCC and M1 hand area), neither of which displayed significant effects for functional connectivity, and there were no significant changes in fALFF in the M1 hand area. This suggests that changes in functional connectivity and fALFF are not distributed universally across the entire brain, strengthening the results observed in these sympathoregulatory brain regions.

While our study has several strengths, we also recognize a few limitations. First, we did not record MSNA responses or measure plasma catecholamine concentrations in these participants. Thus, we are unable to directly relate changes in fALFF or functional connectivity with sympathetic responses. Second, while we recognize the importance of testing women across the menstrual cycle, we tested women who were not using hormonal contraceptives during the follicular phase based on previous studies showing that sex hormones affect osmotic regulation across the menstrual cycle (114). Additional studies are warranted to investigate whether these brain regions respond differently across the menstrual cycle and whether hormonal contraception may affect these responses. Third, our ROIs for this aim are all 2-mm-radius spheres. This, along with the limited anatomical landmarks visible on T1 anatomical scans to define the brainstem ROIs, makes accurate identification of these brain regions challenging. We meticulously checked the normalization of the scans

and selected our ROIs based off previously published neuroimaging studies which functionally or histologically identified these ROIs (152, 217). However, additional advancements in the neuroimaging field would be beneficial to ensure accurate identification and assessment of small brain nuclei. A more thorough discussion of the limitations associated with this approach can be found in our group's previous publication (140). Lastly, while our sample size met our goal, as estimated via an a priori power analysis, it is possible that additional effects of acute hypernatremia and sex differences might emerge with a larger sample size.

3.5 Conclusion

In this study of young, healthy adults, we found that acute relative hypernatremia via an IV hypertonic saline infusion increased functional connectivity between the SFO and left CVLM and between the left RVLM and left NTS. We also observed increases in fALFF in the CVLM, NTS, RVLM, PVN, and SON with this protocol. Overall, all fMRI responses were similar between men and women, consistent with the changes observed for serum sodium, thirst, SBP, and plasma AVP, all of which increased to a similar extent in men and women. Collectively, these results translate preclinical findings into humans, suggesting that the activity of these sympathoregulatory and BP-regulating nuclei increase with acute salt loading. This sets the stage for additional studies to investigate sex differences in and the effects of sex hormones on the response of sympathoregulatory brain regions to acute relative hypernatremia across the lifespan.

Table 4 MNI coordinates for sympathoregulatory brain regions.

Brain Region	MNI: x (mm)	MNI: y (mm)	MNI: z (mm)
PVN	2	-2	-12
SON	6	0	-16
Left CVLM	-6	-38	-56
Right CVLM	6	-38	-56
Left NTS	-4	-42	-48
Right NTS	4	-42	-48
Left RVLM	-8	-34	-46
Right RVLM	8	-34	-46

All nuclei were created as 2-mm-radius spheres centered around these MNI (Montreal Neurological Institute) coordinates. Coordinates were based on previous studies: PVN and SON (217) and CVLM, NTS, and RVLM (152). CVLM, caudal ventrolateral medulla; MNI, Montreal Neurological Institute; NTS, nucleus tractus solitarius; PVN, paraventricular nucleus of the hypothalamus; RVLM, rostral ventrolateral medulla; SON, supraoptic nucleus of the hypothalamus.

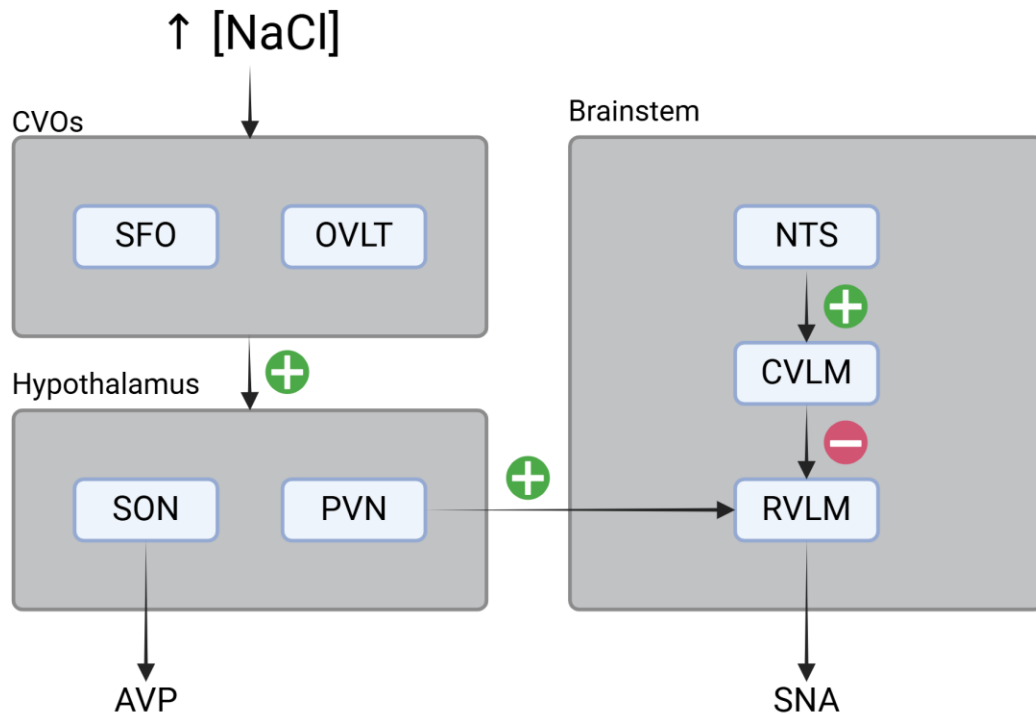


Figure 17 Schematic representing how salt sensing in the SFO and OVLT affects the activity of several hypothalamic and medullary nuclei. The CVOs project to the SON and PVN of the hypothalamus. The SON primarily regulates the release of AVP from the posterior pituitary gland, while the PVN is largely responsible for regulating sympathetic outflow. The PVN has excitatory projections to the RVLN, the primary driver of sympathetic outflow. However, this response is modulated by the baroreceptor reflex as the NTS sends excitatory projections to the CVLM, which tonically inhibits the RVLN. Figure created in Biorender. AVP, arginine vasopressin; CVLM, caudal ventrolateral medulla; CVOs, circumventricular organs; NTS, nucleus tractus solitarius; OVLT, organum vasculosum of the lamina terminalis; PVN, paraventricular nucleus of the hypothalamus; RVLN, rostral ventrolateral medulla; SFO, subfornical organ; SNA, sympathetic nerve activity; SON, supraoptic nucleus of the hypothalamus.

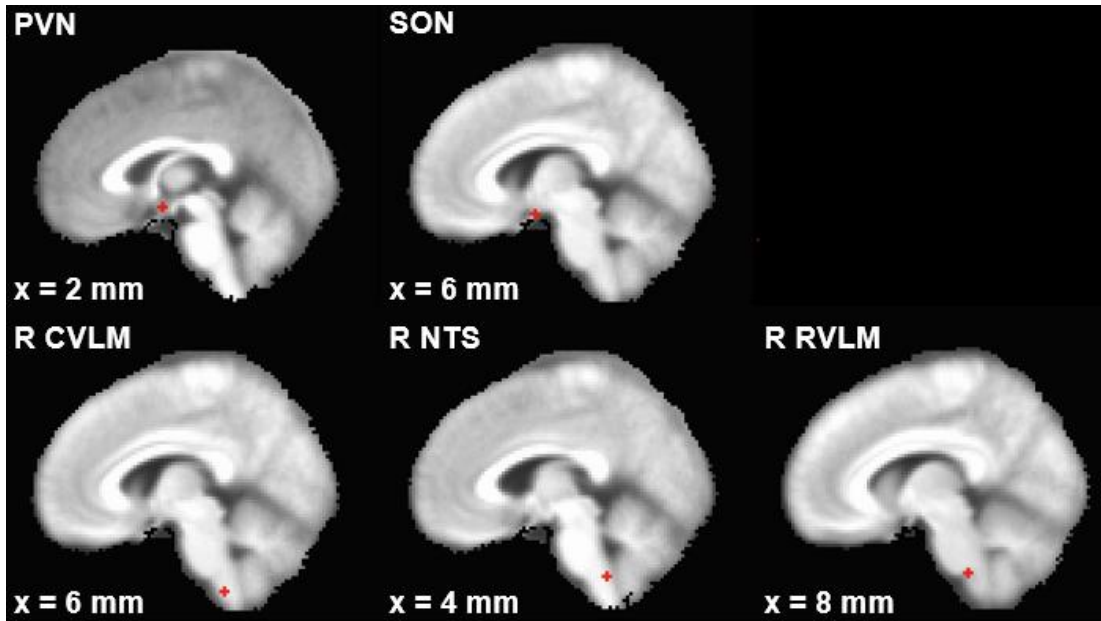


Figure 18 Regions of interest (ROIs) for the resting-state fMRI analysis. The name of each brain region is in the upper left with the slice location indicated in the lower left. The ROIs for the brainstem nuclei (CVLM, NTS, and RVLM) are depicted on the right side only since the ROIs on the left side are symmetrical. CVLM, caudal ventrolateral medulla; L, left; NTS, nucleus tractus solitarius; PVN, paraventricular nucleus of the hypothalamus; R, right; RVLM, rostral ventrolateral medulla; SON, supraoptic nucleus of the hypothalamus.

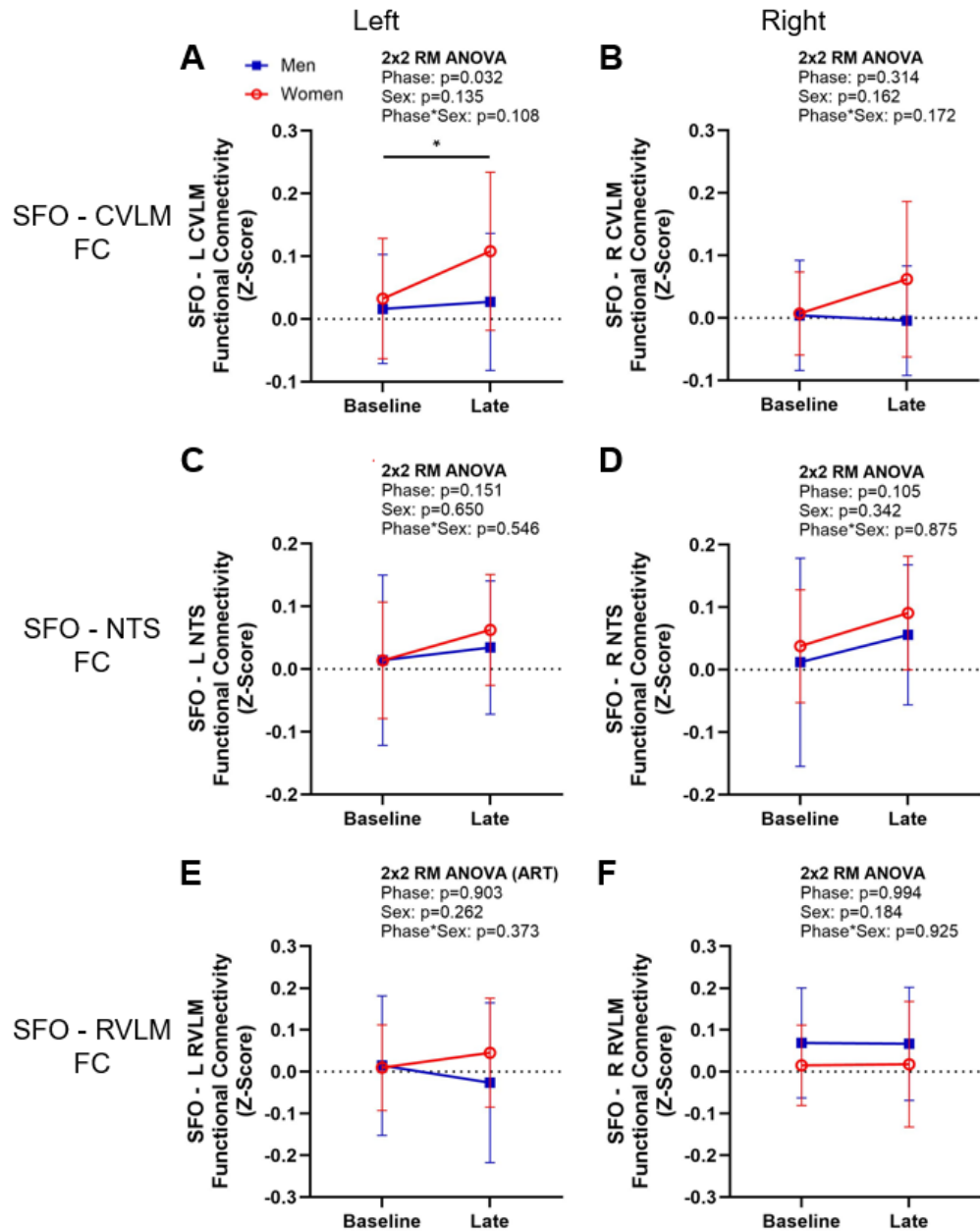


Figure 19 Functional connectivity of the subfornical organ (SFO) with the left and right CVLM (A-B), NTS (C-D), and RVLM (E-F). Data are presented as mean \pm standard deviation. * $p < 0.05$ for baseline vs late phase. ART, aligned rank transformation; CVLM, caudal ventrolateral medulla; FC, functional connectivity; L, left; NTS, nucleus tractus solitarius; RM ANOVA, repeated measures analysis of variance; R, right; RVLM, rostral ventrolateral medulla.

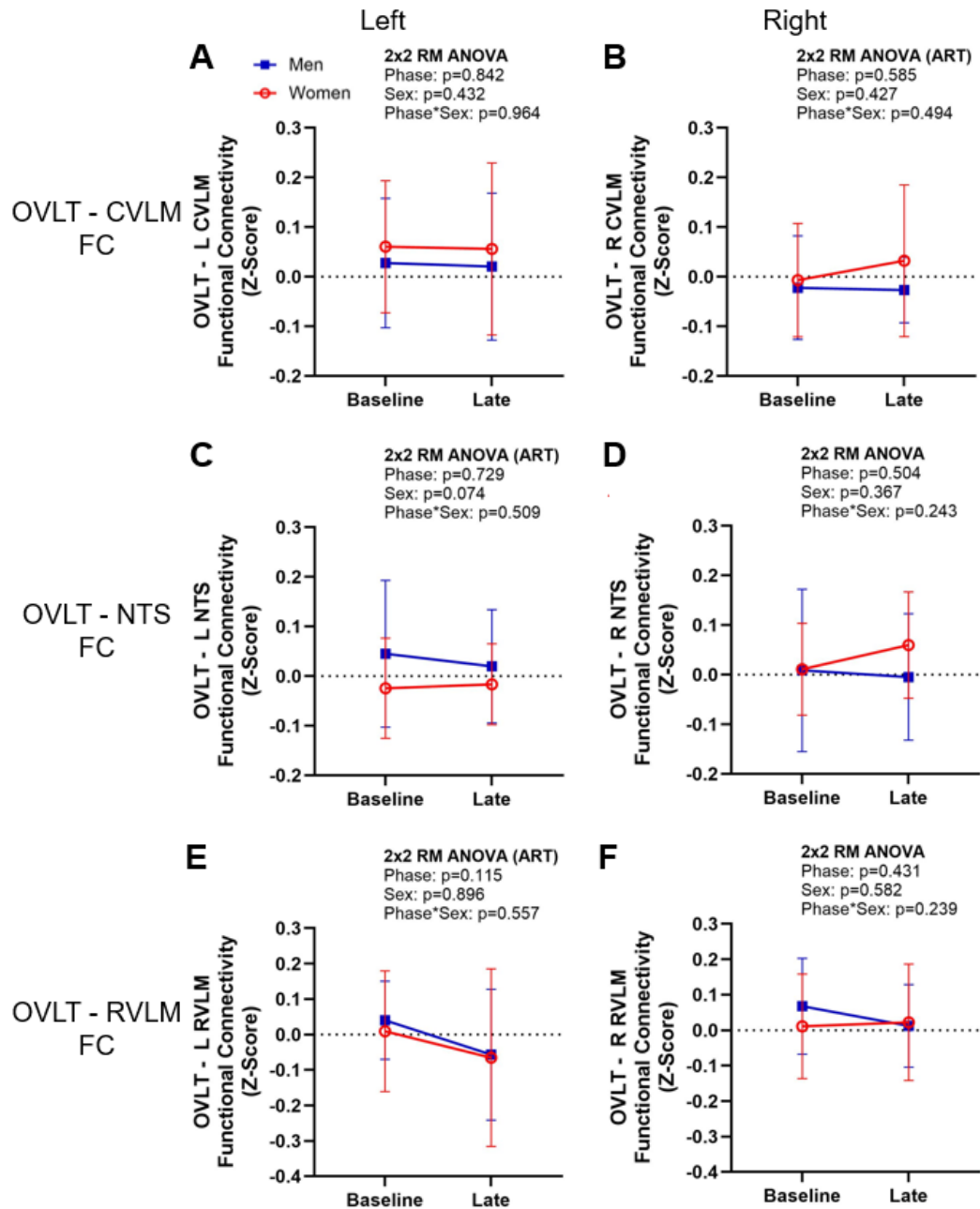


Figure 20 Functional connectivity of the organum vasculosum of the lamina terminalis (OVLT) with the left and right CVLM (A-B), NTS (C-D), and RVLM (E-F). Data are presented as mean \pm standard deviation. ART, aligned rank transformation; CVLM, caudal ventrolateral medulla; FC, functional connectivity; L, left; NTS, nucleus tractus solitarius; R, right; RM ANOVA, repeated measures analysis of variance; RVLM, rostral ventrolateral medulla.

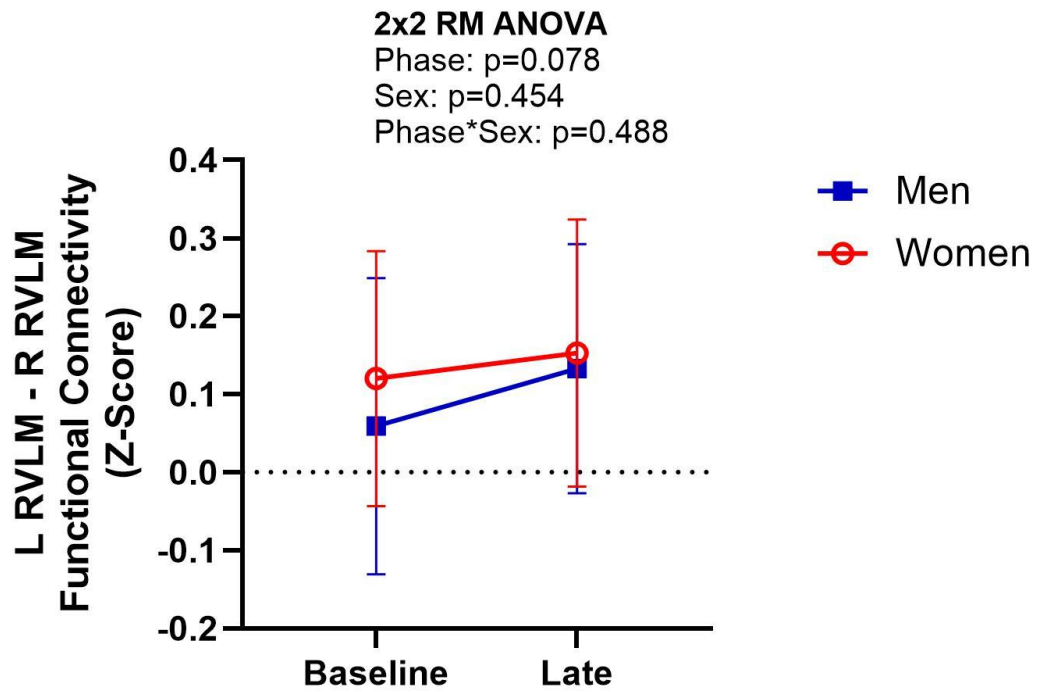


Figure 21 Functional connectivity of the RVLM bilaterally. Data are presented as mean \pm standard deviation. L, left; R, right; RM ANOVA, repeated measures analysis of variance; RVLM, rostral ventrolateral medulla.

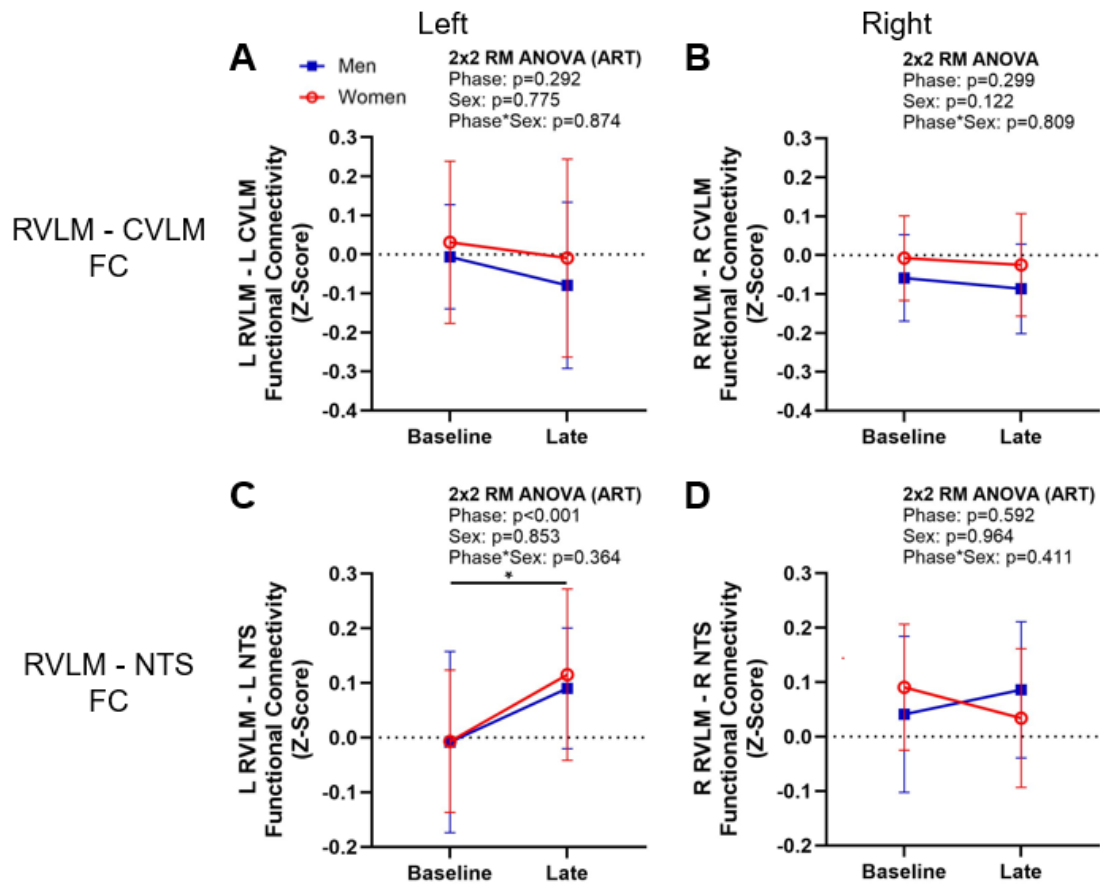


Figure 22 Functional connectivity of the RVLM with the CVLM (A-B) and NTS (C-D). Data are presented as mean \pm standard deviation. * $p<0.001$ for baseline vs late phase. ART, aligned rank transformation; CVLM, caudal ventrolateral medulla; FC, functional connectivity; L, left; NTS, nucleus tractus solitarius; R, right; RM ANOVA, repeated measures analysis of variance; RVLM, rostral ventrolateral medulla.

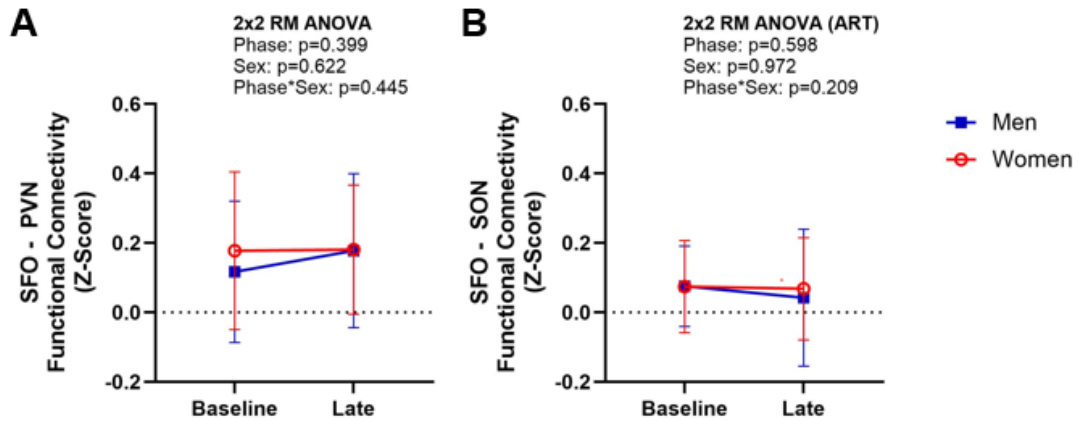


Figure 23 Functional connectivity of the subfornical organ (SFO) with the PVN (A) and SON (B). Data are presented as mean \pm standard deviation. ART, aligned rank transformation; PVN, paraventricular nucleus of the hypothalamus; RM ANOVA, repeated measures analysis of variance; SON, supraoptic nucleus of the hypothalamus.

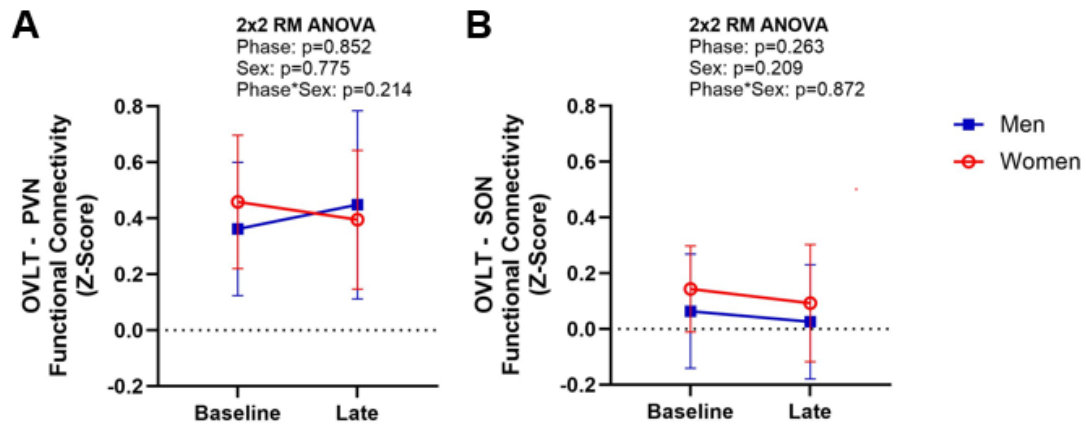


Figure 24 Functional connectivity of the organum vasculosum of the lamina terminalis (OVLT) with the PVN (A) and SON (B). Data are presented as mean \pm standard deviation. PVN, paraventricular nucleus of the hypothalamus; RM ANOVA, repeated measures analysis of variance; SON, supraoptic nucleus of the hypothalamus.

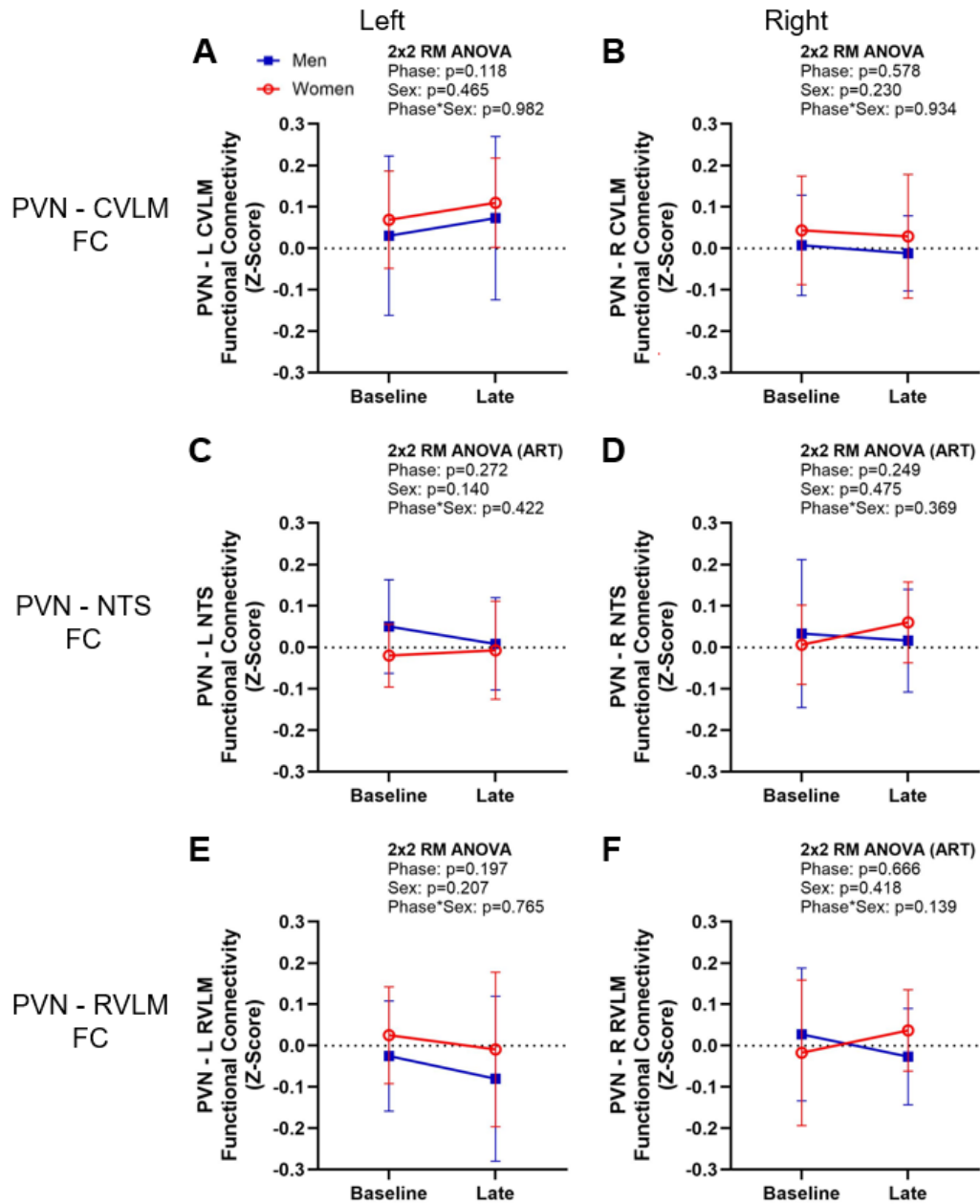


Figure 25 Functional connectivity of the PVN with the left and right CVLM (A-B), NTS (C-D), and RVLM (E-F). Data are presented as mean \pm standard deviation. ART, aligned rank transformation; CVLM, caudal ventrolateral medulla; FC, functional connectivity; L, left; NTS, nucleus tractus solitarius; PVN, paraventricular nucleus of the hypothalamus; R, right; RM ANOVA, repeated measures analysis of variance; RVLM, rostral ventrolateral medulla.

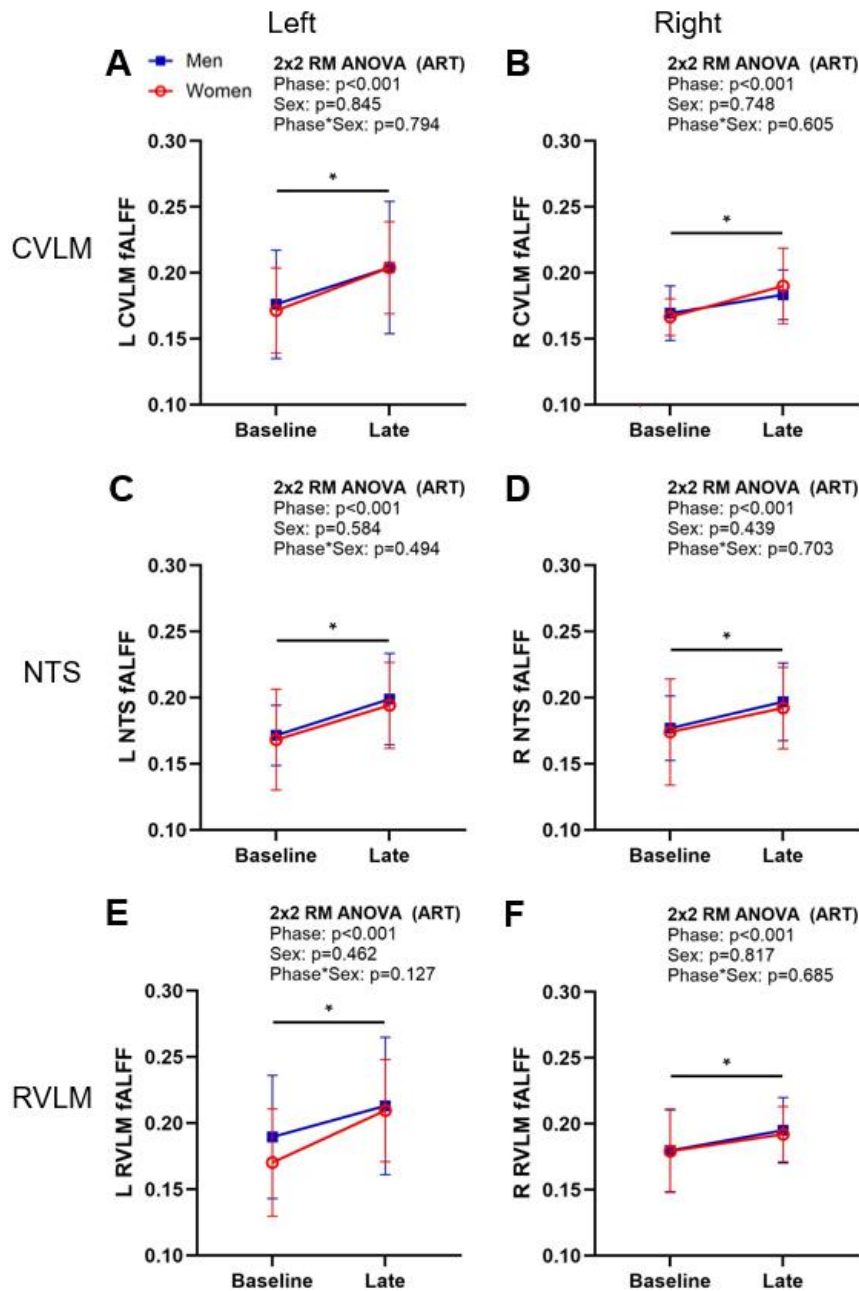


Figure 26 Fractional amplitude of low frequency fluctuations (fALFF) of the left and right CVLM (A-B), NTS (C-D), and RVLM (E-F). Data are displayed as mean \pm standard deviation. * $p < 0.001$ for baseline vs late phase. ART, aligned rank transformation; CVLM, caudal ventrolateral medulla; L, left; NTS, nucleus tractus solitarius; R, right; RM ANOVA, repeated measures analysis of variance; RVLM, rostral ventrolateral medulla.

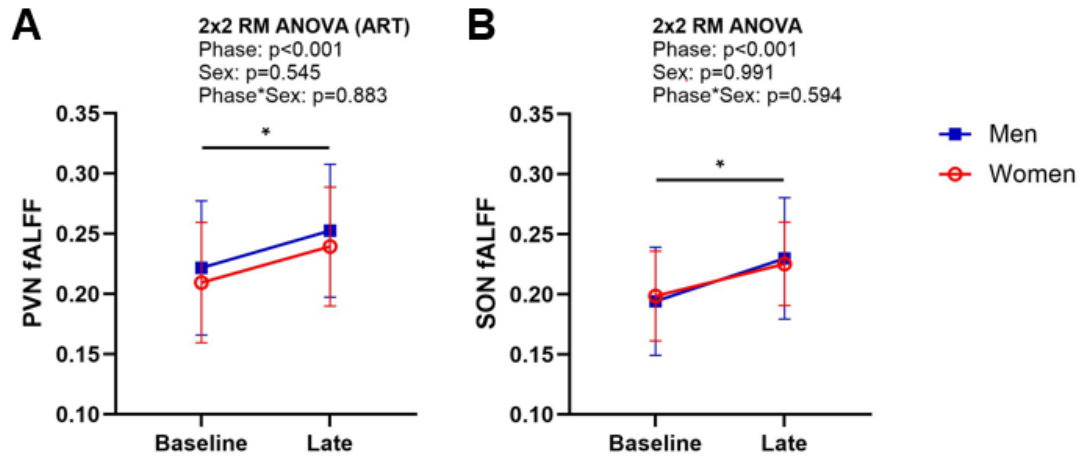


Figure 27 Fractional amplitude of low frequency fluctuations (fALFF) of the PVN (A) and SON (B). Data are displayed as mean \pm standard deviation. * $p < 0.001$ for baseline vs late phase. ART, aligned rank transformation; PVN, paraventricular nucleus of the hypothalamus; RM ANOVA, repeated measures analysis of variance; SON, supraoptic nucleus of the hypothalamus.

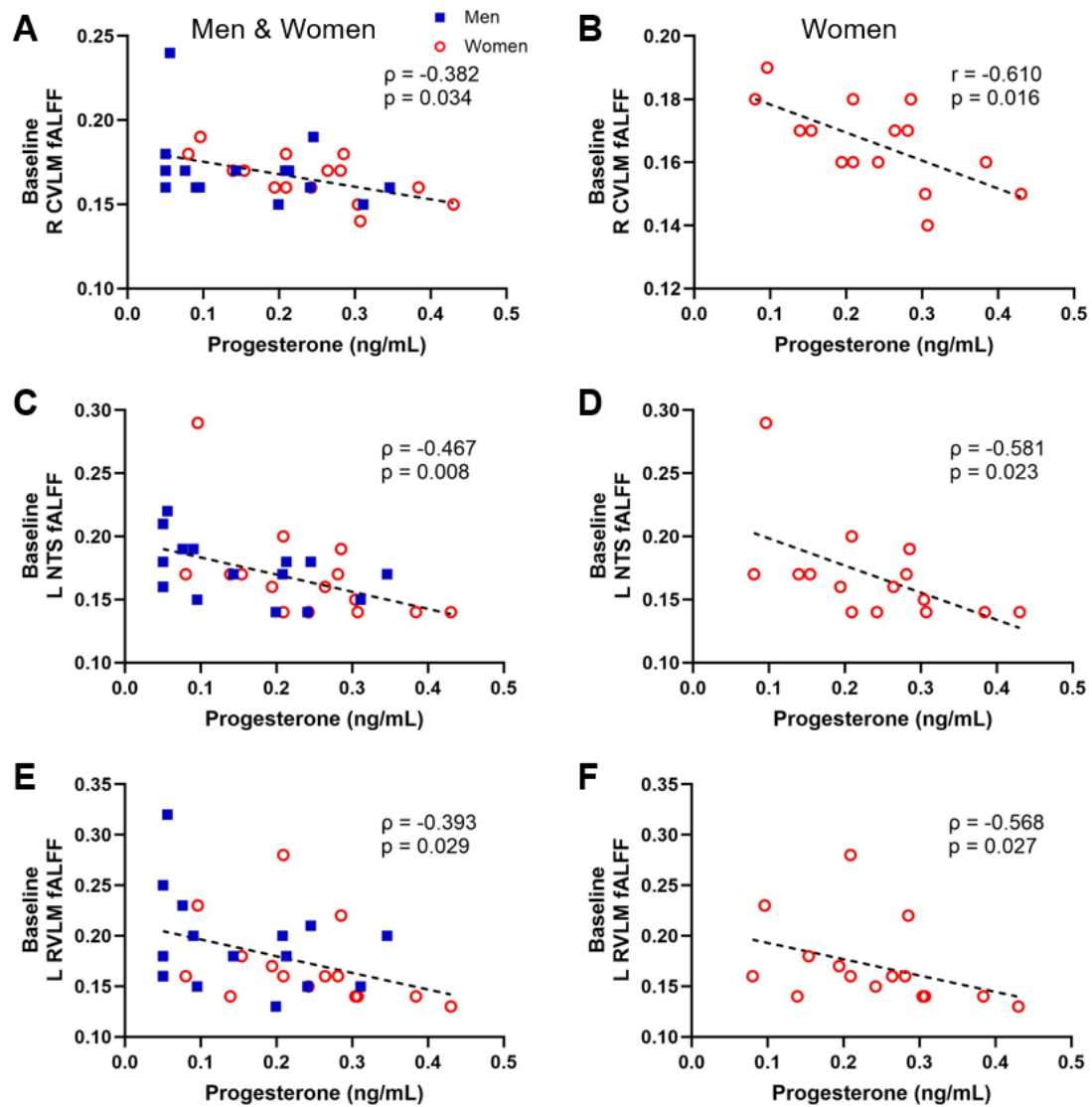


Figure 28 Correlations between serum progesterone and baseline fALFF in the right CVLM (A & B), left NTS (C & D), and left RVLM (E-F). Correlations are displayed for the entire cohort (left) and in only women (right). Women are red open circles; men are blue closed squares. CVLM, caudal ventrolateral medulla; fALFF, fractional amplitude of low frequency fluctuations; L, left; NTS, nucleus tractus solitarius; R, right; RVLM, rostral ventrolateral medulla. Pearson correlations (r) or Spearman's correlations (ρ) were used depending on whether the data were normally distributed.

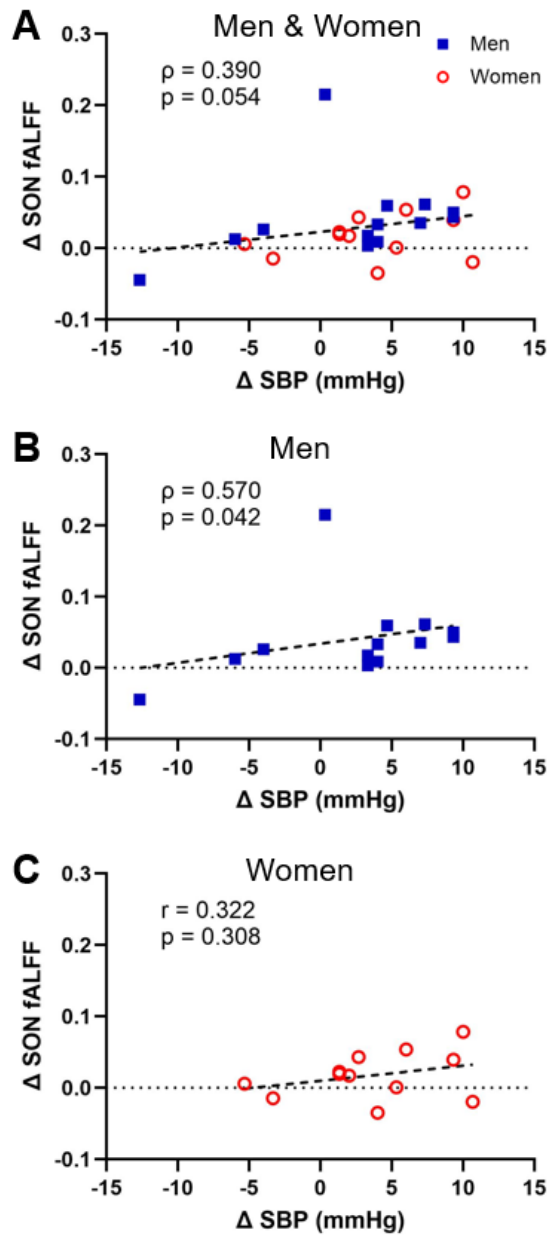


Figure 29 Correlations between change in SBP pre- to post-infusion and change in fALFF in the SON from baseline to the late phase of the infusion. Correlations are presented in the entire cohort (A), in men only (B), and in women only (C). Women are red open circles; men are blue closed squares. fALFF, fractional amplitude of low frequency fluctuations; SBP, systolic blood pressure; SON, supraoptic nucleus of the hypothalamus. Pearson correlations (r) or Spearman's correlations (ρ) were used depending on whether the data were normally distributed.

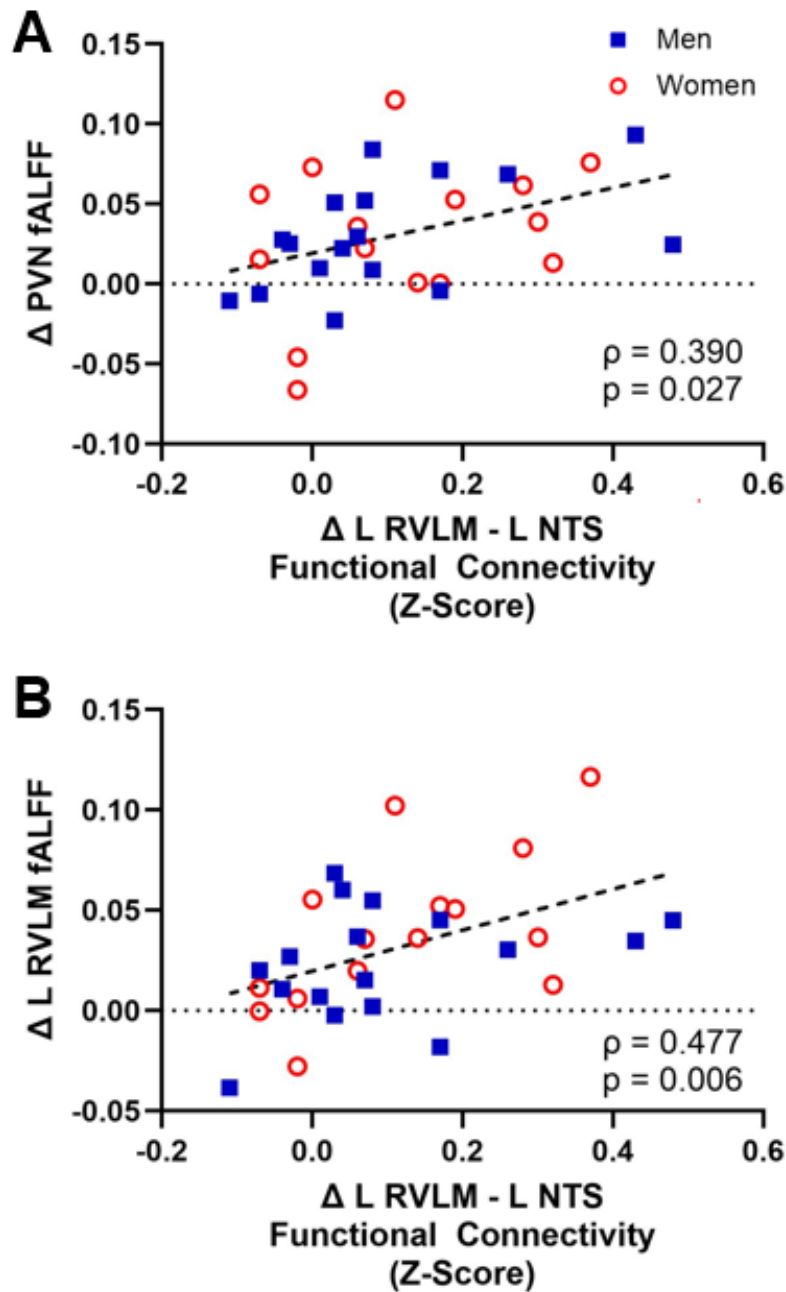


Figure 30 The change in functional connectivity between the left RVLM and left NTS was positively correlated with the change in fALFF in the PVN (A) and in the left RVLM (B). Women are red open circles; men are blue closed squares. fALFF, fractional amplitude of low frequency fluctuations; L, left; NTS, nucleus tractus solitarius; PVN, paraventricular nucleus of the hypothalamus; RVLM, rostral ventrolateral medulla. Spearman's correlations (ρ) were used.

Chapter 4

DISSERTATION CONCLUSIONS

4.1 Summary

In this study of young, healthy adults, we found that acute relative hypernatremia via an IV hypertonic saline infusion elicited changes in the activation patterns of several salt sensing and sympathoregulatory brain regions. Acute hypernatremia increased fALFF in several brain regions associated with salt sensing and thirst, including the SFO, OVLT, ACC, PCC, insula, and thalamus, and in several sympathoregulatory brain regions, including the PVN, SON, RVLM, NTS, and CVLM. Overall, changes in fALFF were similar between men and women; this is consistent with the changes observed for serum sodium, thirst, SBP, and plasma AVP in this cohort, all of which increased to a similar extent between men and women. However, functional connectivity between the SFO and OVLT increased in men but decreased in women, indicating a sex-specific response. Collectively, these results suggest that these salt sensing and sympathoregulatory brain regions are activated similarly in both men and women tested during the follicular menstrual cycle phase in response to acute relative hypernatremia (as assessed by fALFF). However, men seem to have a more

synchronized neural response between the SFO and OVLT (as assessed via functional connectivity), suggesting that these regions are more tightly coupled in their neural response to acute hypernatremia in men compared to women tested during the follicular menstrual cycle phase.

4.2 Perspectives and Future Directions

To date, most research studies investigating central salt sensing have been conducted in preclinical models, and there is limited data investigating central salt sensing in humans. These results translate preclinical findings into humans, suggesting that the activity of these salt sensing and sympathoregulatory brain regions increases with acute salt loading. To our knowledge, this also represents the first time the activity of sympathoregulatory brain regions has been shown to change during acute relative hypernatremia in humans. These findings set the stage for additional studies to investigate the mechanisms of central salt sensing in humans and the effects of chronic salt loading on central salt sensing. These results also lay the groundwork for additional studies to investigate sex differences in central neural activation during acute relative hypernatremia across the menstrual cycle and lifespan, and the impact of sex hormone concentrations on these responses.

REFERENCES

1. Tsao CW, Aday AW, Almarzooq ZI, et al. Heart Disease and Stroke Statistics-2022 Update: A Report From the American Heart Association. *Circulation*. 2022;145(8):e153–639.
2. Virani SS, Alonso A, Aparicio HJ, et al. Heart Disease and Stroke Statistics-2021 Update: A Report From the American Heart Association. *Circulation*. 2021;143(8):e254–743.
3. Appel LJ, Frohlich ED, Hall JE, et al. The Importance of Population-Wide Sodium Reduction as a Means to Prevent Cardiovascular Disease and Stroke. *Circulation*. 2011;123(10):1138–43.
4. Ahmad FB, Cisewski JA, Xu J, Anderson RN. Provisional Mortality Data — United States, 2022. *MMWR Morb Mortal Wkly Rep*. 2023;72(18):488–92.
5. Drury ER, Wu J, Gigliotti JC, Le TH. Sex differences in blood pressure regulation and hypertension: renal, hemodynamic, and hormonal mechanisms. *Physiol Rev*. 2024;104(1):199–251.
6. Robinson AT, Edwards DG, Farquhar WB. The Influence of Dietary Salt Beyond Blood Pressure. *Curr Hypertens Rep*. 2019;21(6).
7. Elliott P, Stamler J, Nichols R, et al. Intersalt revisited: further analyses of 24 hour sodium excretion and blood pressure within and across populations. Intersalt Cooperative Research Group. *BMJ*. 1996;312(7041):1249–53.
8. Weinberger MH. Salt Sensitivity of Blood Pressure in Humans. *Hypertension*. 1996;27(3):481–90.
9. Mente A, O'Donnell MJ, Rangarajan S, et al. Association of Urinary Sodium and Potassium Excretion with Blood Pressure. *New England Journal of Medicine*. 2014;371(7):601–11.

10. Elliott P, Dyer A, Stamler R. The INTERSALT study: results for 24 hour sodium and potassium, by age and sex. INTERSALT Co-operative Research Group. *J Hum Hypertens*. 1989;3(5):323–30.
11. Filippini T, Malavolti M, Whelton PK, Naska A, Orsini N, Vinceti M. Blood Pressure Effects of Sodium Reduction: Dose-Response Meta-Analysis of Experimental Studies. *Circulation*. 2021;143(16):1542–67.
12. Sacks FM, Svetkey LP, Vollmer WM, et al. Effects on Blood Pressure of Reduced Dietary Sodium and the Dietary Approaches to Stop Hypertension (DASH) Diet. *New England Journal of Medicine*. 2001;344(1):3–10.
13. Filippou C, Thomopoulos C, Konstantinidis D, et al. DASH vs. Mediterranean diet on a salt restriction background in adults with high normal blood pressure or grade 1 hypertension: A randomized controlled trial. *Clinical Nutrition*. 2023;42(10):1807–16.
14. Bray GA, Vollmer WM, Sacks FM, Obarzanek E, Svetkey LP, Appel LJ. A further subgroup analysis of the effects of the DASH diet and three dietary sodium levels on blood pressure: Results of the DASH-sodium trial. *American Journal of Cardiology*. 2004;94(2):222–7.
15. Appel LJ, Brands MW, Daniels SR, Karanja N, Elmer PJ, Sacks FM. Dietary Approaches to Prevent and Treat Hypertension. *Hypertension*. 2006;47(2):296–308.
16. He FJ, Tan M, Ma Y, MacGregor GA. Salt Reduction to Prevent Hypertension and Cardiovascular Disease: JACC State-of-the-Art Review. *J Am Coll Cardiol*. 2020;75(6):632–47.
17. Weinberger MH, Miller JZ, Luft FC, Grim CE, Fineberg NS. Definitions and characteristics of sodium sensitivity and blood pressure resistance. *Hypertension*. 1986;8(6_pt_2):II-127-II-134.
18. Romberger NT, Stock JM, Patik JC, et al. Inverse salt sensitivity in normotensive adults: Role of demographic factors. *J Hypertens*. 2023;41(6):934–40.
19. Bailey MA, Dhaun N. Salt Sensitivity: Causes, Consequences, and Recent Advances. *Hypertension* [Internet]. 2023; doi:10.1161/hypertensionaha.123.17959.

20. Oh YS, Appel LJ, Galis ZS, et al. National Heart, Lung, and Blood Institute Working Group Report on Salt in Human Health and Sickness. *Hypertension*. 2016;68(2):281–8.
21. Felder RA, White MJ, Williams SM, Jose PA. Diagnostic tools for hypertension and salt sensitivity testing. *Curr Opin Nephrol Hypertens*. 2013;22(1):65–76.
22. Felder RA, Gildea JJ, Xu P, et al. Inverse Salt Sensitivity of Blood Pressure: Mechanisms and Potential Relevance for Prevention of Cardiovascular Disease. *Curr Hypertens Rep*. 2022;24(9):361–74.
23. Overlack A, Ruppert M, Kolloch R, et al. Divergent hemodynamic and hormonal responses to varying salt intake in normotensive subjects. *Hypertension*. 1993;22(3):331–8.
24. Overlack A, Ruppert M, Kolloch R, Kraft K, Stumpe KO. Age is a major determinant of the divergent blood pressure responses to varying salt intake in essential hypertension. *Am J Hypertens*. 1995;8(8):829–36.
25. Eljovich F, Weinberger MH, Anderson CAM, et al. Salt Sensitivity of Blood Pressure: A Scientific Statement From the American Heart Association. *Hypertension*. 2016;68(3):e7–46.
26. De Leeuw PW, Kroon AA. Salt and sensitivity. *Hypertension*. 2013;62(3):461–2.
27. Sullivan JM. Salt sensitivity definition, conception, methodology, and long-term issues. *Hypertension* [Internet]. 1991 [cited 2021 Dec 29];17(1) Available from: <http://ahajournals.org>. doi:10.1161/01.HYP.17.1_SUPPL.I61.
28. Kurtz TW, DiCarlo SE, Pravenec M, Morris RC. An Appraisal of Methods Recently Recommended for Testing Salt Sensitivity of Blood Pressure. *J Am Heart Assoc* [Internet]. 2017 [cited 2021 Dec 28];6(4) Available from: <https://www.ahajournals.org/doi/10.1161/JAHA.117.005653>. doi:10.1161/JAHA.117.005653.
29. Strazzullo P, Galletti F, Dessì-Fulgheri P, et al. Prediction and consistency of blood pressure salt-sensitivity as assessed by a rapid volume expansion and contraction protocol. Salt-Sensitivity Study Group of the Italian Society of Hypertension. *J Nephrol*. 2000;13(1):46–53.
30. Weinberger MH, Fineberg NS. Sodium and volume sensitivity of blood pressure. Age and pressure change over time. *Hypertension*. 1991;18(1):67–71.

31. Sharma AM, Schorr U, Cetto C, Distler A. *Dietary v Intravenous Salt Loading for the Assessment of Salt Sensitivity in Normotensive Men*. 1994. 1070–1075 p. Available from: <https://academic.oup.com/ajh/article/7/12/1070/162610>.
32. Sharma AM, Schattenfroh S, Kribben A, Distler A. Reliability of salt-sensitivity testing in normotensive subjects. *Klin Wochenschr*. 1989;67(12):632–4.
33. Draaijer P, de Leeuw P, Maessen J, van Hooff J, Leunissen K. Salt-sensitivity testing in patients with borderline hypertension: reproducibility and potential mechanisms. *J Hum Hypertens*. 1995;9(4):263–9.
34. Gu D, Zhao Q, Chen J, et al. Reproducibility of blood pressure responses to dietary sodium and potassium interventions: The GenSalt study. *Hypertension*. 2013;62(3):499–505.
35. Zoccali C, Mallamaci F, Cuzzola F, Leonardis D. Reproducibility of the response to short-term low salt intake in essential hypertension. *J Hypertens*. 1996;14(12):1455–9.
36. Reges O, Krefman AE, Hardy ST, et al. Race- and Sex-Specific Factors Associated With Age-Related Slopes in Systolic Blood Pressure: Findings From the CARDIA Study. *Hypertension*. 2023;80(9):1890–9.
37. Morris RC, Sebastian A, Forman A, Tanaka M, Schmidlin O. *Normotensive Salt Sensitivity Effects of Race and Dietary Potassium*. 1999. Available from: <http://www.hypertensionaha.org>.
38. Faulkner JL, Belin de Chantemèle EJ. Female Sex, a Major Risk Factor for Salt-Sensitive Hypertension. *Curr Hypertens Rep*. 2020;22(12):99.
39. Barris CT, Faulkner JL, Belin de Chantemèle EJ. Salt Sensitivity of Blood Pressure in Women. *Hypertension* [Internet]. 2022 [cited 2022 Sep 28]; Available from: <https://www.ahajournals.org/doi/10.1161/HYPERTENSIONAHA.122.17952>. doi:10.1161/HYPERTENSIONAHA.122.17952.
40. He J, Gu D, Chen J, et al. Gender difference in blood pressure responses to dietary sodium intervention in the GenSalt study. *J Hypertens*. 2009;27(1):48–54.
41. Shukri MZ, Tan JW, Manosroi W, et al. Biological Sex Modulates the Adrenal and Blood Pressure Responses to Angiotensin II. *Hypertension*. 2018;71(6):1083–90.

42. Ishibashi K, Oshima T, Matsuura H, et al. Effects of age and sex on sodium chloride sensitivity: association with plasma renin activity. *Clin Nephrol.* 1994;42(6):376–80.
43. Robinson AT, Wenner MM, Charkoudian N. Differential influences of dietary sodium on blood pressure regulation based on race and sex. *Auton Neurosci.* 2021;236:102873.
44. Murtaugh MA, Beasley JM, Appel LJ, et al. Relationship of sodium intake and blood pressure varies with energy intake: Secondary analysis of the DASH (Dietary Approaches to Stop Hypertension)-sodium Trial. *Hypertension.* 2018;71(5):858–65.
45. Hinojosa-Laborde C, Lange DL, Haywood JR. Role of Female Sex Hormones in the Development and Reversal of Dahl Hypertension. *Hypertension.* 2000;35(1):484–9.
46. Hay M, Xue B, Johnson AK. Yes! Sex Matters: Sex, the Brain and Blood Pressure. *Curr Hypertens Rep.* 2014;16(8):458.
47. Belanger KM, Crislip GR, Gillis EE, et al. Greater T Regulatory Cells in Females Attenuate DOCA-Salt-Induced Increases in Blood Pressure Versus Males. *Hypertension.* 2020;75(6):1615–23.
48. Xue B, Badaue-Passos D, Guo F, Gomez-Sanchez CE, Hay M, Johnson AK. Sex differences and central protective effect of 17beta-estradiol in the development of aldosterone/NaCl-induced hypertension. *Am J Physiol Heart Circ Physiol.* 2009;296(5):H1577-85.
49. Xue B, Pamidimukkala J, Hay M. Sex differences in the development of angiotensin II-induced hypertension in conscious mice. *American Journal of Physiology-Heart and Circulatory Physiology.* 2005;288(5):H2177–84.
50. Xue B, Johnson AK, Hay M. Sex differences in angiotensin II- induced hypertension. *Braz J Med Biol Res.* 2007;40(5):727–34.
51. Quinn R. Comparing rat's to human's age: How old is my rat in people years? *Nutrition.* 2005;21(6):775–7.
52. Sengupta P. *The Laboratory Rat: Relating Its Age with Human's.* 2013. Available from: www.ijpm.ir.
53. Morimoto A, Uzu T, Fujii T, et al. Sodium sensitivity and cardiovascular events in patients with essential hypertension. *The Lancet.* 1997;350(9093):1734–7.

54. Weinberger MH. Salt Sensitivity Is Associated With an Increased Mortality in Both Normal and Hypertensive Humans. *The Journal of Clinical Hypertension*. 2002;4(4):274–6.
55. Weinberger MH, Fineberg NS, Fineberg SE, Weinberger M. Salt Sensitivity, Pulse Pressure, and Death in Normal and Hypertensive Humans. *Hypertension*. 2001;37(2):429–32.
56. Barba G, Galletti F, Cappuccio FP, et al. Incidence of hypertension in individuals with different blood pressure salt-sensitivity: results of a 15-year follow-up study. *J Hypertens*. 2007;25(7):1465–71.
57. He J, Huang J-F, Li C, et al. Sodium Sensitivity, Sodium Resistance, and Incidence of Hypertension: A Longitudinal Follow-Up Study of Dietary Sodium Intervention. *Hypertension*. 2021;78(1):155–64.
58. Babcock MC, Robinson AT, Migdal KU, et al. High Salt Intake Augments Blood Pressure Responses During Submaximal Aerobic Exercise. *J Am Heart Assoc*. 2020;9(10):15633.
59. Ramick MG, Brian MS, Matthews EL, et al. Apocynin and Tempol ameliorate dietary sodium-induced declines in cutaneous microvascular function in salt-resistant humans. *Am J Physiol Heart Circ Physiol*. 2019;317(1):H97–103.
60. Farquhar WB, Edwards DG, Jurkowitz CT, Weintraub WS. Dietary sodium and health: more than just blood pressure. *J Am Coll Cardiol*. 2015;65(10):1042–50.
61. Castiglioni P, Parati G, Lazzeroni D, et al. Hemodynamic and Autonomic Response to Different Salt Intakes in Normotensive Individuals. *J Am Heart Assoc* [Internet]. 2016;5(8) Available from: <https://www.ahajournals.org/doi/10.1161/JAHA.116.003736>. doi:10.1161/JAHA.116.003736.
62. Schmidlin O, Forman A, Sebastian A, Morris RC. What initiates the pressor effect of salt in salt-sensitive humans? Observations in normotensive blacks. *Hypertension*. 2007;49(5):1032–9.
63. Lennon-Edwards S, Ramick MG, Matthews EL, Brian MS, Farquhar WB, Edwards DG. Salt loading has a more deleterious effect on flow-mediated dilation in salt-resistant men than women. *Nutrition, Metabolism and Cardiovascular Diseases*. 2014;24(9):990–5.

64. Eisenach JH, Gullixson LR, Kost SL, Joyner MJ, Turner ST, Nicholson WT. Sex differences in salt sensitivity to nitric oxide dependent vasodilation in healthy young adults. *J Appl Physiol*. 2012;112(6):1049–53.
65. Hay M. Sex, the brain and hypertension: brain oestrogen receptors and high blood pressure risk factors. *Clin Sci*. 2016;130:9–18.
66. Fehrenbach DJ, Abais-Battad JM, Dasinger JH, Lund H, Mattson DL. Salt-sensitive increase in macrophages in the kidneys of Dahl SS rats. *American Journal of Physiology-Renal Physiology*. 2019;317(2):F361–74.
67. Rudemiller N, Lund H, Jacob HJ, Geurts AM, Mattson DL. CD247 modulates blood pressure by altering t-lymphocyte infiltration in the kidney. *Hypertension*. 2014;63(3):559–64.
68. Fehrenbach DJ, Dasinger JH, Lund H, Zemaj J, Mattson DL. Splenocyte transfer exacerbates salt-sensitive hypertension in rats. *Exp Physiol*. 2020;105(5):864–75.
69. Liu Y, Rafferty TM, Rhee SW, et al. CD8+ T cells stimulate Na-Cl co-transporter NCC in distal convoluted tubules leading to salt-sensitive hypertension. *Nat Commun*. 2017;8(1):14037.
70. Bovée DM, Cuevas CA, Zietse R, Danser AHJ, Mirabito Colafella KM, Hoorn EJ. Salt-sensitive hypertension in chronic kidney disease: distal tubular mechanisms. *Am J Physiol Renal Physiol*. 2020;319:729–45.
71. Vogt L, Marques FZ, Fujita T, Hoorn EJ, Danser AHJ. Novel mechanisms of salt-sensitive hypertension. *Kidney Int*. 2023;104(4):690–7.
72. Morris RC, Schmidlin O, Sebastian A, Tanaka M, Kurtz TW. Vasodysfunction That Involves Renal Vasodysfunction, Not Abnormally Increased Renal Retention of Sodium, Accounts for the Initiation of Salt-Induced Hypertension. *Circulation*. 2016;133(9):881–93.
73. Roman RJ, Osborn JL. Renal function and sodium balance in conscious Dahl S and R rats. *American Journal of Physiology-Regulatory, Integrative and Comparative Physiology*. 1987;252(5):R833–41.
74. Pechère-Bertschi A, Maillard M, Stalder H, Brunner HR, Burnier M. Renal segmental tubular response to salt during the normal menstrual cycle. *Kidney Int*. 2002;61(2):425–31.

75. Xue B, Johnson AK, Hay M. Sex differences in angiotensin II- and aldosterone-induced hypertension: the central protective effects of estrogen. *Am J Physiol Regul Integr Comp Physiol* [Internet]. 2013 [cited 2023 Oct 31];305(5) Available from: <https://pubmed.ncbi.nlm.nih.gov/23883676/>. doi:10.1152/AJPREGU.00222.2013.
76. Tatchum-Talom R, Eyster KM, Martin DS. Sexual dimorphism in angiotensin II-induced hypertension and vascular alterations. *Can J Physiol Pharmacol*. 2005;83(5):413–22.
77. Stocker SD, Monahan KD, Browning KN. Neurogenic and Sympathoexcitatory Actions of NaCl in Hypertension. *Curr Hypertens Rep*. 2013;15(6):538–46.
78. Shi P, Stocker SD, Toney GM. Organum vasculosum laminae terminalis contributes to increased sympathetic nerve activity induced by central hyperosmolality. *Am J Physiol Regul Integr Comp Physiol*. 2007;293(6):2279–89.
79. Farquhar WB, Paul EE, Prettyman A V., Stillabower ME. Blood pressure and hemodynamic responses to an acute sodium load in humans. *J Appl Physiol*. 2005;99(4):1545–51.
80. Farquhar WB, Wenner MM, Delaney EP, Prettyman A V, Stillabower ME. Sympathetic neural responses to increased osmolality in humans. *Am J Physiol Heart Circ Physiol*. 2006;291(5):H2181–6.
81. Greaney JL, Ray CA, Prettyman A V., Edwards DG, Farquhar WB. Influence of increased plasma osmolality on sympathetic outflow during apnea. *American Journal of Physiology-Regulatory, Integrative and Comparative Physiology*. 2010;299(4):R1091–6.
82. Brian MS, Matthews EL, Watso JC, et al. The influence of acute elevations in plasma osmolality and serum sodium on sympathetic outflow and blood pressure responses to exercise. *J Neurophysiol*. 2018;119(4):1257–65.
83. Weiss ML, Claassen DE, Hirai T, Kenney MJ. Nonuniform sympathetic nerve responses to intravenous hypertonic saline infusion. *J Auton Nerv Syst*. 1996;57(1–2):109–15.
84. Stocker SD, Lang SM, Simmonds SS, Wenner MM, Farquhar WB. Cerebrospinal Fluid Hypernatremia Elevates Sympathetic Nerve Activity and Blood Pressure via the Rostral Ventrolateral Medulla. *Hypertension*. 2015;66(6):1184–90.

85. Yamauchi K, Tsuchimochi H, Stone AJ, Stocker SD, Kaufman MP. Increased dietary salt intake enhances the exercise pressor reflex. *Am J Physiol Heart Circ Physiol*. 2014;306(3):H450-4.
86. Campese VM, Romoff MS, Levitan D, Saglikes Y, Friedler RM, Massry SG. Abnormal relationship between sodium intake and sympathetic nervous system activity in salt-sensitive patients with essential hypertension. *Kidney Int*. 1982;21(2):371-8.
87. Averina VA, Othmer HG, Fink GD, Osborn JW. A mathematical model of salt-sensitive hypertension: the neurogenic hypothesis. *J Physiol*. 2015;593(14):3065-75.
88. Stocker SD. Altered Neuronal Discharge in the Organum Vasculosum of the Lamina Terminalis Contributes to Dahl Salt-Sensitive Hypertension. *Hypertension*. 2023;80(4):872-81.
89. Ralph AF, Grenier C, Costello HM, et al. Activation of the Sympathetic Nervous System Promotes Blood Pressure Salt-Sensitivity in C57BL/6/J Mice. *Hypertension*. 2021;77(1):158-68.
90. Carlson SH, Roysomutti S, Peng N, Wyss JM. The role of the central nervous system in NaCl-sensitive hypertension in spontaneously hypertensive rats. *Am J Hypertens*. 2001;14(6 Pt 2):155S-162S.
91. Simmonds SS, Lay J, Stocker SD. Dietary Salt Intake Exaggerates Sympathetic Reflexes and Increases Blood Pressure Variability in Normotensive Rats. *Hypertension*. 2014;64(3):583-9.
92. Babcock MC, Brian MS, Watso JC, et al. Alterations in dietary sodium intake affect cardiovagal baroreflex sensitivity. *American Journal of Physiology-Regulatory, Integrative and Comparative Physiology*. 2018;315(4):R688-95.
93. Bayorh MA, Socci RR, Eatman D, Wang M, Thierry-Palmer M. The role of gender in salt-induced hypertension. *Clin Exp Hypertens*. 2001;23(3):241-55.
94. Ouchi Y, Share L, Crofton JT, Iitake K, Brooks DP. Sex difference in pressor responsiveness to vasopressin and baroreflex function in DOC-salt hypertensive rats. *J Hypertens*. 1988;6(5):381-7.
95. Lange DL, Haywood JR, Hinojosa-Laborde C. Role of the Adrenal Medullae in Male and Female DOCA-Salt Hypertensive Rats. *Hypertension*. 1998;31(1):403-8.

96. Hart EC, Charkoudian N, Wallin BG, Curry TB, Eisenach JH, Joyner MJ. Sex Differences in Sympathetic Neural-Hemodynamic Balance. *Hypertension*. 2009;53(3):571–6.
97. Joyner MJ, Barnes JN, Hart EC, Wallin BG, Charkoudian N. Neural Control of the Circulation: How Sex and Age Differences Interact in Humans. *Comprehensive Physiology*. Wiley; 2014. p. 193–215. Available from: <https://onlinelibrary.wiley.com/doi/10.1002/cphy.c140005>.
98. Keir DA, Badrov MB, Tomlinson G, et al. Influence of Sex and Age on Muscle Sympathetic Nerve Activity of Healthy Normotensive Adults. *Hypertension*. 2020;76(3):997–1005.
99. Jarvis SS, VanGundy TB, Galbreath MM, et al. Sex differences in the modulation of vasomotor sympathetic outflow during static handgrip exercise in healthy young humans. *American Journal of Physiology-Regulatory, Integrative and Comparative Physiology*. 2011;301(1):R193–200.
100. Shoemaker JK, Hogeman CS, Khan M, Kimmerly DS, Sinoway LI. Gender affects sympathetic and hemodynamic response to postural stress. *American Journal of Physiology-Heart and Circulatory Physiology*. 2001;281(5):H2028–35.
101. Kimmerly DS, Wong S, Menon R, Shoemaker JK. Forebrain neural patterns associated with sex differences in autonomic and cardiovascular function during baroreceptor unloading. *American Journal of Physiology-Regulatory, Integrative and Comparative Physiology*. 2007;292(2):R715–22.
102. Noda M, Hiyama TY. Sodium sensing in the brain. *Pflugers Arch*. 2015;467(3):465–74.
103. Zimmerman CA, Leib DE, Knight ZA. Neural circuits underlying thirst and fluid homeostasis. *Nat Rev Neurosci*. 2017;18(8):459–69.
104. Kinsman BJ, Browning KN, Stocker SD. NaCl and osmolarity produce different responses in organum vasculosum of the lamina terminalis neurons, sympathetic nerve activity and blood pressure. *J Physiol*. 2017;595(18):6187–201.
105. Kinsman BJ, Simmonds SS, Browning KN, Stocker SD. Organum Vasculosum of the Lamina Terminalis Detects NaCl to Elevate Sympathetic Nerve Activity and Blood Pressure. *Hypertension*. 2017;69(1):163–70.

106. Hochstenbach SL, Ciriello J. *Effect of lesions of forebrain circumventricular organs on c-fos expression in the central nervous system to plasma hypernatremia*. 1996. 17–28 p.
107. Tiruneh MA, Huang BS, Leenen FHH. Role of angiotensin II type 1 receptors in the subfornical organ in the pressor responses to central sodium in rats. *Brain Res*. 2013;1527:79–86.
108. Suckling RJ, He FJ, Markandu ND, MacGregor GA. Dietary salt influences postprandial plasma sodium concentration and systolic blood pressure. *Kidney Int*. 2012;81(4):407–11.
109. Nagakura A, Hiyama TY, Noda M. Nax-deficient mice show normal vasopressin response to dehydration. *Neurosci Lett*. 2010;472(3):161–5.
110. Rundgren M, McKinley MJ, Leksell LG, Andersson B. Inhibition of thirst and apparent ADH release by intracerebroventricular ethacrynic acid. *Acta Physiol Scand*. 1979;105(1):123–5.
111. Konopacka A, Qiu J, Yao ST, et al. Osmoregulation Requires Brain Expression of the Renal Na-K-2Cl Cotransporter NKCC2. *Journal of Neuroscience*. 2015;35(13):5144–55.
112. Stachenfeld NS, Mack GW, Takamata A, DiPietro L, Nadel ER. Thirst and fluid regulatory responses to hypertonicity in older adults. *American Journal of Physiology-Regulatory, Integrative and Comparative Physiology*. 1996;271(3):R757–65.
113. Stachenfeld NS. Sex hormone effects on body fluid regulation. *Exerc Sport Sci Rev*. 2008;36(3):152–9.
114. Stachenfeld NS, Splenser AE, Calzone WL, Taylor MP, Keefe DL. Sex differences in osmotic regulation of AVP and renal sodium handling. *J Appl Physiol (1985)*. 2001;91(4):1893–901.
115. Wenner MM, Stachenfeld NS. Blood pressure and water regulation: understanding sex hormone effects within and between men and women. *J Physiol*. 2012;590(23):5949–61.
116. Stachenfeld NS, Keefe DL. Estrogen effects on osmotic regulation of AVP and fluid balance. *Am J Physiol Endocrinol Metab*. 2002;283(4):E711–21.

117. Stachenfeld NS, DiPietro L, Palter SF, Nadel ER. Estrogen influences osmotic secretion of AVP and body water balance in postmenopausal women. *Am J Physiol*. 1998;274(1):R187-95.
118. Calzone WL, Silva C, Keefe DL, Stachenfeld NS. Progesterone does not alter osmotic regulation of AVP. *Am J Physiol Regul Integr Comp Physiol*. 2001;281(6):R2011-20.
119. Ishunina TA, Swaab DF. Vasopressin and Oxytocin Neurons of the Human Supraoptic and Paraventricular Nucleus; Size Changes in Relation to Age and Sex. *J Clin Endocrinol Metab*. 1999;84(12):4637-44.
120. Spary EJ, Maqbool A, Batten TFC. Oestrogen receptors in the central nervous system and evidence for their role in the control of cardiovascular function. *J Chem Neuroanat*. 2009;38(3):185-96.
121. Simerly RB, Swanson LW, Chang C, Muramatsu M. Distribution of androgen and estrogen receptor mRNA-containing cells in the rat brain: An in situ hybridization study. *J Comp Neurol*. 1990;294(1):76-95.
122. Goto A, Ganguli M, Tobian L, Johnson MA, Iwai J. Effect of an anteroventral third ventricle lesion on NaCl hypertension in Dahl salt-sensitive rats. *American Journal of Physiology-Heart and Circulatory Physiology*. 1982;243(4):H614-8.
123. Collister JP, Nahey DB, Hartson R, Wiedmeyer CE, Banek CT, Osborn JW. Lesion of the OVLT markedly attenuates chronic DOCA-salt hypertension in rats. *Am J Physiol Regul Integr Comp Physiol*. 2018;315:568-75.
124. Stocker SD, Wenner MM, Farquhar WB, Browning KN. Activation of the Organum Vasculosum of the Lamina Terminalis Produces a Sympathetically Mediated Hypertension. *Hypertension*. 2022;79(1):139-49.
125. Ramachandran CD, Gholami K, Lam SK, Hoe SZ. A preliminary study of the effect of a high-salt diet on transcriptome dynamics in rat hypothalamic forebrain and brainstem cardiovascular control centers. *PeerJ*. 2020;8(3):e8528.
126. Adams JM, Bardgett ME, Stocker SD. Ventral Lamina Terminalis Mediates Enhanced Cardiovascular Responses of Rostral Ventrolateral Medulla Neurons During Increased Dietary Salt. *Hypertension*. 2009;54(2):308-14.
127. Xue B, Hay M. 17 β -estradiol inhibits excitatory amino acid-induced activity of neurons of the nucleus tractus solitarius. *Brain Res*. 2003;976(1):41-52.

128. Ciriello J, Roder S. 17β -Estradiol alters the response of subfornical organ neurons that project to supraoptic nucleus to plasma angiotensin II and hypernatremia. *Brain Res.* 2013;1526:54–64.
129. Xue B, Pamidimukkala J, Lubahn DB, Hay M. Estrogen receptor-alpha mediates estrogen protection from angiotensin II-induced hypertension in conscious female mice. *Am J Physiol Heart Circ Physiol* [Internet]. 2007 [cited 2023 Nov 1];292(4) Available from: <https://pubmed.ncbi.nlm.nih.gov/17142339/>. doi:10.1152/AJPHEART.01011.2005.
130. Pamidimukkala J, Hay M. 17 beta-Estradiol inhibits angiotensin II activation of area postrema neurons. *Am J Physiol Heart Circ Physiol* [Internet]. 2003 [cited 2023 Nov 1];285(4) Available from: <https://pubmed.ncbi.nlm.nih.gov/12829428/>. doi:10.1152/AJPHEART.00174.2003.
131. Xue B, Zhang Z, Beltz TG, et al. Estrogen receptor- β in the paraventricular nucleus and rostroventrolateral medulla plays an essential protective role in aldosterone/salt-induced hypertension in female rats. *Hypertension.* 2013;61(6):1255–62.
132. Xue B, Zhang Z, Beltz TG, Guo F, Hay M, Johnson AK. Genetic knockdown of estrogen receptor-alpha in the subfornical organ augments ANG II-induced hypertension in female mice. *Am J Physiol Regul Integr Comp Physiol.* 2015;308(6):R507–16.
133. Xue B, Zhao Y, Johnson AK, Hay M. Central estrogen inhibition of angiotensin II-induced hypertension in male mice and the role of reactive oxygen species. *Am J Physiol Heart Circ Physiol* [Internet]. 2008 [cited 2023 Nov 1];295(3) Available from: <https://pubmed.ncbi.nlm.nih.gov/18599599/>. doi:10.1152/AJPHEART.00021.2008.
134. Xue B, Singh M, Guo F, Hay M, Johnson AK. Protective actions of estrogen on angiotensin II-induced hypertension: role of central nitric oxide. *Am J Physiol Heart Circ Physiol* [Internet]. 2009 [cited 2023 Nov 1];297(5) Available from: <https://pubmed.ncbi.nlm.nih.gov/19734362/>. doi:10.1152/AJPHEART.00502.2009.
135. Xue B, Zhang Z, Beltz TG, Guo F, Hay M, Johnson AK. Estrogen regulation of the brain renin-angiotensin system in protection against angiotensin II-induced sensitization of hypertension. *Am J Physiol Heart Circ Physiol* [Internet]. 2014 [cited 2023 Oct 31];307(2) Available from:

<https://pubmed.ncbi.nlm.nih.gov/24858844/>.
doi:10.1152/AJPHEART.01012.2013.

136. Egan G, Silk T, Zamarripa F, et al. Neural correlates of the emergence of consciousness of thirst. *Proceedings of the National Academy of Sciences*. 2003;100(25):15241–6.
137. Denton D, Shade R, Zamarripa F, et al. Correlation of regional cerebral blood flow and change of plasma sodium concentration during genesis and satiation of thirst. *Proc Natl Acad Sci U S A*. 1999;96(5):2532–7.
138. Farrell MJ, Bowala TK, Gavrilesco M, et al. Cortical activation and lamina terminalis functional connectivity during thirst and drinking in humans. *Am J Physiol Regul Integr Comp Physiol*. 2011;301(3):R623-31.
139. Huettel SA, Song AW, McCarthy G. *Functional Magnetic Resonance Imaging*. Third Edition. Sunderland, MA: Sinauer Associates, Inc; 2014.
140. Stock JM, Romberger NT, McMillan RK, et al. Acute hypernatremia increases functional connectivity of NaCl sensing regions in the human brain: An fMRI pilot study. *Auton Neurosci* [Internet]. 2024;254
doi:10.1016/j.autneu.2024.103182.
141. Macefield VG, Henderson LA. Identifying Increases in Activity of the Human RVLM Through MSNA-Coupled fMRI. *Front Neurosci* [Internet]. 2019 [cited 2022 Apr 27];13 Available from:
<http://www.ncbi.nlm.nih.gov/pubmed/32038124>.
doi:10.3389/fnins.2019.01369.
142. Macefield VG, Henderson LA. Real-time imaging of the medullary circuitry involved in the generation of spontaneous muscle sympathetic nerve activity in awake subjects. *Hum Brain Mapp*. 2009;31(4):539–49.
143. James C, Macefield VG, Henderson LA. Real-time imaging of cortical and subcortical control of muscle sympathetic nerve activity in awake human subjects. *Neuroimage*. 2013;70:59–65.
144. Coulson JM, Murphy K, Harris AD, Fjodorova M, Cockcroft JR, Wise RG. Correlation between baseline blood pressure and the brainstem FMRI response to isometric forearm contraction in human volunteers: a pilot study. *J Hum Hypertens*. 2015;29(7):449–55.
145. Kobuch S, Macefield VG, Henderson LA. Resting regional brain activity and connectivity vary with resting blood pressure but not muscle sympathetic nerve

- activity in normotensive humans: An exploratory study. *Journal of Cerebral Blood Flow & Metabolism*. 2019;39(12):2433.
146. Kobuch S, Fatouleh RH, Macefield JM, Henderson LA, Macefield VG. Differences in regional grey matter volume of the brain are related to mean blood pressure and muscle sympathetic nerve activity in normotensive humans. *J Hypertens*. 2020;38(2):303–13.
 147. Taylor KS, Kucyi A, Millar PJ, et al. Association between resting-state brain functional connectivity and muscle sympathetic burst incidence. *J Neurophysiol*. 2015;115(2):662–73.
 148. Sander M, Macefield VG, Henderson LA. Cortical and brain stem changes in neural activity during static handgrip and postexercise ischemia in humans. *J Appl Physiol (1985)*. 2010;108(6):1691–700.
 149. Wong SW, Massé N, Kimmerly DS, Menon RS, Shoemaker JK. Ventral medial prefrontal cortex and cardiovagal control in conscious humans. *Neuroimage*. 2007;35(2):698–708.
 150. Topolovec JC, Gati JS, Menon RS, Shoemaker JK, Cechetto DF. Human cardiovascular and gustatory brainstem sites observed by functional magnetic resonance imaging. *J Comp Neurol*. 2004;471(4):446–61.
 151. Kobuch S, Fazalbhoy A, Brown R, Henderson LA, Macefield VG. Central circuitry responsible for the divergent sympathetic responses to tonic muscle pain in humans. *Hum Brain Mapp*. 2017;38(2):869.
 152. Gerlach DA, Manuel J, Hoff A, et al. Novel Approach to Elucidate Human Baroreflex Regulation at the Brainstem Level: Pharmacological Testing During fMRI. *Front Neurosci*. 2019;13:193.
 153. Macefield VG, Henderson LA. Identification of the human sympathetic connectome involved in blood pressure regulation. *Neuroimage*. 2019;202:116119.
 154. Wong SW, Kimmerly DS, Massé N, Menon RS, Cechetto DF, Shoemaker JK. Sex differences in forebrain and cardiovagal responses at the onset of isometric handgrip exercise: a retrospective fMRI study. *J Appl Physiol*. 2007;103(4):1402–11.
 155. Grover VPB, Tognarelli JM, Crossey MME, Cox IJ, Taylor-Robinson SD, McPhail MJW. Magnetic Resonance Imaging: Principles and Techniques: Lessons for Clinicians. *J Clin Exp Hepatol*. 2015;5(3):246–55.

156. Geva T. Magnetic resonance imaging: historical perspective. *J Cardiovasc Magn Reson*. 2006;8(4):573–80.
157. Plewes DB, Kucharczyk W. Physics of MRI: a primer. *J Magn Reson Imaging*. 2012;35(5):1038–54.
158. Ridgway JP. Cardiovascular magnetic resonance physics for clinicians: part I. *J Cardiovasc Magn Reson*. 2010;12(1):71.
159. de Figueiredo EHMSG, Borgonovi AFNG, Doring TM. Basic Concepts of MR Imaging, Diffusion MR Imaging, and Diffusion Tensor Imaging. *Magn Reson Imaging Clin N Am*. 2011;19(1):1–22.
160. Buxton RB. The physics of functional magnetic resonance imaging (fMRI). *Rep Prog Phys*. 2013;76(9):096601.
161. Logothetis NK. The underpinnings of the BOLD functional magnetic resonance imaging signal. *J Neurosci*. 2003;23(10):3963–71.
162. Hillman EMC. Coupling Mechanism and Significance of the BOLD Signal: A Status Report. *Annu Rev Neurosci*. 2014;37(1):161–81.
163. Soares JM, Magalhães R, Moreira PS, et al. A Hitchhiker’s Guide to Functional Magnetic Resonance Imaging. *Front Neurosci*. 2016;10(2):891–901.
164. Logothetis NK, Pauls J, Augath M, Trinath T, Oeltermann A. Neurophysiological investigation of the basis of the fMRI signal. *Nature*. 2001;412(6843):150–7.
165. Mumford JA, Nichols TE. Power calculation for group fMRI studies accounting for arbitrary design and temporal autocorrelation. *Neuroimage*. 2008;39(1):261–8.
166. Huettel SA, McCarthy G. The effects of single-trial averaging upon the spatial extent of fMRI activation. *Neuroreport*. 2001;12(11):2411–6.
167. Brinker G, Bock C, Busch E, Krep H, Hossmann KA, Hoehn-Berlage M. Simultaneous recording of evoked potentials and T2*-weighted MR images during somatosensory stimulation of rat. *Magn Reson Med*. 1999;41(3):469–73.
168. Rees G, Friston K, Koch C. A direct quantitative relationship between the functional properties of human and macaque V5. *Nat Neurosci*. 2000;3(7):716–23.

169. Xue G, Chen C, Lu Z-L, Dong Q. Brain Imaging Techniques and Their Applications in Decision-Making Research. *Xin Li Xue Bao*. 2010;42(1):120–37.
170. Crosson B, Ford A, McGregor KM, et al. Functional imaging and related techniques: An introduction for rehabilitation researchers. *The Journal of Rehabilitation Research and Development*. 2010;47(2):vii.
171. Kameyama M, Murakami K, Jinzaki M. Comparison of [15O] H₂O positron emission tomography and functional magnetic resonance imaging in activation studies. *World J Nucl Med*. 2016;15(01):3–6.
172. Zhang K, Huang D, Shah NJ. Comparison of resting-state brain activation detected by bold, blood volume and blood flow. *Front Hum Neurosci* [Internet]. 2018;12 doi:10.3389/fnhum.2018.00443.
173. Viviani R, Messina I, Walter M. Resting state functional connectivity in perfusion imaging: Correlation maps with Bold connectivity and resting state perfusion. *PLoS One* [Internet]. 2011;6(11) doi:10.1371/journal.pone.0027050.
174. Lee MH, Smyser CD, Shimony JS. Resting-state fMRI: a review of methods and clinical applications. *AJNR Am J Neuroradiol*. 2013;34(10):1866–72.
175. Biswal B, Zerrin Yetkin F, Haughton VM, Hyde JS. Functional connectivity in the motor cortex of resting human brain using echo-planar mri. *Magn Reson Med*. 1995;34(4):537–41.
176. Van Dijk KRA, Hedden T, Venkataraman A, Evans KC, Lazar SW, Buckner RL. Intrinsic Functional Connectivity As a Tool For Human Connectomics: Theory, Properties, and Optimization. *J Neurophysiol*. 2010;103(1):297–321.
177. Fukunaga M, Horovitz SG, van Gelderen P, et al. Large-amplitude, spatially correlated fluctuations in BOLD fMRI signals during extended rest and early sleep stages. *Magn Reson Imaging*. 2006;24(8):979–92.
178. Lv H, Wang Z, Tong E, et al. Resting-State Functional MRI: Everything That Nonexperts Have Always Wanted to Know. *AJNR Am J Neuroradiol*. 2018;39(8):1390–9.
179. Zuo XN, Kelly C, Adelstein JS, Klein DF, Castellanos FX, Milham MP. Reliable intrinsic connectivity networks: Test-retest evaluation using ICA and dual regression approach. *Neuroimage*. 2010;49(3):2163–77.

180. Beckmann CF. Modelling with independent components. *Neuroimage*. 2012;62(2):891–901.
181. Shehzad Z, Kelly AMC, Reiss PT, et al. The resting brain: unconstrained yet reliable. *Cereb Cortex*. 2009;19(10):2209–29.
182. Chou Y, Panych LP, Dickey CC, Petrella JR, Chen N. Investigation of long-term reproducibility of intrinsic connectivity network mapping: a resting-state fMRI study. *AJNR Am J Neuroradiol*. 2012;33(5):833–8.
183. Zang Y, Jiang T, Lu Y, He Y, Tian L. Regional homogeneity approach to fMRI data analysis. *Neuroimage*. 2004;22(1):394–400.
184. Zou QH, Zhu CZ, Yang Y, et al. An improved approach to detection of amplitude of low-frequency fluctuation (ALFF) for resting-state fMRI: Fractional ALFF. *J Neurosci Methods*. 2008;172(1):137–41.
185. Yang H, Long XY, Yang Y, et al. Amplitude of low frequency fluctuation within visual areas revealed by resting-state functional MRI. *Neuroimage*. 2007;36(1):144–52.
186. Deng S, Franklin CG, O’Boyle M, et al. Hemodynamic and metabolic correspondence of resting-state voxel-based physiological metrics in healthy adults. *Neuroimage*. 2022;250:118923.
187. Mente A, O’Donnell M, Yusuf S. Sodium Intake and Health: What Should We Recommend Based on the Current Evidence? *Nutrients*. 2021;13(9):3232.
188. Wenner MM, Shenouda N, Shoemaker L, et al. Characterizing vascular and hormonal changes in women across the life span: a cross-sectional analysis. *Am J Physiol Heart Circ Physiol*. 2024;327(5):H1286–95.
189. Romberger NT, Stock JM, Burciu RG, et al. Acute Hypernatremia Increases Functional Connectivity Between the SFO and OVLT: Time Course of the Response. *International Journal of Exercise Science: Conference Proceedings* [Internet]. 2023;9(11).
190. Mumford JA, Nichols TE. Power calculation for group fMRI studies accounting for arbitrary design and temporal autocorrelation. *Neuroimage*. 2008;39(1):261–8.
191. Verheggen ICM, de Jong JJA, van Boxtel MPJ, et al. Permeability of the windows of the brain: feasibility of dynamic contrast-enhanced MRI of the

- circumventricular organs. *Fluids Barriers CNS* [Internet]. 2020;17(1)
doi:10.1186/s12987-020-00228-x.
192. Naidich TP, Duvernoy HM, Delman BN, Sorensen AG, Kollias SS, Haacke EM. Duvernoy's Atlas of the Human Brain Stem and Cerebellum. *Duvernoy's Atlas of the Human Brain Stem and Cerebellum* [Internet]. 2009 [cited 2024 Dec 2]; doi:10.1007/978-3-211-73971-6.
 193. Rolls ET, Huang CC, Lin CP, Feng J, Joliot M. Automated anatomical labelling atlas 3. *Neuroimage* [Internet]. 2020;206
doi:10.1016/j.neuroimage.2019.116189.
 194. Behrens TEJ, Johansen-Berg H, Woolrich MW, et al. Non-invasive mapping of connections between human thalamus and cortex using diffusion imaging. *Nat Neurosci*. 2003;6(7):750–7.
 195. Johansen-Berg H, Behrens TEJ, Sillery E, et al. Functional-anatomical validation and individual variation of diffusion tractography-based segmentation of the human thalamus. *Cerebral Cortex*. 2005;15(1):31–9.
 196. Behrens TEJ, Woolrich MW, Jenkinson M, et al. Characterization and Propagation of Uncertainty in Diffusion-Weighted MR Imaging. *Magn Reson Med*. 2003;50(5):1077–88.
 197. Buckner RL, Krienen FM, Castellanos A, Diaz JC, Thomas Yeo BT. The organization of the human cerebellum estimated by intrinsic functional connectivity. *J Neurophysiol*. 2011;106:2322–45.
 198. Andrews-Hanna JR. The brain's default network and its adaptive role in internal mentation. *Neuroscientist*. 2012;18(3):251–70.
 199. Elkin LA, Kay M, Higgins JJ, Wobbrock JO. An Aligned Rank Transform Procedure for Multifactor Contrast Tests. *The 34th Annual ACM Symposium on User Interface Software and Technology*. New York, NY, USA: ACM; 2021. p. 754–68. Available from: <https://dl.acm.org/doi/10.1145/3472749.3474784>.
 200. Wobbrock JO, Findlater L, Gergle D, Higgins JJ. The aligned rank transform for nonparametric factorial analyses using only anova procedures. *Proceedings of the SIGCHI Conference on Human Factors in Computing Systems*. New York, NY, USA: ACM; 2011. p. 143–6. Available from: <https://dl.acm.org/doi/10.1145/1978942.1978963>.

201. Watso JC, Babcock MC, Robinson AT, et al. Water deprivation does not augment sympathetic or pressor responses to sciatic afferent nerve stimulation in rats or to static exercise in humans. *J Appl Physiol*. 2019;127(1):235–45.
202. Wenner MM, Paul EP, Robinson AT, Rose WC, Farquhar WB. Acute NaCl loading reveals a higher blood pressure for a given serum sodium level in African American compared to Caucasian adults. *Front Physiol* [Internet]. 2018;9(OCT) doi:10.3389/fphys.2018.01354.
203. Hall JE, Hall ME. *Guyton and Hall Textbook of Medical Physiology*. 14th Edition. Philadelphia, PA: Elsevier; 2021.
204. Verdonk SJE, Vesper HW, Martens F, Sluss PM, Hillebrand JJ, Heijboer AC. Estradiol reference intervals in women during the menstrual cycle, postmenopausal women and men using an LC-MS/MS method. *Clinica Chimica Acta*. 2019;495:198–204.
205. Grisendi V, Spada E, Argento C, et al. Age-specific reference values for serum FSH and estradiol levels throughout the reproductive period. *Gynecological Endocrinology*. 2014;30(6):451–5.
206. Khalid M, Ilhami N, Giudicelli Y, Dausse J-P. Testosterone dependence of salt-induced hypertension in Sabra rats and role of renal alpha(2)-adrenoceptor subtypes. *J Pharmacol Exp Ther*. 2002;300(1):43–9.
207. Yanes LL, Sartori-Valinotti JC, Iliescu R, et al. Testosterone-dependent hypertension and upregulation of intrarenal angiotensinogen in Dahl salt-sensitive rats. *Am J Physiol Renal Physiol* [Internet]. 2009;296(4) doi:10.1152/ajprenal.90389.2008.
208. Ciura S, Liedtke W, Bourque CW. Hypertonicity Sensing in Organum Vasculosum Lamina Terminalis Neurons: A Mechanical Process Involving TRPV1 But Not TRPV4. *Journal of Neuroscience*. 2011;31(41):14669–76.
209. Ciura S, Prager-Khoutorsky M, Thirouin ZS, et al. Trpv4 Mediates Hypotonic Inhibition of Central Osmosensory Neurons via Taurine Gliotransmission. *Cell Rep*. 2018;23(8):2245–53.
210. Nishimura M, Ohtsuka K, Nanbu A, Takahashi H, Yoshimura M. Benzamil blockade of brain Na⁺ channels averts Na⁽⁺⁾-induced hypertension in rats. *American Journal of Physiology-Regulatory, Integrative and Comparative Physiology*. 1998;274(3):R635–44.

211. Abrams JM, Osborn JW. A role for benzamil-sensitive proteins of the central nervous system in the pathogenesis of salt-dependent hypertension. *Clin Exp Pharmacol Physiol*. 2008;35(5–6):687–94.
212. Huang BS, Leenen FHH. Brain Amiloride-Sensitive Phe-Met-Arg-Phe-NH₂ – Gated Na⁺ Channels and Na⁺-Induced Sympathoexcitation and Hypertension. *Hypertension*. 2002;39(2):557–61.
213. Nomura K, Hiyama TY, Sakuta H, et al. [Na⁺] Increases in Body Fluids Sensed by Central Nax Induce Sympathetically Mediated Blood Pressure Elevations via H⁺-Dependent Activation of ASIC1a. *Neuron*. 2019;101(1):60-75.e6.
214. Noda M, Hiyama TY. Sodium sensing in the brain. *Pflugers Arch*. 2015;467(3):465–74.
215. Konopacka A, Qiu J, Yao ST, et al. Osmoregulation requires brain expression of the renal Na-K-2Cl cotransporter NKCC2. *Journal of Neuroscience*. 2015;35(13):5144–55.
216. Sims ST, Heather AK. Myths and Methodologies: Reducing scientific design ambiguity in studies comparing sexes and/or menstrual cycle phases. *Exp Physiol*. 2018;103(10):1309–17.
217. Baroncini M, Jissendi P, Balland E, et al. MRI atlas of the human hypothalamus. *Neuroimage*. 2012;59(1):168–80.
218. Agarwal SK, Calaresu ER. *Reciprocal connections between nucleus tractus solitarius and rostral ventrolateral medulla*. 1990. 305–308 p.
219. Kline DD, King TL, Austgen JR, Heesch CM, Hasser EM. Sensory afferent and hypoxia-mediated activation of nucleus tractus solitarius neurons that project to the rostral ventrolateral medulla. *Neuroscience*. 2010;167(2):510–27.

Appendix A

IRB APPROVAL LETTER



Institutional Review Board
210H Hullen Hall
Newark, DE 19716
Phone: 302-831-2137
Fax: 302-831-2828

DATE: July 30, 2024

TO: Nathan Romberger
FROM: University of Delaware IRB

STUDY TITLE: [2054185-7] Sex Differences in Central Neural Activation During Acute Hypertremia
SUBMISSION TYPE: Amendment/Modification

ACTION: APPROVED
APPROVAL DATE: July 30, 2024
EXPIRATION DATE: May 16, 2025
REVIEW TYPE: Expedited Review
REVIEW CATEGORY: Expedited review category *per 45 CFR 46.110 (b) (1) (ii)*

Thank you for your Amendment/Modification submission to the University of Delaware Institutional Review Board (UD IRB). The UD IRB has reviewed and APPROVED the proposed research and submitted documents via Expedited Review in compliance with the pertinent federal regulations.

As the Principal Investigator for this study, you are responsible for and agree that:

- All research must be conducted in accordance with the protocol and all other study forms as approved in this submission. Any revisions to the approved study procedures or documents must be reviewed and approved by the IRB prior to their implementation. Please use the UD amendment form to request the review of any changes to approved study procedures or documents.
- Informed consent is a process that must allow prospective participants sufficient opportunity to discuss and consider whether to participate. IRB-approved and stamped consent documents must be used when enrolling participants and a written copy shall be given to the person signing the informed consent form.
- Unanticipated problems, serious adverse events involving risk to participants, and all non-compliance issues must be reported to this office in a timely fashion according with the UD requirements for reportable events. All sponsor reporting requirements must also be followed.

Oversight of this study by the UD IRB REQUIRES the submission of a CONTINUING REVIEW seeking the renewal of this IRB approval, which will expire on May 16, 2025. A continuing review/progress report form and up-to-date copies of the protocol form and all other approved study materials must be submitted to the UD IRB at least 45 days prior to the expiration date to allow for the required IRB review of that report.

If you have any questions, please contact the UD IRB Office at (302) 831-2137 or via email at hsrb-research@udel.edu. Please include the study title and reference number in all correspondence with this office.

Appendix B

BIORENDER PUBLICATION LICENSE



49 Spadina Ave. Suite 200
Toronto ON M5V 2J1 Canada
www.biorender.com

Confirmation of Publication and Licensing Rights

January 16th, 2025

Subscription Type: Institution - Academic
Agreement number: KZ27SS0VLH
Publisher Name: ProQuest

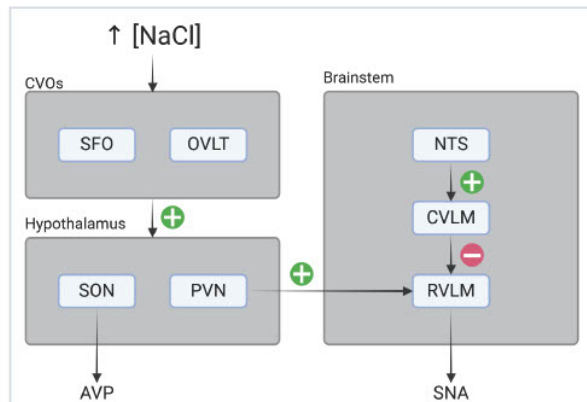
Citation to Use: Created in BioRender. Romberger, N. (2025) <https://BioRender.com/a41u352>

To whom this may concern,

This document is to confirm that Nate Romberger has been granted a license to use the BioRender Content, including icons, templates, and other original artwork, appearing in the attached Completed Graphic pursuant to BioRender's [Academic License Terms](#). This license permits BioRender Content to be sublicensed for use in publications (journals, textbooks, websites, etc.).

All rights and ownership of BioRender Content are reserved by BioRender. All Completed Graphics must be accompanied by the following citation: "Created in BioRender. Romberger, N. (2025) <https://BioRender.com/a41u352>".

BioRender Content included in the Completed Graphic is not licensed for any commercial uses beyond use in a publication. For any commercial use of this figure, users may, if allowed, recreate it in BioRender under an Industry BioRender Plan.



For any questions regarding this document, or other questions about publishing with BioRender, please refer to our [BioRender Publication Guide](#), or contact BioRender Support at support@biorender.com.